

# Adaptive process planning of rapid prototyping and manufacturing for complex biomedical models

Jin, Guoqing

*Award date:*
2012

# Adaptive Process Planning of Rapid Prototyping and Manufacturing for Complex Biomedical Models

**GUOQING JIN**

**A thesis submitted in partial fulfilment**
**of the University's requirements**
**for the Degree of Doctor of Philosophy**

**SEPTEMBER 2012**

**Coventry University**

# ABSTRACT

In this research, a set of novel, integrated and systematic adaptive process planning algorithms and strategies, which include adaptive tool-path generation algorithms and strategies, adaptive slicing algorithms and strategies, adaptive approach for FGM-based biomedical model and build time and geometrical accuracy analysis and control modules, for complex biomedical model fabrication in the RP/M process, have been developed to balance and optimise the geometrical accuracy and build efficiency.

In the developed adaptive tool-path generation algorithms and strategies, directly slicing algorithm and NURBS-based curves have been developed to represent the boundary contours of the sliced layers to maintain the geometrical accuracy of original biomedical models. The developed mixed tool-path generation algorithm can be used to generate mixed contour and zigzag tool-paths to preserve geometrical accuracy and speed up fabrication. Based on the developed build time and geometrical accuracy analysis modules, the developed adaptive speed algorithms can be used to further reduce build time of biomedical model fabrication in RP/M.

In the developed adaptive slicing approach, rotating slicing and two thresholds have been introduced to extract surface feature of biomedical models. Then, an adaptive slicing thickness determination algorithm has been developed to decide the thickness of each slicing layer based on the outside surface complexity of the model. In addition, the user can balance the geometrical accuracy and the build efficiency during RP/M processing with the different values of two pre-setting thresholds. Furthermore, by choosing the right value of the pre-setting thresholds, it can also effectively reduce the build time and improve the accuracy of biomedical model fabrication in RP/M.

In the developed adaptive approach for FGM-based biomedical model fabrication, FGM-based modelling features can represents typical FGM-based biomedical models effectively, and the linear and non-linear control parameters for FGM composition and distributions can enable users to address their specific functional needs of FGM-based biomedical model. The proposed mixed tool-path generation algorithm and adaptive speed algorithm can be used to generate a series of contour/offset tool-paths to represent the material gradual change, and zigzag tool-path is generated for the internal area of a single material to support the realizable and customized FGM-based biomedical models fabrication in RP/M efficiently.

# ACKNOWLEDGEMENTS

Firstly, I would like to express my sincere gratitude and appreciation to my supervisor Dr. Weidong Li (Reader, Faculty of Engineering and Computing, Coventry University, UK) for his continued encouragement, expert guidance and wise advices to help me to explore my potential and broaden the horizons of my capabilities. He is always willing to provide great helps on my study and living. Without his support and encouragement, I could not finish my research and get the chance to obtain a Ph.D degree in UK. I feel so fortunate to have a chance to work with him and it is really difficult to express my gratitude to him in these few words.

I also would like to say thanks to my parents. Without their support and understanding, it will be difficult for me to finish present work. Thanks also to my wife for her great support and encouragement during these years. Meanwhile, I would like to take this opportunity to thank my grandma, she is always the best in my heart.

I would like to thank the Coventry University for their financial support during these three years.

Finally, I would like to take this opportunity to thank everyone who gives me helps in UK. Especially, Irtaza Syed. They give me a lot of happy memories during these three years in UK.

# TABLE OF CONTENTS

**ABSTRACT** I

**ACKNOWLEDGEMENTS** II

**TABLE OF CONTENTS** III

**GLOSARY** VII

**LIST OF FIGURES** IX

**LIST OF TABLES** XIII

**PUBLICATIONS FOR THE RESEARCH** XV

**CHAPTER 1 INTRODUCTION** 1

1.1 Background on complex biomedical model fabrication in using RP/M techniques 1

1.2 Research problems and challenges 7

1.3 Aim and objectives 9

1.4 Summary of contributions 12

1.5 Outline of thesis 13

**CHAPTER 2 LITERATURE REVIEW** 16

2.1 Introduction 16

2.2 Historical development and biomedical application of RP/M technology 16

2.2.1 Historical development of RP/M technology 16

2.2.2 Biomedical application of RP/M technology 21

2.3 Tool-path generation strategies 24

2.4 Slicing strategies 27

2.4.1 Directly slicing and parametric representation 27

2.4.2 Adaptive slicing 30

2.5 RP/M for FGM-based biomedical models 33

2.5.1 FGM-based product representation 33

2.5.2 FGM-based RP/M fabrication process planning 35

2.6 Build time and geometric accuracy analysis modelling 37

2.6.1 Build time analysis modelling 38

2.6.2 Geometric accuracy analysis modelling 39
2.7 Summary 40

**CHAPTER 3 ADAPTIVE TOOL-PATH GENERATION OF RP/M FOR COMPLEX BIOMEDICAL MODELS** 42

3.1Introduction 42
3.2 The developed adaptive tool-path generation approach for biomedical models in RP/M 43
3.2.1 Phase 1 – Directly slicing and NURBS-based contour curve representation 46
3.2.2 Phase 2 - Offset curve generation and an adaptive speed algorithm along the contour tool-paths 48
3.2.2.1 Offset curve generation for a Type I or Type II contour curve 48
3.2.2.2 Adaptive speed algorithm of the RP/M nozzle/print head along the contour tool-paths 51
3.2.3 Phase 3 - Zigzag-based tool-path generation and adaptive algorithm along the zigzag tool-paths 54
3.3 The geometrical accuracy analysis model 60
3.4 Case studies and algorithm validation 62
3.4.1 Case study 1 – a tibia model 62
3.4.2 Case study 2 – an iliac model 63
3.4.3 Case study 3 – an ear model 65
3.4.4 Case study 4 – a calcaueus model 66
3.5 Build efficiency and geometrical accuracy comparisons 68
3.5.1 Build efficiency comparisons 68
3.5.2 Geometrical accuracy comparisons 70
3.6 Summary 73

**CHAPTER 4 ADAPTIVE SLICING APPROACH OF RP/M FOR COMPLEX BIOMEDICAL MODELS** 74

4.1Introduction 74
4.2 The developed adaptive slicing approach for biomedical models in RP/M 75
4.2.1 Phase 1 – Adaptive slicing algorithms and strategies 76

4.2.1.1 Part 1 – NURBS-based representation of slicing boundary 77
4.2.1.2 Part 2 – Rotating slicing and two controlling thresholds 79
4.2.1.3 Part 3 – Adaptive slicing thickness determination 82
4.2.2 Phase 3 – Geometrical accuracy and build time control strategies 88
4.3 Case studies 90
4.3.1 Case study 1 – a navicular bone model 90
4.3.2 Case study 2 – a calcaneus bone model 93
4.4 Geometrical Accuracy and Build Time Analysis and Control 95
4.5 Summary 98

**Chapter 5 ADAPTIVE RP/M FOR FGM-BASED BIOMEDICAL MODELS** 99

5.1 Introduction 99
5.2 Developed adaptive RP/M approach for FGM-based biomedical models 102
5.3 FGM-based representation of sliced layer 102
5.4 Contour/offset and zigzag FGM-based tool-path generation 110
5.5 Case studies and analysis 112
5.5.1 Case study I: Demonstration of the algorithms and the flow 112
5.5.2 Case Study II: Benchmarking the efficiency and geometrical quality 115
5.6 Summary 119

**Chapter 6 SYSTEMATIC APPLICATION OF THE DEVELOPED ADAPTIVE APPROACH AND CONCEPT DESIGN OF MULTI-MATERIAL RP/M SYSTEM** 121

6.1 Introduction 121
6.2 Systematic application of the developed adaptive process planning approach 122
6.2.1 Part 1(systematic application) - The adaptive slicing algorithms and strategies 122
6.2.2 Part 2 (systematic application) - The adaptive

tool-path generation algorithms and strategies 127
6.2.3 Part 3 (Systematic application) - The adaptive approach for FGM-biomedical model 131
6.3 Concept design of a multi-material RP/M system 134
6.4 Summary 141

**CHAPTER 7 CONCLUSIONS AND FUTURE WORK** 142

7.1 Conclusions 142
7.2 Recommendations for future work 146

**LIST OF REFERENCES** 149

# GLOSSARY

| | | |
|---|---|---|
| 2D | = | Two-Dimensional |
| 2.5D | = | Two and Half Dimensional |
| 3D | = | Three-Dimensional |
| 3DP | = | Three-Dimensional Printing |
| 3MMs | = | 3D Measurement Devices |
| AF | = | Additive Fabrication |
| AM | = | Additive Manufacturing |
| ANOVA | = | Analysis of Variance |
| CAD | = | Computer Aided Design |
| CAE | = | Computer-Aided Engineering |
| CCD | = | Charge Coupled Device |
| CNC | = | Computer Numerical Control |
| CT | = | Computed Tomography |
| DLP | = | Digital light processing |
| DMD | = | Direct Metal Deposition |
| DSPC | = | Direct Shell Production Casting |
| EOS | = | Electro Optical Systems |
| FDM | = | Fused Deposition Modelling |
| FDMC | = | Fused Deposition of Multiple Ceramic |
| FFF | = | Free-Form Fabrication |
| FGM | = | Functionally Graded Material |
| GA | = | Genetic Algorithm |
| IGES | = | Initial Graphics Exchange Specification |
| IJD | = | Ink-Jet Deposition |
| LAM | = | Laser Additive Manufacturing |
| LEM | = | Laminated Engineering Materials |
| LENS | = | Laser Engineered Net Shaping |
| LM | = | Layer Manufacturing |
| LOM | = | Laminated Object Manufacturing |
| MEM | = | Melted Extrusion Modelling |
| MEMS | = | Micro Electromechanical System |
| MJM | = | Multi Jet Modelling Systems |

| | | |
|---|---|---|
| MJS | | Multiphase Jet Solidification |
| M-RPM | = | Multi Functional RPM Systems |
| MRI | = | Magnetic Resonance Imaging |
| NURBS | = | Non-Uniform Rational B-Spline |
| POM | = | Precision Optical Manufacturing |
| QSR | = | Quick Surface Reconstruction |
| RE | = | Reverse Engineering |
| RM | = | Rapid Manufacturing |
| RP | = | Rapid Prototyping |
| RP/M | = | Rapid Prototyping and Manufacturing |
| RTM | = | Rapid Tool Maker |
| SCS | = | Solid Creation System |
| SGC | = | Solid Ground Curing |
| SLA | = | Stereo Lithography Apparatus |
| SLM | = | Selective Laser Melting |
| SLS | = | Selective Laser Sintering |
| SOUP | = | Solid Object  Ultraviolet laser plotter |
| STL | = | StereoLithography File |
| TSP-IP | = | Asymmetric Traveling Salesman Problem and Integer Programming |
| UV | = | Ultraviolet |
| WAAM | = | Wire and Arc Additive Manufacturing |

# LIST OF FIGURES


| | | |
|---|---|---|
| Figure. 1.1 | RP/M manufacturing systems | 2 |
| Figure. 1.2 | Some examples of biomedical models | 3 |
| Figure. 1.3 | The workflow and stages for biomedical model fabrication of RP/M | 4 |
| Figure. 1.4 | CT/MRI/3MMs scanners | 5 |
| Figure. 1.5 | Developed systematic adaptive process planning approach framework | 10 |
| Figure. 1.6 | Framework of dissertation organisation. | 15 |
| Figure. 2.1 | Different materials of RP/M systems | 18 |
| Figure. 2.2 | SLA process | 19 |
| Figure. 2.3 | SLS process | 20 |
| Figure. 2.4 | FDM process | 21 |
| Figure. 2.5 | Applications of RP/M technologies | 22 |
| Figure. 2.6 | Human implants fabricated by RP/M process | 24 |
| Figure. 2.7 | Different tool-path types of RP/M | 25 |
| Figure. 2.8 | CAD and STL format model of human being | 28 |
| Figure. 2.9 | A NURBS curve with 6 control points | 28 |
| Figure. 2.10 | Different slicing strategies of RP/M | 31 |
| Figure. 2.11 | Three examples of FGM-based model | 33 |
| Figure. 3.1 | Adaptive algorithms for RP/M process planning | 44 |
| Figure. 3.2 | The flowchart of the developed approach | 45 |
| Figure. 3.3 | An example to illustrate the developed approach | 46 |
| Figure. 3.4 | The flow of generating a NURBS-based contour curve of a sliced layer | 47 |
| Figure. 3.5 | Examples of two types of contour curves | 48 |
| Figure. 3.6 | An example for computing the new control points of an offset contour curve | 49 |
| Figure. 3.7 | An example for handling a *Type II* contour | 50 |
| Figure. 3.8 | Contour and offset tool-paths generated for the tibia model | 50 |
| Figure. 3.9 | Examples to illustrate the segmentation process for the adaptive speed algorithm | 51 |
| Figure. 3.10 | The flow of the segmentation and adaptive speed algorithm | 52 |

| | | |
|---|---|---|
| Figure. 3.11 | Illustration of the concepts in the contour based curve adaptive speed strategy | 53 |
| Figure. 3.12 | Two type lines in zigzag tool-paths | 55 |
| Figure. 3.13 | Incremental degrees of slopes for the minimum build time computing | 56 |
| Figure. 3.14 | Three cases of a segment and the speed of the RP/M nozzle/print head | 57 |
| Figure. 3.15 | Different tolerance distribution methods of RP/M | 58 |
| Figure. 3.16 | Geometrical errors of RP/M | 61 |
| Figure. 3.17 | Model 1 - a tibia model | 63 |
| Figure. 3.18 | Model 2 - an iliac model | 64 |
| Figure. 3.19 | Model 3 – an ear model | 65 |
| Figure. 3.20 | Model 4 - a calcaueus model | 67 |
| Figure. 3.21 | Build time comparisons - Model 1 | 68 |
| Figure. 3.22 | Build time comparisons - Model 2 | 69 |
| Figure. 3.23 | Build time comparisons - Model 3 | 69 |
| Figure. 3.24 | Build time comparisons - Model 4 | 70 |
| Figure. 3.25 | Geometrical accuracy comparisons - Model 1 | 71 |
| Figure. 3.26 | Geometrical accuracy comparisons - Model 2 | 71 |
| Figure. 3.27 | Geometrical accuracy comparisons - Model 3 | 72 |
| Figure. 3.28 | Geometrical accuracy comparisons - Model 4 | 72 |
| Figure. 4.1 | The developed adaptive slicing approach for biomedical models | 76 |
| Figure. 4.2 | An example to illustrate the directly slicing and NURBS representation | 78 |
| Figure. 4.3 | An example to illustrate the rotating slicing strategy | 79 |
| Figure. 4.4 | An example to illustrate the two thresholds | 82 |
| Figure. 4.5 | The main process of the developed adaptive slicing thickness determination algorithm | 84 |
| Figure. 4.6 | The main flow of the developed adaptive slicing thickness determination algorithm | 85 |
| Figure. 4.7 | The main flow of the smart adaptive slicing strategy | 87 |
| Figure. 4.8 | The relationship between the thresholds and geometrical accuracy and build time | 89 |
| Figure. 4.9 | The adaptive slicing of the biomedical model with the different | 90 |

| | | |
|---|---|---|
| | value of the threshold one ($D^1_{threshold}$) | |
| Figure. 4.10 | The process of the developed approach for the navicular model | 92 |
| Figure. 4.11 | The process of the developed approach for the calcaneus model | 94 |
| Figure. 4.12 | The results of geometrical accuracy and build time with different value of threshold one | 96 |
| Figure. 5.1 | An example of FGM-based model | 99 |
| Figure. 5.2 | The algorithms and strategies for RP/M processing of FGM-based biomedical models | 102 |
| Figure. 5.3 | Direct slicing and NURBS representation for one layer | 103 |
| Figure. 5.4 | FGM-based feature representation of the sliced layer | 104 |
| Figure. 5.5 | An example of material composition from two material grading sources | 105 |
| Figure. 5.6 | The computation of the material composition based on geometrical variable | 106 |
| Figure. 5.7 | Representations of linear and non-linear FGM distribution | 107 |
| Figure. 5.8 | $r_1(u)$ with different tensions is plotted | 108 |
| Figure. 5.9 | The example of a FGM-based sliced layer | 109 |
| Figure. 5.10 | A FGM-based NURBS surface | 110 |
| Figure. 5.11 | Contour/offset and zigzag tool-paths generation for a FGM-based sliced layer | 111 |
| Figure. 5.12 | Case Study I for a bone model | 114 |
| Figure. 5.13 | The interpolated curve for the relation between the build times and slope degrees of zigzag tool-paths | 115 |
| Figure. 5.14 | Case Study II – Model one: an ear model | 116 |
| Figure. 5.15 | Case Study II – Model three: an iliac bone model | 117 |
| Figure. 5.16 | Case Study II – Model four: a calcaneus model | 118 |
| Figure. 6.1 | Systematic application of the developed approach | 122 |
| Figure. 6.2 | A biomedical talus bone model | 123 |
| Figure. 6.3 | The developed adaptive slicing process for the talus model | 124 |
| Figure. 6.4 | The results of geometrical accuracy and build time with changed threshold one | 126 |
| Figure. 6.5 | The developed adaptive tool-path generation process for the talus model | 128 |
| Figure. 6.6 | Build time comparisons | 129 |

| | | |
|---|---|---|
| Figure. 6.7 | Geometrical accuracy comparisons | 130 |
| Figure. 6.8 | The developed adaptive process for FGM-based model | 131 |
| Figure. 6.9 | The curve for the relation between the build times and slope degrees of zigzag tool-paths | 132 |
| Figure. 6.10 | Five different layers of the FGM-based model | 133 |
| Figure. 6.11 | Concept design of multi-material RP/M 3D nozzle deposition system | 134 |
| Figure. 6.12 | Concept design of the feeding process | 135 |
| Figure. 6.13 | Concept design of the deposition process | 136 |
| Figure. 6.14 | Concept design of the Z-axis | 137 |
| Figure. 6.15 | Concept design of the nozzle apparatus | 138 |
| Figure. 6.16 | Concept design of material deposition control process | 139 |
| Figure. 6.17 | Concept design of curing process | 140 |
| Figure. 7.1 | Two examples of tissue scaffold | 147 |
| Figure. 7.2 | Two examples of complex FGM-based model | 148 |

# LIST OF TABLES


| | | |
|---|---|---|
| Table 2.1 | Categorisation of RP/M Systems | 17 |
| Table 2.2 | A summary of RP/M tool-path generation | 25 |
| Table 2.3 | A summary of RP/M model representation | 29 |
| Table 2.4 | A summary of the adaptive slicing works | 31 |
| Table 2.5 | RP/M methods and their characteristics for FGM objects fabrication | 35 |
| Table 2.6 | A summary of the RP/M build time and geometrical accuracy modules | 38 |
| Table 3.1 | The RP/M nozzle/print head speed of the contour tool-paths for the tibia model | 63 |
| Table 3.2 | Comparisons of the different slope degrees of zigzag tool-paths for the tibia model | 63 |
| Table 3.3 | The RP/M nozzle/print head speed of the contour tool-paths for the iliac model | 64 |
| Table 3.4 | Comparisons of the different slope degrees of zigzag tool-paths for the iliac model | 64 |
| Table 3.5 | The RP/M nozzle/print head speed of the contour tool-paths for the ear model | 65 |
| Table 3.6 | Comparisons of the different slope degrees of zigzag tool-paths for the ear model | 66 |
| Table 3.7 | The RP/M nozzle/print head speed of the contour tool-paths for the calcaueus model | 67 |
| Table 3.8 | Comparisons of the different slope degrees of zigzag tool-paths for the calcaueus model | 67 |
| Table 4.1 | The characteristics of the three phases of the developed adaptive slicing approach | 76 |
| Table 4.2 | The volume and bi-data for each layer of the navicular model | 93 |
| Table 4.3 | Comparison of computational results of different threshold one for the navicular model | 93 |
| Table 4.4 | The volume and bi-data for each layer of the calcaneus model | 95 |
| Table 4.5 | Comparison of computational results of different threshold one for the calcaneus model | 95 |

| | | |
|---|---|---|
| Table 4.6 | The change results of the different value of threshold one | 97 |
| Table 5.1 | Build time of the contour/offset tool-paths for the bone model | 115 |
| Table 5.2 | Results of the build time with different sliced layers in the developed approach | 118 |
| Table 5.3 | Results of the build time comparison in the same layer (layer 13) | 119 |
| Table 5.4 | Comparison of the geometrical accuracy of the models (layer 13) | 119 |
| Table 6.1 | The volume and bi-data for each layer of the talus model. | 125 |
| Table 6.2 | Comparison of computational results of different threshold one for the talus model | 125 |
| Table 6.3 | The results of the build time and geometrical accuracy of changed threshold one | 126 |
| Table 6.4 | The RP/M nozzle/print head speed of the contour tool-paths for the talus model | 128 |
| Table 6.5 | Comparisons of the different slope degrees of zigzag tool-paths for the talus model | 128 |
| Table 6.6 | Build time of the contour/offset tool-paths for the bone model | 132 |
| Table 6.7 | Results of the build time with different sliced layers of developed appraoch | 133 |
| Table 6.8 | Results of the build time comparison in the same layer (layer 13) | 133 |

# PUBLICATIONS FOR THE RESEARCH

G.Q. Jin, W.D. Li, L. Gao. An Adaptive Process Planning Approach of Rapid Prototyping and Manufacturing. Robotics and Computer-Integrated Manufacturing, 2013, 29: 23-38.

G.Q. Jin, W.D. Li. Adaptive Rapid Prototyping/Manufacturing for Functionally Graded Material-based Biomedical Models. International Journal of Advanced Manufacturing Technology, 2012, in press. (Online available on April 29, 2012)

G.Q. Jin, W.D. Li, C.F. Tsai, L. Wang. Adaptive tool-path generation of rapid prototyping for complex product models. Journal of Manufacturing Systems, 2011, 30(3): 154-164.

G.Q. Jin, W.D. Li, L. Gao, K. Popplewell. A Combined and Adaptive Tool-path Generation Approach of Rapid Prototyping and Manufacturing for Biomedical Models. Computer In Industrial, 2012, Accepted.

G.Q. Jin, W.D. Li. An Adaptive Slicing Approach of Rapid Prototyping and Manufacturing for Complex Biomedical Models, 2012, preparing for submission.

G.Q. Jin, W.D. Li, L. Gao. Tool-paths Optimization of Rapid Prototyping to Support Product Verification and Collaboration, CSCWD2011 conference: 120-124.

W.D. Li, G.Q. Jin, L. Gao, C. Page, K. Popplewell. The current status of process planning for multi-material rapid prototyping fabrication, PDR2010 conference: 625-629.

W. D. Li, K.M. Chao, G. Q. Jin, K. Xia, L. Gao. Sustainable information management for Waste Electrical and Eletronic Equipment. CSCWD2012 conference: 875-881.

# CHAPTER 1
# INTRODUCTION

## 1.1 Background on complex biomedical model fabrication in using Rapid Prototyping and Manufacturing (RP/M) techniques

The Rapid Prototyping and Manufacturing (RP/M) technology (the technology is also called Layer Manufacturing (LM), Free-form Fabrication (FFF), Additive Manufacturing (AM) or Additive Fabrication (AF). In the following, the terminology is standardized as RP/M) has been identified as an innovative manufacturing technology in recent years (Bourell et al., 2009). Different from conventional forming and machining processes, it is an additive build process by adding materials, layer-by-layer, as specified by a Computer-Aided Design (CAD) system. Based on this working principle, various RP/M machines have been developed, including Stereolithography Apparatus (SLA), 3D Printing (3DP), Fused Deposition Modelling (FDM), Selective Laser Sintering or Melting (SLS/SLM), Laminated Object Manufacturing (LOM), etc (shown in Figure 1.1). The distinguished advantage of RP/M is that it is a mouldless process, suitable for free-form and complex geometry product realisation. For instance, compared with the traditional Computer Numerical Control (CNC) system, the PR/M system can fabricate parts with almost any geometrical complexity without significant requirements in technical expertise (Chua et al., 2005). Meanwhile, biomedical models such as anatomy model and patient specific implant are usually characterised with highly customised and complex geometry (shown in Figure 1.2). It is difficult for the conventional manufacturing and machining processes such as forming, casting, turning and milling, etc. to fabricate the models. This kind of geometric flexibility of RP/M technologies and the complexity of biomedical models are the main reasons that RP/M is increasingly used in non-industrial applications like biomedical (Giannatsis and Dedoussis, 2009).

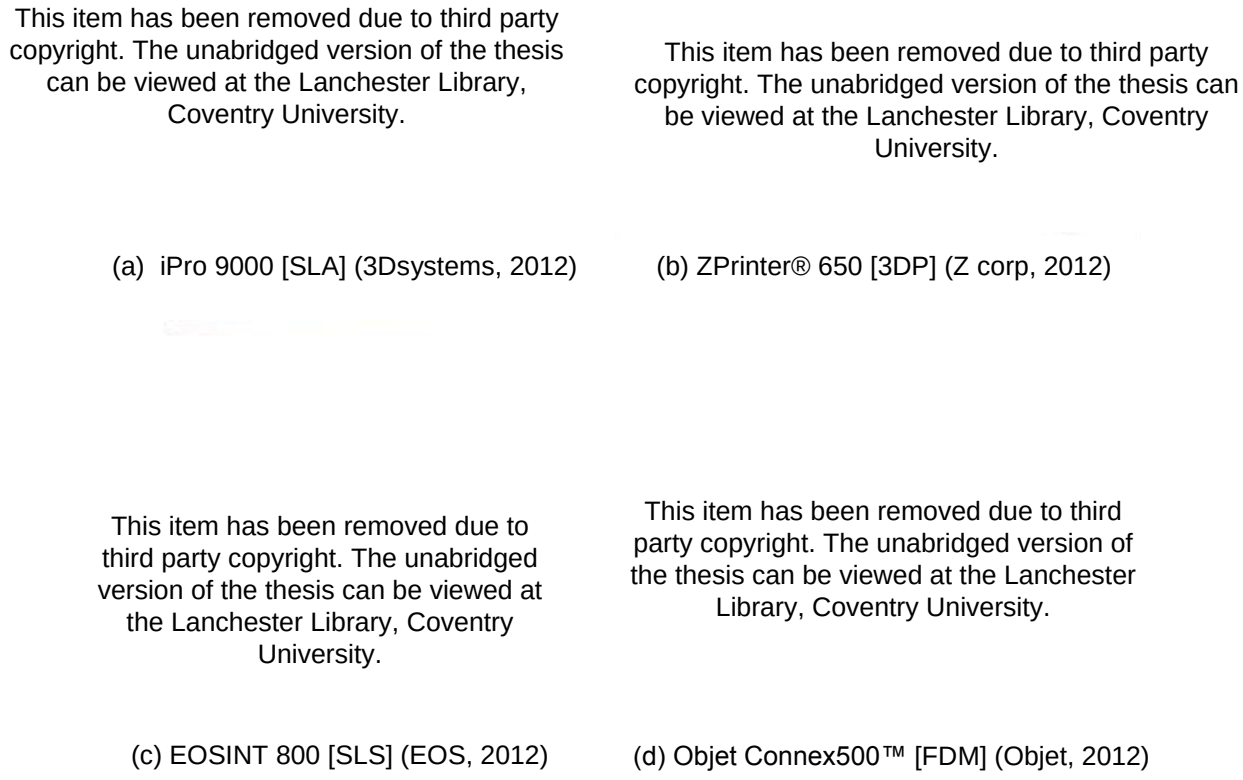


**Figure 1.1** RP/M manufacturing systems.

One of the major biomedical applications of RP/M is to fabricate biomedical models of human anatomy of patient as an aiding tool for rehearsal and surgical planning. Owing to the fact that every patient is unique, a biomedical model of a patient offers surgeons a direct, full understanding of the patient's anatomy which cannot be obtained from X-ray, Computed Tomography (CT) and Magnetic Resonance Imaging (MRI) images, helps surgeons identify a disease more easily on disease diagnosis and treatment planning, and reduce the risk of medical and operation problems. Meanwhile, such a biomedical model is very useful in medical teaching and as a communication tool between medical personals.

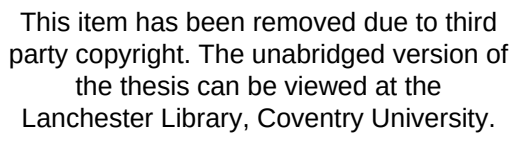


(a) A skull model

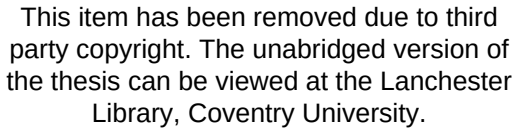


(b) A bone model

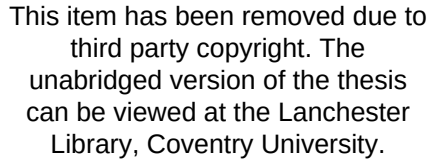


(c) A human body model

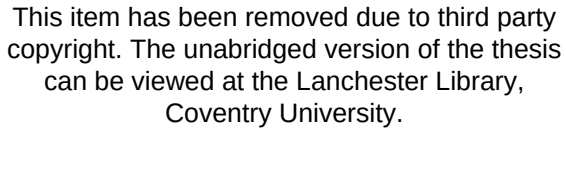


(d) A feet model

**Figure 1.2** Some examples of biomedical models (Object, 2012).

The fabrication process of a biomedical model in RP/M systems is generally composed by three stages: (1) modelling, (2) process planning, and (3) fabrication. Each stage includes more tasks in Figure 1.3.

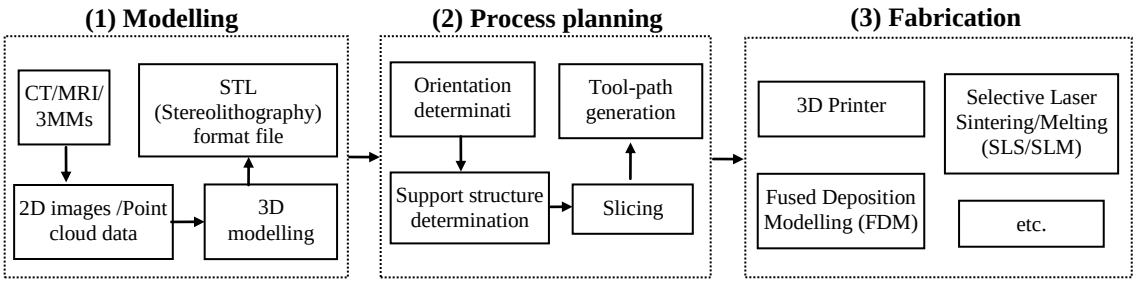


**Figure 1.3** The workflow and stages for biomedical model fabrication of RP/M.

The modelling stage is to use CT, MRI and 3D Measurement Devices (3MMs) scanners (shown in Figure 1.4) to obtain the data such as 2D images or point cloud data of the patient's area of interest. The data is next manipulated employing special image processing software for instance Mimic software (Materialise, 2012) to deal with the tissues and represent the area of the biomedical model, and allow the conversion from 2D images or point cloud data to 3D representation. Generally, the Stereolithography (STL) file, which is a de facto data representation standard to support RP/M, is utilised for the commercial application.

This item has been removed due to third party copyright. The unabridged version of the thesis can be viewed at the Lanchester Library, Coventry University.

(a) MRI scanner

This item has been removed due to third party copyright. The unabridged version of the thesis can be viewed at the Lanchester Library, Coventry University.

(b) CT scanner

This item has been removed due to third party copyright. The unabridged version of the thesis can be viewed at the Lanchester Library, Coventry University.

(c) 3MMs scanner

**Figure 1.4** CT/MRI/3MMs scanners (ultrasound-scanners, 2012).

Then the biomedical 3D modelling is sent to the process planning stage, which is a critical task in RP/M to determine the build efficiency and surface quality of complex biomedical model fabrication (Ren et al., 2008). The process consists of four essential tasks, i.e., orientation determination, support structure determination, slicing and tool-path generation (Marsan and Dutta, 1997):

1. **Orientation determination.** It is used to define the fabrication direction of the biomedical model. Different build orientation for a CAD model will affect the surface quality, the build time, the complexity of support structure and the total number of sliced layers. The build orientation is usually determined based on the

height, surface quality requirement, mechanical properties and external support structure requirement of the model (Thompson, 1995; Xu et al., 1999);

2. **Support structure determination.** It is used to uphold overhanging build materials during RP/M forming to avoid structural collapse or deformation of the biomedical model. Different designs of the support structure will affect the build time, surface quality and mechanical properties of the fabrication model (Allen and Dutta, 1995; Byun and Lee, 2005). In the past years, some software packages have been developed in this research field to automatically generate the support of RP/M fabrication, such as Materials' Magics RP and Marcam Engineering's VisCAM RP, etc. (Materialise, 2012). Meanwhile, some of the RP/M technologies do not need support structures during their fabrication processing such as Wire and Arc Additive Manufacturing (WAAM), SLA and LOM (Ding et al., 2011).

3. **Slicing.** It is to transfer the biomedical model into a series of two-half Dimensional (2.5D) sliced layers perpendicular to the orientation direction with a thickness. It can be generally divided into uniform slicing and adaptive slicing. In uniform slicing, the distance between two consecutive layers is the same, while in adaptive slicing, the distance between two layers varies depending on the surface curvatures of the model. Most of the commercial RP/M systems use uniform slicing while research is being conducted to explore adaptive slicing (Kulkarni et al., 2000; Ma et al., 2004; Rianmora and Koomsap et al., 2010);

4. **Tool-path generation.** It is the trajectory of the nozzle (e.g., in a FDM system)/print head (e.g., in a 3DP system) in a RP/M process to fill the boundary and interior areas of each sliced layer of the biomedical model. Several types of tool-path strategies and algorithms such as zigzag, contour, spiral and partition patterns have been developed with different considerations of the build time, cost, surface quality, warpage, strength and stiffness of RP/M models. A well-developed tool-path strategy can significantly optimise the build time of fabrication, surface quality and mechanical properties of the models (Misra et al., 2005; Chiu et al., 2006; Luo et al., 2010).

Finally, the biomedical model is fabricated by a selected RP/M system with suitable raw materials followed by possible manual finishing if it is necessary.

In the above RP/M process, there are a number of elements affecting the surface quality and build time of fabrication. This research focuses on the improvement of slicing and tool-path generation approaches, which are the major technical challenges in RP/M process planning.

## 1.2 Research problems and challenges

The biomedical branch in particular has attracted the attention of many researchers since the first introduction of RP/M technologies, and a lot of research efforts have been devoted to biomedical models fabrication in using RP/M techniques as they have great potential due to their additive nature and distinct features (Kruth et al., 2007). However, there are still a few problems remaining unresolved. Some of the problems and challenges in this research field include:

A STL file is a triangular representation of a 3D surface geometry, where a surface is tessellated into a series of small triangles facets. It is the widely adopted data standard in the RP/M industry recently. However, there are some problems in STL files such as gaps, holes, missing/degenerated/overlapping facets, etc. Meanwhile, STL is inherently inaccurate in geometrical representation and needs much more storage spaces to represent a highly complex model such as biomedical model. In addition, STL file is hard to represent the heterogeneous material-based products with varied material compositions and distributions such as Functionally Graded Material (FGM)-based biomedical models (Chua et al., 2005). It is becoming a strong desire to develop a better representation approach in RP/M for complex biomedical models.

Geometrical errors inherent from the layer-by-layer and additive forming mechanism of RP/M have brought great challenges on achieving high geometrical accuracy with less time consuming for complex biomedical models (Sabourin et al., 1997). In addition, owing to quickly developed healthcare markets with stronger requirements for more complex

applications, it is becoming a strong desire to develop better algorithms and strategies in the current process planning of RP/M to reduce build time and improve geometrical accuracy so as to meet the high-quality design and functional requirements of complex biomedical models.

The zigzag tool-path generation is the most typical method used in RP/M systems. It is easy to implement, but if a biomedical model is complex or has some hollow structures inside, the nozzle/print heads have to be turned frequently, leading to a poor geometrical quality and it will also has a warpage problem as the tool-path along the same direction to build the whole model. The contour tool-path generation can address the above geometrical quality issue effectively by following the geometrical trend of the boundary contour. However, when a boundary contour is irregular or has a hollow, island or ring structure such as biomedical models, the computation of the algorithms will be complicated and sometime could not work for the whole model fabrication (Misra et al., 2005; Chiu et al., 2006). It is expected to develop a smart and hybrid strategy to leverage the advantages of various tool-path generation strategies to be suitable for complex biomedical models in RP/M process.

Uniform slicing has been widely used for commercial RP/M systems recently. However, uniform slicing is difficult to achieve an optimised balance of build efficiency and geometrical accuracy. For instance, if the layer is too thick, the build time is reduced but the geometrical accuracy of the product could be relatively poor. Otherwise, the geometrical accuracy is improved but the build time is also extended significantly (Ma et al., 2004). Adaptive slicing can effectively reduce the staircase effect of RP/M and balance the build time and the geometrical accuracy of RP/M with varied thickness of layers to address the different geometrical characteristics of models' surfaces. However, a research gap still exists between the adaptive slicing thickness determination, and an analysis and control solution to balance and optimise the geometrical accuracy and build time for complex biomedical model in the RP/M process.

The current RP/M systems have been developed mainly for homogenous material-based product modelling. It is desired to develop a FGM-based design model integrative to the current RP/M systems so as to take advantage of the best practices and simulation

methods developed in the RP/M systems (Bourell and Leu, 2009). Apart from the representation of regular product shapes, the new design features are also expected to be extensible and adaptive to represent more complex shapes such as FGM-based biomedical models.

Manufacturing technologies of FGM-based biomedical model are essential because FGM-based biomedical models need to be not only theoretically correct in design and modelling but also realisable in manufacturing. In recent years, the RP/M technology has been increasingly used in FGM-based model applications (Sun et al., 2005). Considering the characteristics of FGM-based models, an important research issue is how to develop more efficient and adaptive RP/M algorithms and strategies to support the realisable, customised and free-form FGM-based biomedical models.

Most of the existing analysis and prediction modules rely on the simple geometric product models and they are difficult to be applied to complex biomedical models which include highly customised and complex geometry (Chen and Sullivan, 1996; Han et al., 2003). It is expect to develop more suitable and sensible geometrical accuracy and build time analysis and control modules to enable the user to calculate and analyse the build time and geometrical accuracy for complex biomedical model during RP/M processing.

This research is motivated to tackle the above problems in the context of complex biomedical model fabrication in using the RP/M technologies. The objectives of this research are presented in below.

## 1.3 Aim and objectives

This study aims at developing a systematic adaptive process planning approach to effectively balance and optimise the geometrical accuracy and build efficiency of biomedical model in RP/M process (shown in Figure 1.5). It includes a directly slicing algorithm and Non-Uniform Rational B-Spline (NURBS)-based representation, adaptive tool-path generation algorithms and strategies, adaptive slicing algorithms and strategies, FGM-based biomedical model representation and adaptive process planning approach,

geometrical accuracy and build time analysis modules, geometrical accuracy and build time control strategy. The objectives of this research are listed as follows:

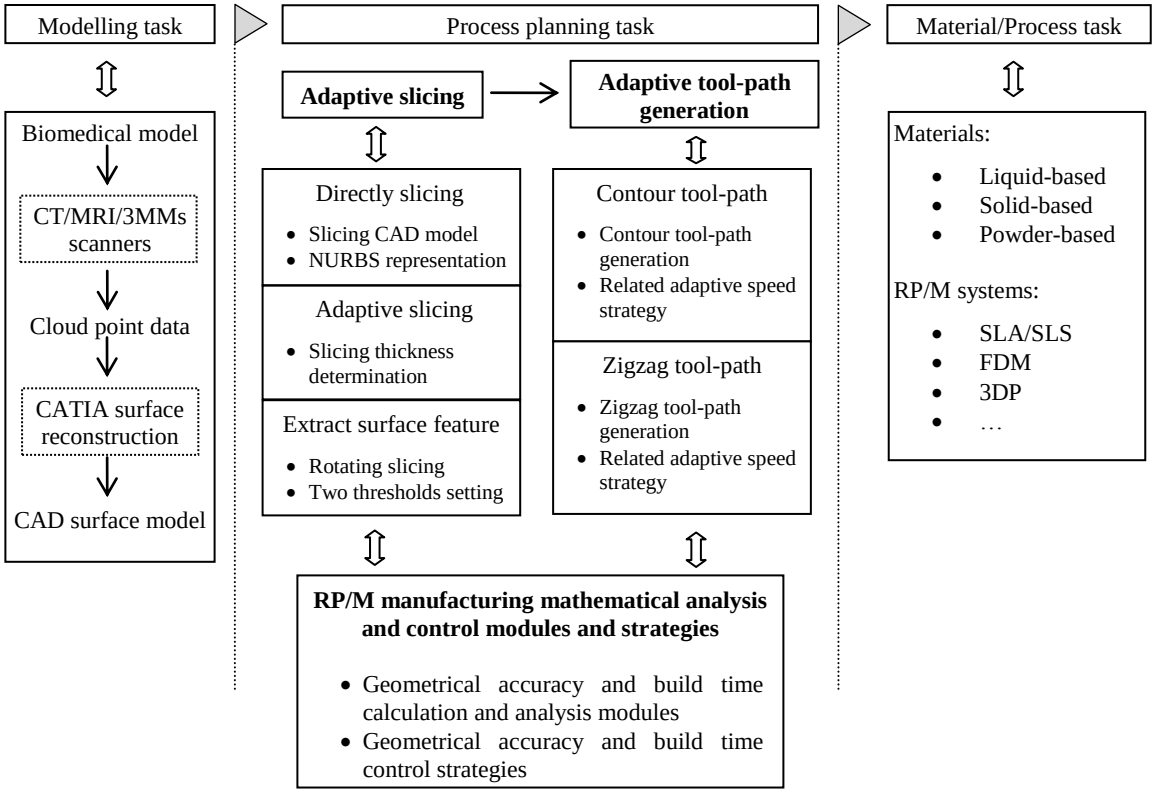


**Figure 1.5** Developed systematic adaptive process planning approach framework.

1. In literature, to review the related research work on the RP/M technology, tool-path generation, slicing strategies, Functionally Graded Material (FGM)-based biomedical model representation and fabrication process, and build time and geometrical accuracy analysis modules.

2. To identify major factors that affect the build time and geometrical accuracy in the process planning of RP/M.

3. To develop a direct slicing algorithm to directly slice complex biomedical models and use NURBS-based curves to represent the contour of the sliced layers.

4. To develop adaptive tool-path generation algorithms and strategies to reduce build time and improve geometrical accuracy of biomedical models. It consists of some algorithms and strategies that are as follows:
   i) To develop a mixed tool-path algorithm to meet both the geometrical accuracy and build efficiency requirements of biomedical models.
   ii) To develop an adaptive speed strategies to optimise the speed of the RP/M nozzle/print head along the tool-paths.
   iii) To develop a slope degree optimisation algorithm to obtain the best slope degree of the RP/M nozzle/print head along the zigzag tool-paths.

5. To develop adaptive slicing algorithms and strategies to reduce build time and improve geometrical accuracy of biomedical models. It consists of some algorithms and strategies that are as follows:
   i) To develop a rotating slicing and two thresholds strategy to extract the surface feature of biomedical models.
   ii) To develop an adaptive slicing thickness determination algorithm to decide the thickness for each slicing layer of the models.

6. To develop an adaptive approach to fabricate FGM-based biomedical models. It consists of some contents that are as follows:
   i) To develop a FGM-based biomedical model representation approach and integrate it to the current RP/M systems.
   ii) To develop more efficient and adaptive RP/M process planning approach to support the realisation of FGM-based biomedical models in RP/M.

7. To develop geometrical accuracy and build time analysis modules to calculate and analyse the build time and geometrical accuracy during RP/M processing of biomedical models.

8. To develop a geometrical accuracy and build time control strategy to control and optimise the geometrical accuracy and build time of fabrication in RP/M of biomedical models.

9. To concept design a multi-material RP/M nozzle deposition system to fabricate multi-material objects including FGM-based biomedical models.

10. To make some recommendations to users to balance and optimise the build time and the geometrical accuracy of the RP/M fabrication.

## 1.4 Summary of contributions

The geometrical accuracy of the original CAD models is maintained through introducing directly slicing and NURBS-based curve to represent the contours of sliced layers of biomedical models to keep high-fidelity information. It also establishes a good original data source for further RP/M adaptive tool-path generation and slicing thickness determination.

The developed mixed tool-path generation algorithms can effectively balance RP/M geometrical quality and build efficiency. The contour tool-paths are used to fabricate the area along the boundary of each sliced layer to improve the geometrical quality of a biomedical model. The zigzag tool-paths are used to fabricate the interior area of the biomedical model to improve the efficiency.

The developed adaptive speed strategies of contour and zigzag tool-paths for RP/M nozzle/print head can be used to reduce build time towards a minimum target. The slope degree optimisation algorithm can be used to further optimise build time by choosing the best slope degree of the RP/M nozzle/print head along the zigzag tool-paths.

Rotating slicing and two thresholds are first used to extract the surface feature of the biomedical model. Based on the obtained surface feature information of the biomedical model, the developed adaptive slicing algorithm can be used to decide the thickness of each slicing layer to balance the geometrical accuracy and build efficiency during the fabrication processes of RP/M.

The developed FGM-based modelling features can represent typical FGM-based biomedical models effectively. The linear and non-linear control parameters for FGM

composition and distributions can enable users to address their specific functional needs. The developed adaptive algorithms and strategies can be used to support the realizable, customized and free-form FGM-based biomedical models.

The introduced concept design of a Multi-material RP/M 3D nozzle deposition system can be used to fabricate multi-material objects which include FGM-based biomedical model.

The developed geometrical accuracy and build time analysis modules can be used to calculate and analyse the geometrical accuracy and build time during RP/M processing with the different values of parameters. It provides an effective guideline for parameter setting of a RP/M system for reducing build time and improving geometrical accuracy.

The developed geometrical accuracy and build time control strategy can be used to control the geometrical accuracy and build time in RP/M. It provides an effective guideline for a user to balance the geometrical accuracy and build efficiency and can achieve significantly improvement by choosing the right threshold values.

## 1.5 Outline of thesis

The framework of this dissertation is shown in figure 1.6. Each chapters are organised as follows:

Chapter 2 reviews the literatures that provide the support of this research. Firstly, the historical development and biomedical application of RP/M are reviewed. Secondly, the tool-path generation strategies are reviewed including the advantages and disadvantages of typical tool-path of zigzag and contour in RP/M and some novel space filling curves tool-path. Thirdly, slicing strategies included direct slicing, uniform slicing and adaptive slicing are reviewed. Fourthly, FGM-based model representation and fabrication process of RP/M are reviewed. Finally, the build time and geometric accuracy analysis and control modules of RP/M are reviewed. After reviewing such related works, it is desirable to develop an integrated adaptive systematic approach for tool-path generation, slicing and build time

and geometrical accuracy analysis and control of complex biomedical models fabrication in RP/M process.

Chapter 3 reports an adaptive tool-path generation algorithms and strategies of biomedical models in RP/M. Firstly, NURBS-based curves are introduced to represent the boundary contours of the sliced layers in RP/M to maintain the geometrical accuracy of original biomedical models. Secondly, a mixed tool-path generation algorithm is developed to generate contour tool-paths along the boundary and offset curves of each sliced layer to preserve geometrical accuracy, and zigzag tool-paths for the internal area of the layer to simplify computing processes and speed up fabrication. Thirdly, based on the developed build time and geometrical accuracy analysis models of tool-paths, adaptive algorithms is designed to generate an adaptive speed of the RP/M nozzle/print head for the contour tool-paths to address the geometrical characteristics of each layer, and to identify the best slope degree of the zigzag tool-paths towards achieving the minimum build time. Finally, four case studies of biomedical models are used to verify and demonstrate the improved performance of the developed approach in terms of processing effectiveness and geometrical accuracy.

Chapter 4 reports an adaptive slicing algorithms and strategies of biomedical models in RP/M. Firstly, rotating slicing and two thresholds are introduced to extract the surface feature of the biomedical model. Secondly, an adaptive slicing algorithm is developed to decide the thickness for each slicing layer based on the number of feature points that pass the two thresholds. Thirdly, geometrical accuracy and build time analysis modules of adaptive slicing are introduced to calculate and analyse the geometrical accuracy and build time during RP/M processing with different values of two pre-setting thresholds. Fourthly, geometrical accuracy and build time control strategy is used to control and optimise the geometrical accuracy and build time of fabrication of complex biomedical model in RP/M. Finally, some case studies of biomedical models are used to demonstrate and verify the performance of the adaptive slicing strategies and algorithms.

Chapter 5 reports the research on developing adaptive approach for FGM-based biomedical models. Firstly, a NURBS-based slicing algorithm is introduced to represent the geometrical boundary of each layer of a biomedical model, and FGM-based features are

designed to represent the model with control parameters on multiple material composition. Secondly, a tool-path generation algorithm is developed to generate tool-paths for different materials of the FGM-based model, and the developed adaptive algorithm is also used to optimise the build time and geometrical accuracy of fabrication. Finally, some case studies of FGM-based biomedical models are used to demonstrate the effectiveness and robustness of the developed approach.

Chapter 6 reports a systematic application of the developed adaptive approach for a biomedical talus bone model. Meanwhile, a concept designed multi-material RP/M fabrication system has been introduced.

Chapter 7 gives conclusions of this research and suggests recommendations for future work.

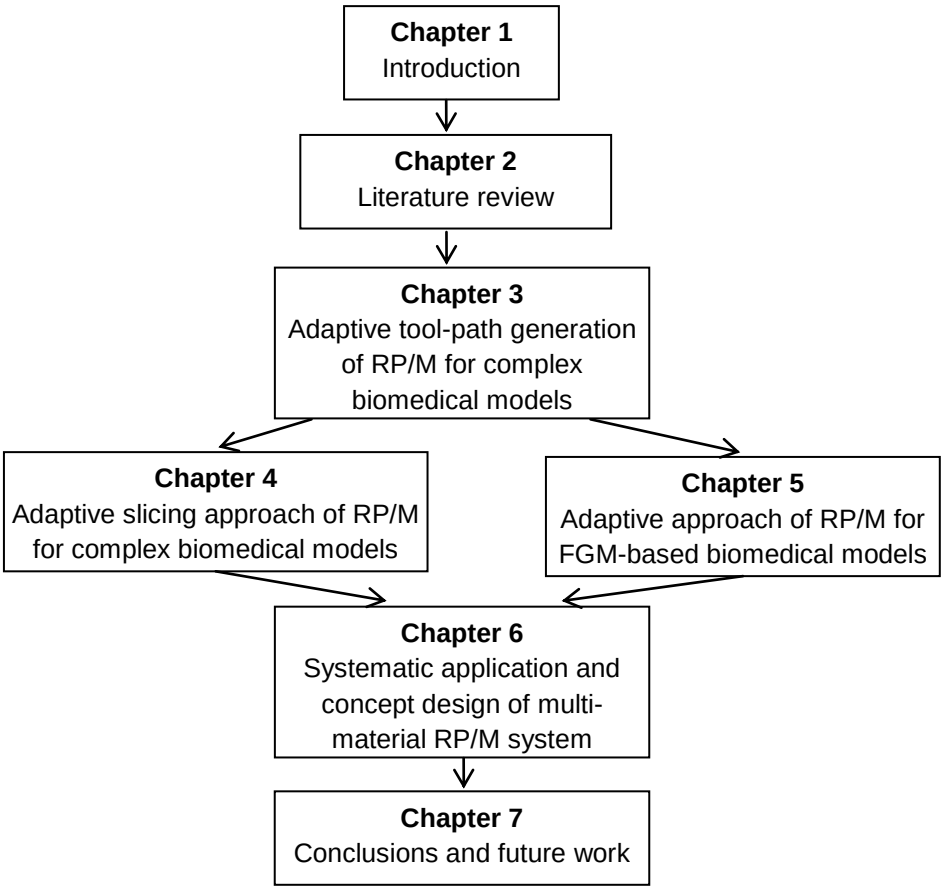


**Figure 1.6** Framework of dissertation organisation.

# CHAPTER 2
# LITERATURE REVIEW

## 2.1 Introduction

This chapter presents a review of RP/M technologies and its related work to this research. In section 2.2, the historical development and biomedical application of RP/M are reviewed. The RP/M tool-path generation strategies are reviewed and the strengths and weaknesses of each existing tool-path strategies are analysed in Section 2.3. In Section 2.4, existing slicing strategies include direct slicing, uniform slicing and adaptive slicing are reviewed, and the advantages and disadvantages are investigated and compared. FGM-based model representation and fabrication process of RP/M are reviewed in Section 2.5. The development of geometrical accuracy and build time analysis and control modules are reviewed in Section 2.6. Finally this chapter is summarised in Section 2.7.

## 2.2 Historical development and biomedical application of RP/M technology

### 2.2.1 Historical development of RP/M technology

The RP/M technology is an innovative manufacturing technology that has only about 25 years of history. In 1987, 3D Systems invented the world's first RP/M SLA system (Grimm, 2004). Since the commercialisation of the first RP/M machine by 3D systems in 1988, the RP/M industry has evolved and expanded continuously and several dozens of new RP/M processes appeared, such as SLS/SLM, LOM, FDM and 3DP. All of these RP/M processes are additive build process by adding materials, layer-by-layer, to build a 3D model from bottom to top along the fabrication direction. Based on the initial material used in each RP/M system, the technology can be generally categorised into three groups (Chua et al., 2005): (1) liquid based systems, (2) powder based systems, and (3) solid based systems (shown in Figure 2.1). The categorisation of the most existed RP/M systems is shown in Table 2.1.

**Table 2.1** Categorisation of RP/M Systems (Syed, 2011)

| *(1) Liquid Based Systems* | *(2)Solid Based Systems* | *(3) Powder Based Systems* |
|---|---|---|

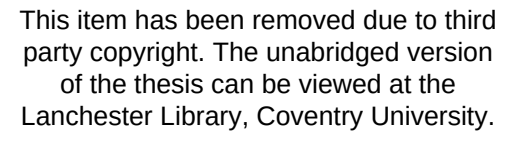


(a) Liquid materials

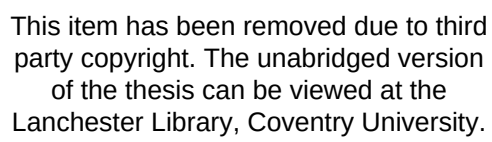


(b) Powder materials

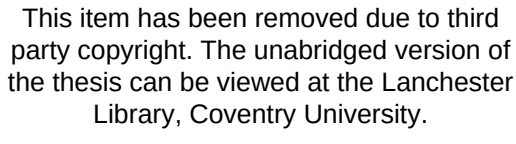


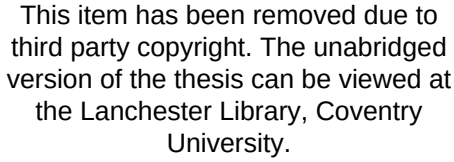


(c) Solid materials

**Figure 2.1** Different materials of RP/M systems (Chua et al., 2005).

**(1) Liquid based RP/M systems**

In liquid based RP/M systems, the liquid materials are the initial materials used to build 3D models through a process commonly known as curing convert into solid state. SLA is a classical liquid based RP/M system and most of available commercial SLA systems build 3D models from liquid photosensitive polymers that solidify when exposed to a Ultraviolet (UV) light. There are a large number of photopolymer resins available for SLA systems, which may contain fillers and other chemical modifiers to meet the desired physical and mechanical properties requirement. The SLA process is as follows (shown in Figure 2.2) (McDonald et al., 2001):

- Parts are built from a photo curable liquid resin that solidifies when sufficiently exposed to a laser beam which scans across the surface of the resin.
- The building is done layer by layer, each layer being scanned by the optical scanning system and controlled by an elevation mechanism, which lowers at the completion of each layer.



**Figure 2.2** SLA process (xpress3d, 2012).

**(2) Powder based RP/M systems**

In the powder based RP/M systems, there are many varying powder materials are available for powder based RP/M systems and the main types of powder materials used in RP/M are safe and non toxic, easy to use, and can be easily stored, recycled and disposed of such as polycarbonate, nylon, ceramics and metals. SLS system is a classical powder based RP/M process that was patented by the 3D Systems in 1989. It is a layered manufacturing method that creates solid, 3D objects by fusing powdered materials with a laser (shown in Figure 2.3). The process is shown as follows (Chua et al., 2005):

- A thin layer of powder material is laid down and the laser draws on the layer, sintering together the powder hit by the laser.

- After each layer is completed, the layer is then lowered and a new layer of powder is spread across the surface on top.
- This process is repeated layer by layer, until the powders are gradually bonded by the laser beam into a solid mass that forms the 3D model.
- In areas not sintered, the powders are loose and can be poured out of completed part.



**Figure 2.3** SLS process (martello, 2012).

**(3) Solid based RP/M systems**

Solid based RP/M systems are meant to encompass all forms of materials in the solid state. The solid form can include the shape in the form of wire, a roll, laminates and pallets. FDM is a classical solid based RP/M system that was first introduced by Stratasys in 1992. This process builds using wax, rigid plastic polymer, and elastomeric materials.

In the FDM process, two types of material are used in filament form, support material and build material. Both materials are fed into a FDM liquefier head where heating elements melt the material, which is then deposited through the nozzle in ultra thin layers, one layer at a time along tool-path. Material solidifies on cooling and the process continues by moving the FDM head to create next layer (shown in Figure 2.4) (Chua et al., 2005).

**Figure 2.4** FDM process (custompartnet, 2012).

In recent years, with the development of CAD design, modelling and control technology and the innovation of new materials of RP/M, the process of RP/M continues to grow in terms of both commercial and scholarly activities. The development of new process of RP/M for biomedical application is a hot topic in the current RP/M research field.

### 2.2.2 Biomedical application of RP/M technology

RP/M, as a new-generation manufacturing process, has opened a new horizon for design and manufacturing companies to develop new products with reduced design and production cost especially for low volume customised products (Wohlers, 2008). In the last few years, RP/M has been increasingly used in a large number of industrials such as biomedical, automotive, jewellery, aerospace and electronics, etc (shown in Figure 2.5).

**Figure 2.5** Applications of RP/M technologies (Bourell and Leu, 2009).

Biomedical models are usually characterised with highly customised and complex geometry. It is hard for the traditional manufacturing and machining processes such as CNC, casting, turning to be applied in this research field. Meanwhile, RP/M is a mould-less process, suitable for free-form and complex geometrical model realisation such as biomedical models. In recent years, the research to exploit the RP/M technology to support biomedical applications is becoming increasingly active. Many universities and research institutes, such as Carnegie Mellon University, Massachusetts Institute of Technology, the University of Texas, Drexel University, the University of Michagen, Loughborough University and so on, are exploring ways in which RP/M can be applied to medical implant design and manufacturing, tissue engineering, artificial organs and biomedical models and products, etc (Jackson, 2000; Jafari et al., 2000; Khalil et al., 2005; Weiss et al., 2005).

Biomedical modelling has a wide range of applications in anatomical representation, implant and prosthesis design, and surgical planning and rehearsal. With the RP/M process, a computer tomography image can be accurately reproduced in a few hours or days as a physical model, which can be handled by the surgeon, allowing a more intuitive understanding of the most complex 3D geometry used to plan and practise an operative procedure. On another hand, the RP/M process produces extremely detailed physical biomedical models that can serve as excellent templates for the creation of custom implants. A physical biomedical model made by RP/M from CT, MRI and CMMs data can be held, offering surgeons a direct, intuitive understanding of complex anatomical details which cannot be obtained from imaging on the screen. A precise physical model can also help determine implant size and type, and surgical planning and rehearsal (Bourell and Leu, 2009). In last few years, many implants have been fabricated by the RP/M process. For instance, the Walter Reed Army Medical Centre has produced 37 cranial implants using electron beam melting with a RP/M process from Arcam of Sweden (WRAMC, 2012). Meanwhile, companies in Italy have used RP/M to fabricate more than 10,000 metal hip implants, and most of them have been implanted into human beings (shown in Figure 2.6). In addition, RP/M fabricated biomedical models can be used to display local regions of interest, which may, for example, help a surgeon identify a tumor on the CT image and use it for disease diagnosis. Thus, RP/M technology offers the surgeon a tool that is not available anywhere else.

The RP/M technology has been successfully applied to fabrication of customised implants, prostheses, and biomedical models. However, owing to quickly developed healthcare markets with stronger requirements for more complex applications, it is becoming a strong desire to develop better algorithms and strategies in the RP/M process planning to reduce build time and improve geometrical accuracy so as to meet the high-quality design and functional requirements of complex biomedical models and products.

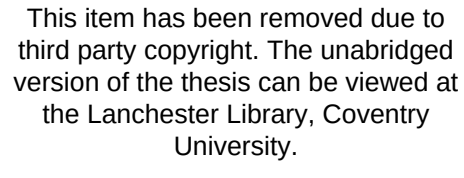


(a) Cranial implants

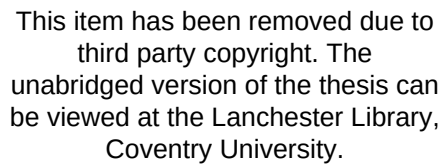


(b) Hip implants

**Figure 2.6** Human implants fabricated by RP/M process (worldmedassist, 2012).

## 2.3 Tool-path generation strategies

A tool-path is the trajectory of the nozzles/print head in a RP/M process to fill the boundary and interior of each sliced layer. It is an important factor that affects the geometrical quality, strength and stiffness of a building model, and efficiency of the RP/M process. There are various types of tool-path patterns developed for RP/M, such as zigzag, contour, spiral and some space filling curves (shown in Figure 2.7). A summary is shown in Table 2.2, and more explanations are given below.

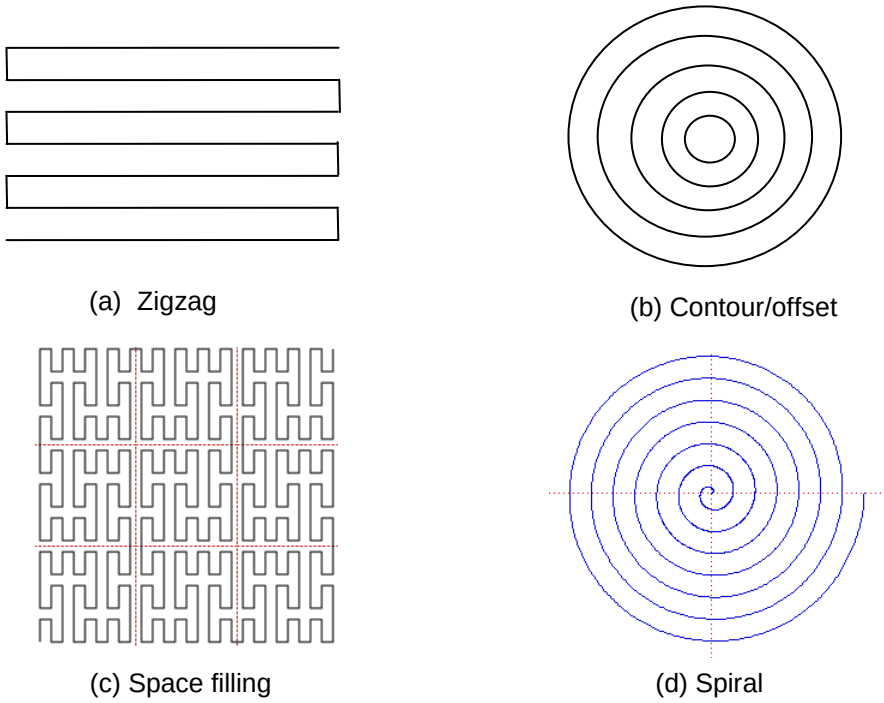


**Figure 2.7** Different tool-path types of RP/M.

**Table 2.2** A summary of RP/M tool-path generation.

| ***Works*** | ***Tool-path patterns*** | ***Major characteristics*** |
|---|---|---|
| Chang, 1997; Misra et al., 2005 | Zigzag | The approach fills a layer along the X, Y or a specific direction, and it is easy for approach implementation but poor on geometrical quality. |
| Genesan and Fadel, 1994; Yang et al., 2002 | Contour | The approach builds a layer along its contour and offset curves following the boundary of the model. It ensures good geometrical quality but takes longer during model build compared to the zigzag tool-path generation. |
| Bertoldi et al., 1998 | Recursive Hilbert's curve | More suitable for some regular boundaries and special geometric models. The build time will be longer than that of other conventional tool-path generation methods. |
| Lou et al., 2010 | Spiral | More suitable for some special geometrical models due to improved computation. |
| Chiu et al., 2006 | Fractal curve | It is only suitable for some special fractal models. |

The zigzag tool-path generation is the most typical method used in RP/M systems. It fills models line-by-line along the X or Y direction (Chang, 1997; Misra et al., 2005). This method is easy to implement, but it has the following drawbacks: (1) if a model for RP/M is complex or has some hollow structures inside, the tools such as the laser of SLS/SLM and the nozzle of FDM have to be turned frequently, leading to a poor building quality; (2) the model will have a warpage problem as the tool-path will be along the same direction to build the whole model. The contour tool-path generation, which is another typical method, can address the above geometrical quality issue effectively by following the geometrical trend of the boundary contours (Genesan and Fadel, 1994; Yang et al., 2002). Meanwhile, the method overcomes the warpage problem as the tool-path direction is changed constantly along the contour curves of sliced layers. However, when a boundary contour is irregular or has a hollow, island or ring structure such as biomedical models, the computation of the algorithms will be complicated. In a number of biomedical cases, the algorithms are unable to generate proper contour tool-paths.

Some space filling curves with pre-defined shapes were also been used for the tool-path generation in RP/M for some special purposes such as strength, stiffness and model bonding. Bertoldi et al. (1998) developed a fractal approach to generate Hilbert curve-based tool-paths for a FDM RP/M system. The method can reduce shrinkage during RP/M fabrication process but build time will be longer than that of traditional tool-path generation methods. The spiral tool-path generation was widely used in CNC machining, especially for Two-Dimensional (2D) pocket milling and uniform pocket cutting (Lou et al., 2010). It can also be applied to solve the problems of zigzag tool-paths in the FDM process, but be more suitable for some special geometrical models due to complex computation. Chiu et al. (2006) proposed a novel method to generate the tool-path of RP/M from the mathematical model of a fractal model. It first generates a slab grid in each layer that consists of a number of pixels, and then checks the interior property of each pixel in the slab grid to create the slab model of the fractal object. The boundary of slab model is refined and the tool-path of RP/M can be generated from these boundaries. However, these research works are only suitable for fractal models.

Based on the potentials of the above research in different conditions, it is expected to develop a smart and hybrid strategy to leverage the advantages of various tool-path generation strategies to be suitable for complex biomedical models in the RP/M processes.

## 2.4 Slicing strategies

### 2.4.1 Directly slicing and parametric representation

STL, which has been a widely adopted data standard in the RP/M industry, is an approximation representation scheme of product models based on triangles or quadrilaterals. However, there are some intrinsic problems in STL files such as gaps, holes, missing/degenerated/overlapping facets, etc. during the conversion process from native CAD files. Therefore, repairing algorithms of errors in STL files and simplification algorithms of STL files were developed (Nagy and Matyasi, 2003; Wang and Chang, 2008; Liu et al., 2009). On the other hand, STL is less inaccurate in geometrical representation and needs much more storage spaces for a complex model than parametric mathematical representation themes such as NURBS, Bezier, B-Spline, etc. Figure 2.8 shows a CAD and STL format model of human head. Figure 2.9 shows a NURBS curve with 6 control points. Recently, there are active research and development to introduce parametric mathematical representation to better support RP/M. A short summary of the previous work is given in Table 2.3, and the detailed discussions are expanded below.

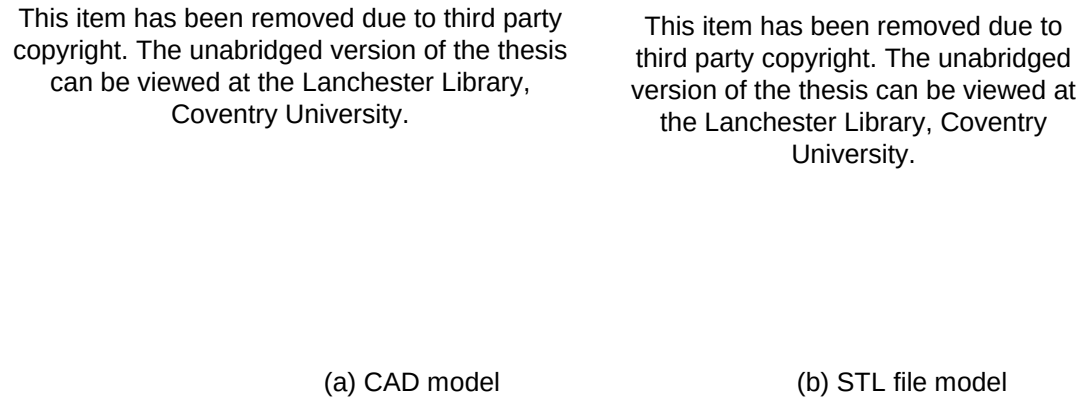


(a) CAD model (b) STL file model

**Figure 2.8** CAD and STL format model of human being (InstaTuts, 2012).

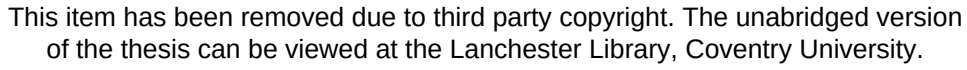


**Figure 2.9** A NURBS curve with 6 control points (TECHSOFT3D, 2012).

**Table 2.3** A summary of RP/M model representation.

| *Research* | *Original models* | *RP/M models* | *Major characteristics* |
|---|---|---|---|
| Chen et al., 2001; Shi et al., 2004 | PowerSHAPE models | Lines, arcs and Bezier curves for sliced contours | A macro-AutoSection software package was developed to collect sliced contour data and produce PIC files; Another software package PDSlice was devised to support the RP/M process. |
| Cao and Miyamoto, 2003 | AutoCAD models | Lines, arcs, circles for sliced contours | An ASCII DXF file was used to store sliced layer data. Material information can also be stored in this file. |
| Ma et al., 2004 | 3D CAD models | NURBS representation for sliced contours | A NURBS surface model was used to obtain more accurate and smoother surface for RP/M, and a selective hatching strategy was developed to further reduce build time and improve geometrical quality. |
| Starly et al., 2005 | 3D CAD models | STEP based NURBS-represented contours | A slicing algorithm was designed to determine the optimal direction, and an adaptive subdivision strategy was also applied for geometrical refinement. |

In Chen and Shi's approaches, arcs, lines and Bezier curves were used to describe the cross-sectional contour geometries of sliced layers (Chen et al., 2001; Shi et al., 2004). A macro-AutoSection software package was developed to collect the sliced contour data, and a software package, i.e., PDSlice, was devised to support the RP/M process for a commercial SLS machine called HRPD-III. Some prototypes were fabricated to demonstrate that the proposed mathematical representation improved the accuracy and quality of complex products compared to the STL format. Cao and Miyamoto (2003) developed an approach to use lines, arcs and circles to represent the sliced contours of an AutoCAD solid model in an ASCII DXF file. Material information such as material type can also be saved in this approach to support RP/M. Ma et al. (2004) used NURBS to represent a RP/M model so as to obtain more accurate and smoother surface, and applied a selective hatching strategy to further reduce build time and improve geometrical quality by fabricating the kernel region of the model using thicker sliced layers and the skin region of the model using thinner sliced layers. Starly et al. (2005) developed a slicing algorithm to represent a RP/M model as a STEP- and NURBS- represented model. The algorithm is comprised of five steps: (1) to determine the orientation of a model to minimise build height, (2) to define the NURBS surface of the model, (3) to generate a boundary volume data

structure, (4) to use a bi-sectional iteration routine method to solve the inter-sectional points, and (5) to categorize inter-sectional points to support an optimised RP/M process. Four models in different representation formats were used to validate the developed algorithm.

Some of the above research successfully adopted parametric representation such as Bezier, B-Spline and NURBS to improve the geometrical quality of RP/M models. However, a research gap exists between the parametric representation and the following process planning, and a smart solution is imperative to address the different geometrical characteristics of complex biomedical models in order to improve the build efficiency and geometrical accuracy of RP/M.

### 2.4.2 Adaptive slicing

Compared with uniform slicing, which the thickness between two consecutive layers is the same, adaptive slicing can better reduce the staircase effect and balance the build time and geometrical accuracy during RP/M processing (shown in Figure 2.10). For this reason, there are lots of adaptive slicing approaches have been developed in the past years. A short summary of the previous work is given in Table 2.4, and the detailed discussions are expanded below.

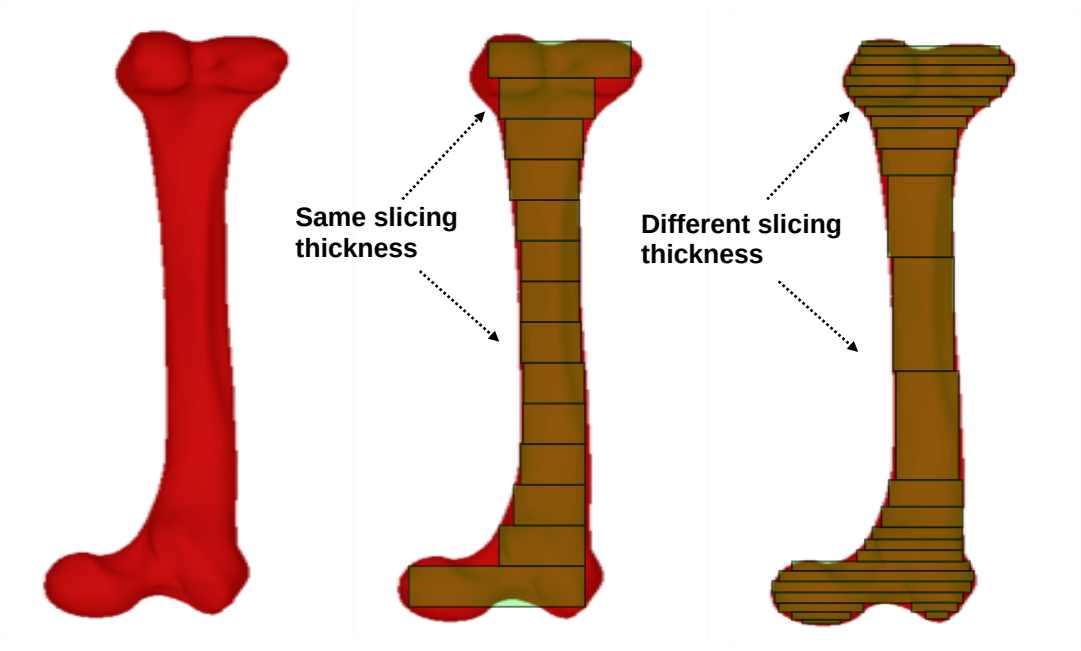


(a) A biomedical bone model (b) Uniform slicing (c) Adaptive slicing

**Figure 2.10** Different slicing strategies of RP/M.

**Table 2.4** A summary of the adaptive slicing works.

| Works | Slicing models | Major characteristics |
|---|---|---|
| Dolenc and Makela, 1994 | tessellated models | The layer thickness was computed based on the cusp height within the maximum allowable cusp height |
| Suh and Wozny, 1994 | non-polyhedral models | The layer thickness is calculated by approximating the part surface geometry using a sphere |
| Sabourin,1996 | STL models | Develop an adaptive high-precision exterior, high-speed interior slicing procedure |
| Zhao and Laperriere,2000 | AutoCAD B-rep model | The model firstly divided into corresponding blocks and then determined the layer thickness based on an allowable staircase tolerance |
| Yin, 2004 | Point cloud data | Build a bridge between scattered points and adaptive slicing |
| Liu et al., 2006 | Contour data from CCD camera | An NC milling machine and a CCD camera was used to capture the cross-sectional image of the model which was used to generated the contour data for directly adaptive slicing |

The concept of maximum allowable cusp height is widely used to determine the slice thickness. It was firstly introduced by Dolenc and Makela (1994). In their paper, the variable layer thickness was computed based on the cusp height within the maximum allowable cusp height. They also used the cusp height concept for evaluating the staircase effect and discussed adaptive slicing methods for dealing with peaks and flat areas of tessellated models. Based on the cusp height concept, Suh and Wozny (1994) addressed the adaptive slicing of non-polyhedral objects. They calculated the layer thickness of adaptive slicing by approximating the part surface geometry using a sphere. Sabourin (1996) proposed an adaptive slicing processing to obtain high-precision outside surface and high-speed inside of the model for RP/M fabrication. The model was first divided into the maximum available layer thickness parts. Then each maximum thickness part was further subdivided into much thin slicing thickness to satisfy the cusp height requirement. Zhao and Laperriere (2000) presented a method used to directly and adaptively slice a solid model in RP/M. The developed system reads into AutoCAD B-rep models, imports DXF files and SAT files, and then uses two stages to directly slice the models: (1) the features of the models are detected and the models are divided into corresponding blocks, and (2) the layer thickness of each block is optimised based on an allowable staircase tolerance.

Some methods have also been developed to integrating of Reverse Engineering (RE) and RP/M by directly slicing point cloud data from 3D measurement device (3MMs) to instead of CAD model. It reduces the product development time and short the overall time-to-market for new products. Yin (2004) developed a novel algorithm to build a bridge between scattered points and adaptive slicing for the integration of RE data and RP/M. It used four steps to carry out the work: (1) part digitization, (2) segmentation, (3) construction of NURBS or B-Spline surfaces, and (4) adaptive slicing. Liu et al. (2006) presented an approach to generated a RP/M slice file directly from the contour data. It used an CNC milling machine to mill the object that encased within resin. A Charge Coupled Device (CCD) camera was used to capture the cross-sectional image of the object. Based on the surface complexity of the contour images data, the slicing thickness and position were recommended for adaptive slicing in RP/M. The proposed approach combined the advantages of RE and RP/M for rapid reproduction of complex objects. However, it is not suitable for some expensive objects as it is a destructive approach.

Some of the above researches successfully adaptive slicing the STL model, or original CAD model and point cloud data model. However, most of them are rely on simple geometric product models, and a research gap still exists between adaptive slicing thickness determination, and analysis and control solution to balance the geometrical accuracy and build time for complex biomedical model in RP/M.

## 2.5 RP/M for FGM-based biomedical models

### 2.5.1 FGM-based product representation

In recent years, active research and development has been carried out to introduce new modelling and presentation methods for FGM-based products (shown in Figure 2.11). A short summary of the previous work is made below.

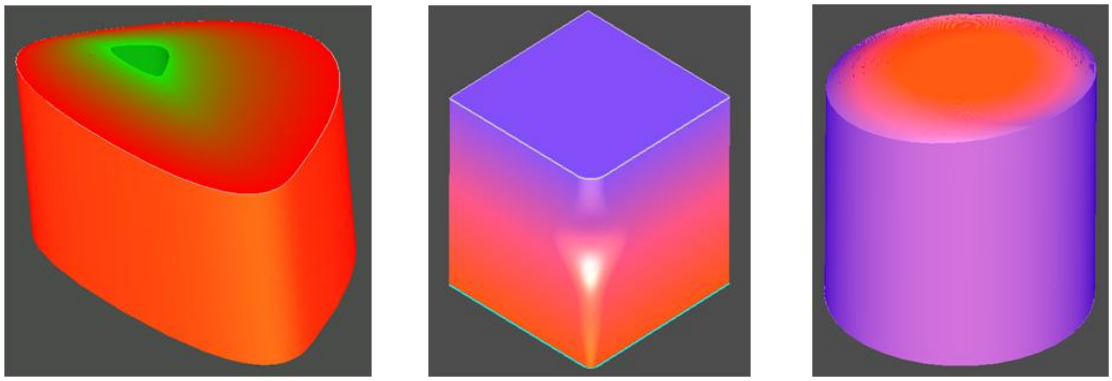

**Figure 2.11** Three examples of FGM-based model.

Parametric and feature-based FGM models with a local composition control were developed (Jackson et al., 1999; Liu, 2000; Liu et al., 2004). In the methods, design features were implemented to enable designers to specify geometrical and material composition features using an editable distance function. Nemat-Alla (2003) developed a 2D FGM design method with a target to withstand super high temperatures and to reduce the thermal and residual stresses. Multi-functional material criteria were summarised in

macro- and micro- levels to design FGM products (Das and Chung, 2006; Xia and Wang, 2008). The research was also extended to optimise FGM design in the aspects of strength, weight and mesoscopic structure. Chiu (2008) developed a multi-criteria decision-making process to decide the best arrangement of FGM compositions. An optimisation algorithm was introduced to fabricate FGM products using a RP/M machine. Computer-Aided Engineering (CAE) was triggered to evaluate and optimise the mechanical or thermal properties during the process. Samanta and Koc (2005) proposed a new feature-based method to model FGM products. Inter-relations between features that control material composition and attributes were established by constraining geometric and material features. Free-form B-Spline functions were used to represent the complex shapes of geometry and material features. Siu and Tan (2002) developed geometrical distance functions from Material 1 to Material 2 and so on as variables to control the material composition in FGM-based products. B-Spline or NURBS-based modelling algorithms were devised to represent complex FGM-based features and products (Qian and Dutta, 2003; Yang and Qian, 2007; Warkhedkar and Bhatt, 2009). In the researches, multiple materials can be diffused smoothly. The developed algorithms were applied to case studies such as turbine blade design, Micro Electromechanical System (MEMS) fabrication processes, biomedical prosthesis design, etc. (Kasaeian et al., 2011; Prakash et al., 2011; Zhu et al., 2011; Torshizian et al., 2011) applied finite element approach was applied to study wave propagation, thermal conductivity, large amplitude flexural vibration characteristics and internal crack problem of FGM plates. Kou et al. (2012) updated the recent status and advance of the FGM-based modelling methods.

Some of the above research adopted a parametric representation such as B-Spline and NURBS to represent FGM-based products. However, a research gap still exists between the FGM modelling and the process planning of RP/M. It is timely to develop a generic presentation method with extensibility and flexibility to support complex FGM-based products such as biomedical models for layer-based RP/M processing.

### 2.5.2 FGM-based RP/M fabrication process planning

**Table 2.5** RP/M methods and their characteristics for FGM objects fabrication.

| *Refs* | *Fabrication technology* | *Functionally Graded Materials* | *Process* | *Strength and Weakness* |
|---|---|---|---|---|
| Jackson et al., 1999 | Powder + Binder + 3-DP | Plaster powder + multiple binding fluids | Local Composition Control (LCC) is accompanied by a print-head with several jets, each depositing binders and/or slurries of a material. The material composition is on the scale of the binder droplets 100 μm. | Strength: Flexible in controlling of composition and porosity; Lower temperature involved; Lower cost and faster speed.<br>Weakness: Low mechanical strength. |
| Yakovlev et al., 2005 | Powder injection + Laser Melting | Stainless steel AISI 316L + Stellite grade 12 | Powders are injected on working zone by coaxial nozzles, controlled by CNC table, and then molten by 5KWatt Nd:YAG laser or CO2 laser. Layer thickness is 30-50 μm. | Strength: Good mechanical strength; Easy control of material composition.<br>Weakness: High temperature; Complex controlling system and shielding gas involved; Materials must be in powder form. |
| Hao et al., 2006 | Powder + Selective Laser Sintering | Hydroxyapatite (HAp) and polymer composites | HAp and polyethylene are incorporated into a FGM-based matrix for bone implants. The average size of internal pores is 60–68 μm with about 20% of the pores larger than 100 μm for bone regeneration. The laser is a 10Watt CO2. | Strength: Good porosity control; Good mechanical strength.<br>Weakness: High temperature; Complex controlling system; Materials must be in powder. |
| Han et al., 2002 | Filament + Fused Deposition Modeling | Ceramic + polymer composites | Ceramic and polymer materials are fused and deposited. The properties of the composites can be tailored by changing the connectivity of the phases.<br>Two piezoelectric test parts have been built to demonstrate the process. | Strength: Good control of composition and location of deposition.<br>Weakness: Complex controlling system; Lower mechanical strength. |
| Chua et al., 2004 | Powder + Selective Laser Sintering | Poly(vinyl alcohol) PVA + hydroxyapatite (HAp) | PLA and HAp are mixed and sintered by SLS RP to fabricate tissue scaffolds. Layer thickness is 50 μm. | Strength: Good control of composition; Good implementation of tissue scaffold.<br>Weakness: Expensive equipment; Difficult to remove the loose powder within pores. |

In recently years, RP/M has been one of the primary and flexible methods to fabricate FGM-based products. Kieback et al. (2003) surveyed the processing technologies for FGMs, including powder metallurgy, centrifugal casting, centrifugal casting, sedimentation casting, controlled mould filling, directional solidification, infiltration processing and reactive infiltration. Zhou (2004) reviewed various available RP/M technologies for FGM-based products fabrication, such as the 3DP, SLS, FDM and SLS. Chang summarised the RP/M technologies for biomedical products including FGM-based bio-products. Some developed RP/M technologies to fabricate FGM objects are compared in Table 2.5.

All of the above researches focused on developing some new mixed materials such as a ceramic and polymer mixed material and a PLA and HAp mixed material for RP/M systems to fabricate FGM objects, or design some key components of RP/M systems such as print-heads and injection nozzles to fabricate FGM objects. However, due to the continuously varying material composition in each sliced layer during RP/M processing, it is a quite time-consuming computational process in fabricating FGM-based objects. At the same time, the precision of the RP/M process is difficult to be managed and optimised. Therefore, it is vital to develop intelligent methods to optimise tool-path planning and multiple material planning in RP/M to minimise the lead time and expense of processing.

Shin (2002) proposed an algorithm to generate multiple tool-paths for FGMs and avoid redundant tool movements to enhance the processing efficiency. Another efficiency improvement algorithm was designed in (Choi and Cheung, 2006). FGMs were divided into some small homogenous sub-regions by the algorithm. After that, tool-paths and process parameters for each sub-region were created separately using optimised contour/raster path patterns. Chen (2007) developed a virtual machine for FGM objects, in which multiple material nozzles and three working subtractive stations for spreading, grinding/milling, and engraving were configured. In this designed virtual machine, some materials are removed using the grinding/milling operations apart from the additive processing of RP/M so that the machine is more flexible for complex products with stricter technical requirements such as surface smoothness and strength. In the machine, strategies of planning and optimizing each nozzle and machining tool were proposed. In the meantime, functional gradation is an important characteristic of human tissues, and FGM can mimic such gradation. As thus, there is an increasing need in tissue engineering

to adopt FGM and RP/M to process materials and relevant products. More details can be found in (Gupta et al., 2007; Ryan et al., 2008; Watanabe et al., 2011). Further research is imperative below:

- Majority of the developed RP/M tool-path generation strategies are based on zigzag. Smart and hybrid tool-path generation algorithms are expected to improve the geometrical accuracy of FGM-based biomedical models;
- The developed speed strategies for RP/M nozzles/print heads are mainly unified. Adaptive speed algorithms are desirable to optimise the build time of FGM-based biomedical models.

## 2.6 Build time and geometric accuracy analysis modelling

Build time and geometric accuracy are the important factors of the RP technology. There are a number of researches that have been done in this research field. A short summary of the previous work is given in Table 2.6, and the detailed discussions are expanded in below sections.

**Table 2.6** A summary of the RP/M build time and geometrical accuracy modules.

| *Works* | *Build time* | *Geometrical accuracy* | *Major characteristics* |
|---|---|---|---|
| Chen and Sullivan, 1996 | ○ | | To predict the build time of a SLS process with different laser powers, beam diameters and input cure depths. |
| Han et al., 2003 | ○ | | To calculate the build time for a FDM process by separating it as a deposition time and an idle time. A nozzle repositioning time and a cleaning time were also taken into account. |
| Wah et al., 2002 | ○ | | Two enhanced GA algorithms were used to reduce build time for non-fabrication motion of a RP/M system. |
| Castelino et al., 1999 | ○ | | An algorithm was developed for minimizing non-fabrication time by optimally connecting different tool-path segments. |
| Liu et al., 1998 | | ○ | To predict the geometrical errors of a RP/M process with profiling error, layer inclination and layer thickness variations. |
| Bacchewar et al., 2007 | | ○ | Surface roughness was studied based on a set of process parameters such as build orientation, laser power, layer thickness, beam speed, and hatch spacing for obtaining the best surface finish in a SLS process. |
| Armillotta, 2006 | | ○ | It analyzed the verification of surface quality with different texture dimensional parameters on textured surfaces of the model. |

### 2.6.1 Build time analysis modelling

As the build time is an important factor of the RP technology, some build time prediction modules and optimisation strategies have been developed in the past.

Chen and Sullivan (1996) made a detailed study of the laser scan mechanism of the SLS process, and based on the results of the measurement results of different scan patterns and cure depths, they developed some equations which can be used to predict the total build time and the resultant cure depth with different laser power, beam diameter and input cure depth of the SLS process. However, it only combines the total laser scan time and total recoating time to predict the whole build time. Information which affects the total build

time still needs to be added to further improve the predictor. Han et al (2003) presented a build time analysis model for a FDM process. In the proposed method, the total build time is separated as deposition time and idle time. Meanwhile, nozzle repositioning time and cleaning time are also taken into account in the analysis model. Some parameters which can be used to speed up the build time of FDM, including layer thickness, road width, table speed and repositioning distance and so on were identified. However, the research can only be suitable for some deposition-based RP processes.

Wah et al. (2002) introduced a Genetic Algorithm (GA)-based approach to reduce the build time of RP/M. A new strategy using a combination of the Asymmetric Travelling Salesman Problem and Integer Programming (TSP-IP) was developed. Based on these approaches, two enhanced GA formulations were deployed to reduce the time for non-fabrication motion of a RP/M system. Castelino et al. (1999) developed an algorithm for minimising the non-fabrication time by optimally connecting different tool-path segments. The non-fabrication time problem was first formulated as a standard TSP problem with precedence constraints, and then some heuristic methods were applied to solve this problem. However, the method is difficult to be applied for complex product models which include hollows and complex contours.

Based on the above reviews, it is expected to develop a more suitable and sensible build time analysis mathematical model to calculate the totally build time during the RP/M process of complex product models. Some adaptive strategies are also expected for further reducing the build time of RP/M process.

### 2.6.2 Geometric accuracy analysis modelling

The geometrical quality is another important factor in RP/M. Liu et al. (1998) studied the geometrical errors interaction and transferring mechanisms in RP/M process. A physical model was used to define the error interactions and transferring mechanisms. Based on the geometrical approximation techniques, a geometrical model was developed to describe the relationships of geometrical errors. A mathematical model was then developed to analyse the effect of transformation of local errors to multiple layer global

errors. However, the described geometrical errors only involve profiling error, layer inclination and layer thickness variations. Other elements that affect the geometrical accuracy of RP/M process should be added to further improve the mathematical analysis model. Bacchewar et al. (2007) studied the effect of process parameters on the surface roughness of SLS with the help of central rotatable composite design of experiments. Analysis of Variance (ANOVA) was used to study various surface roughness based on different build orientation, laser power, layer thickness, beam speed, and hatch spacing. A trust-region-based optimisation method was employed to obtain a set of process parameters for obtaining the best surface finish. Armillotta (2006) proposed an approach to assess surface quality on textured surface in a FDM system. A benchmark polygon model with different feature sizes and aspect ratios was fabricated in a FDM system with different build orientations. It analyzed the verification of surface quality with different texture dimensional parameters on textured surfaces of the model. However, the testing results are limited to a specific process.

Based on the above observations, innovative and adaptive strategies are imperative to develop more suitable and sensible geometrical accuracy and build time analysis and control modules to enable the user to balance the efficiency and geometrical accuracy of complex biomedical product model during RP/M processes.

## 2.7 Summary

This chapter has provided a comprehensive review of development of RP/M and its biomedical applications related to this project. The tool-path generation strategies, various slicing approaches, FGM-based model representation and fabrication process, and geometrical accuracy and build time analysis modules have also been reviewed and discussed in this chapter.

It can be seen from the above review that different RP/M processes have been widely used in biomedical applications. However, there are some new issues that have hindered the further proliferation of the RP/M technology, particularly on software for process planning of biomedical models. Some researchers have made important contributions to

develop suitable process planning for biomedical model applications. However, the proposed approaches could only deal with simple biomedical models and required huge build time for complex biomedical objects. Besides, the geometrical errors inherent from the layer-by-layer and additive forming mechanism of RP/M have brought challenges on achieving high geometrical accuracy of biomedical models.

Tool-path generation and slicing strategies are two key tasks of process planning for RP/M technology. However, few researchers have attracted to study some issues relating to adaptive tool-path generation, adaptive slicing and related build time and geometrical accuracy analysis modules to reduce the build time and improve the geometrical accuracy of biomedical models fabrication in RP/M. It is expected to develop some adaptive process planning for reducing build time and improve geometrical accuracy of RP/M. Meanwhile, more suitable and sensible build time and geometrical accuracy analysis and control modules are also expected to calculate and optimise the build time and geometrical accuracy during the RP/M process of complex product models. The following chapters will present the proposed adaptive process planning approach to reduce the build time and improve geometrical accuracy for biomedical models in RP/M in detail.

# CHAPTER 3
# ADAPTIVE TOOL-PATH GENERATION OF RP/M FOR COMPLEX BIOMEDICAL MODELS

## 3.1 Introduction

A tool-path is the trajectory of the nozzle/print head in a RP/M process to fill the boundary and interior areas of each sliced layer. Various types of tool-path strategies and algorithms such as zigzag, contour, spiral and partition patterns have been developed with different considerations on the build time, cost, geometrical quality, warpage, shrinkage, strength and stiffness of a RP/M model (Genesan and Fadel, 1994; Genesan and Fadel, 1994; Chang, 1997; Bertolodi et al., 1998; Yang et al., 2002; Misra et al., 2005; Chiu et al., 2006; Luo et al., 2010).

As reviewed in Chapter 2, the zigzag tool-path is the most typical method used in RP/M systems recently. However, as biomedical model is generally complex or has hollow structures inside, the nozzle/print head have to be turned frequently, leading to a poor build quality. In addition, the biomedical model will have a warpage problem as the zigzag tool-path along the same direction to build the whole biomedical model. The contour tool-path is another typical tool-path in RP/M which can address the geometrical quality issue of zigzag tool-path effectively by following the geometrical trend of the boundary contours. Meanwhile, the contour tool-path overcomes the warpage problem as the tool-path direction is changed constantly along the contour curves of sliced layers. However, when a boundary contour is irregular or has a hollow or complex structure such as biomedical models, the computation of the contour tool-path algorithm will be complicated and always has island problem, which means the inside areas (i.e., islands) could not be fully filled by the contour tool-paths and therefore these areas in the layer will be left without material filling. In a number of biomedical cases, the contour tool-path algorithm is unable to generate proper contour tool-paths.

This chapter presents the details of the proposed adaptive mixed tool-path generation algorithms and strategies to combine the advantages of the zigzag and contour tool-paths for nozzle/print head speed to adapt to the various geometrical properties of complex biomedical models in RP/M, based on the developed build time and geometrical accuracy analysis modules.

Firstly, NURBS-based curves are introduced to represent the boundary contours of the sliced layers in RP/M to maintain the geometrical accuracy of original biomedical models. Secondly, a mixed tool-path generation algorithm is then developed to generate contour tool-paths along the boundary and offset curves of each sliced layer to preserve geometrical accuracy, and zigzag tool-paths for the internal area of the layer to simplify computing processes and speed up fabrication. Thirdly, based on the developed build time and geometrical accuracy analysis models of tool-paths, adaptive algorithms is designed to generate an adaptive speed of the RP/M nozzle/print head for the contour tool-paths to address the geometrical characteristics of each layer, and to identify the best slope degree of the zigzag tool-paths towards achieving the minimum build time. Finally, four case studies of biomedical models are used to verify and demonstrate the improved performance of the approach in terms of processing effectiveness and geometrical accuracy.

## 3.2 The developed adaptive tool-path generation approach for biomedical models in RP/M

The overview of the developed tool-path generation algorithms and strategies is presented as follows:

1. A slicing algorithm was developed to represent the boundary contour of each sliced layer as a closed NURBS curve to maintain the representation accuracy of an original biomedical model;
2. A mixed tool-path algorithm was developed to generate contour and zigzag tool-paths to meet both the geometrical accuracy and build efficiency requirements. The contour tool-paths are used to fabricate the area along the boundary of each sliced layer to

improve the geometrical quality of a product model. The zigzag tool-paths are used to fabricate the interior area of the model to improve the efficiency;

3. Build time and geometrical accuracy analysis models for contour and zigzag tool-paths were formulated. Based on the models, two adaptive algorithms were designed to address the different geometrical characteristics of a product model and to achieve minimum build time. They include an algorithm to optimise the speed of the RP/M nozzle/print head along the contour tool-paths, and an algorithm to obtain the best slope degree of the RP/M nozzle/print head along the zigzag tool-paths.

The developed algorithms in the RP/M process planning are shown in Figure. 3.1. The flowchart of the algorithms, which is detailed in Figure 3.2, consists of three phases:

Phase 1: The slicing process and NURBS-based contour curve representation

Phase 2: The contour tool-path generation and adaptive speed algorithm of the RP/M nozzle/print head along the contour tool-paths

Phase 3: The zigzag tool-path generation and adaptive speed algorithm of the RP/M nozzle/print head along the zigzag tool-paths

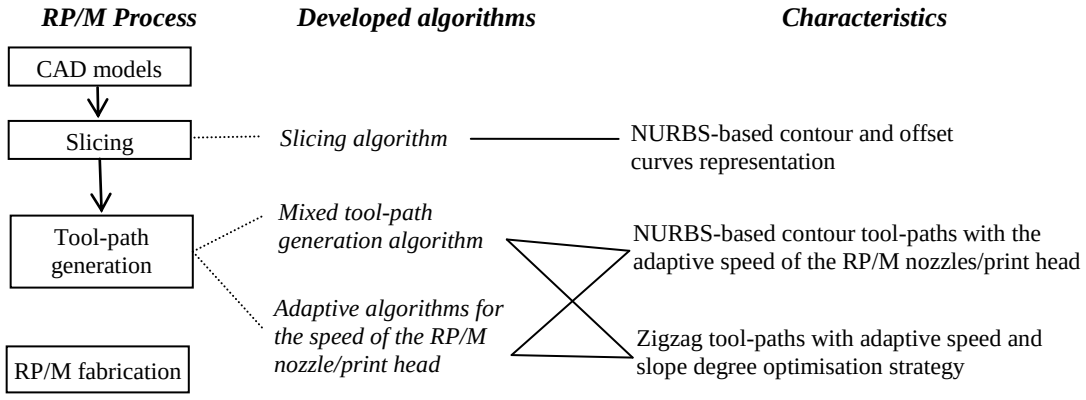


**Figure 3.1** Adaptive algorithms for RP/M process planning.

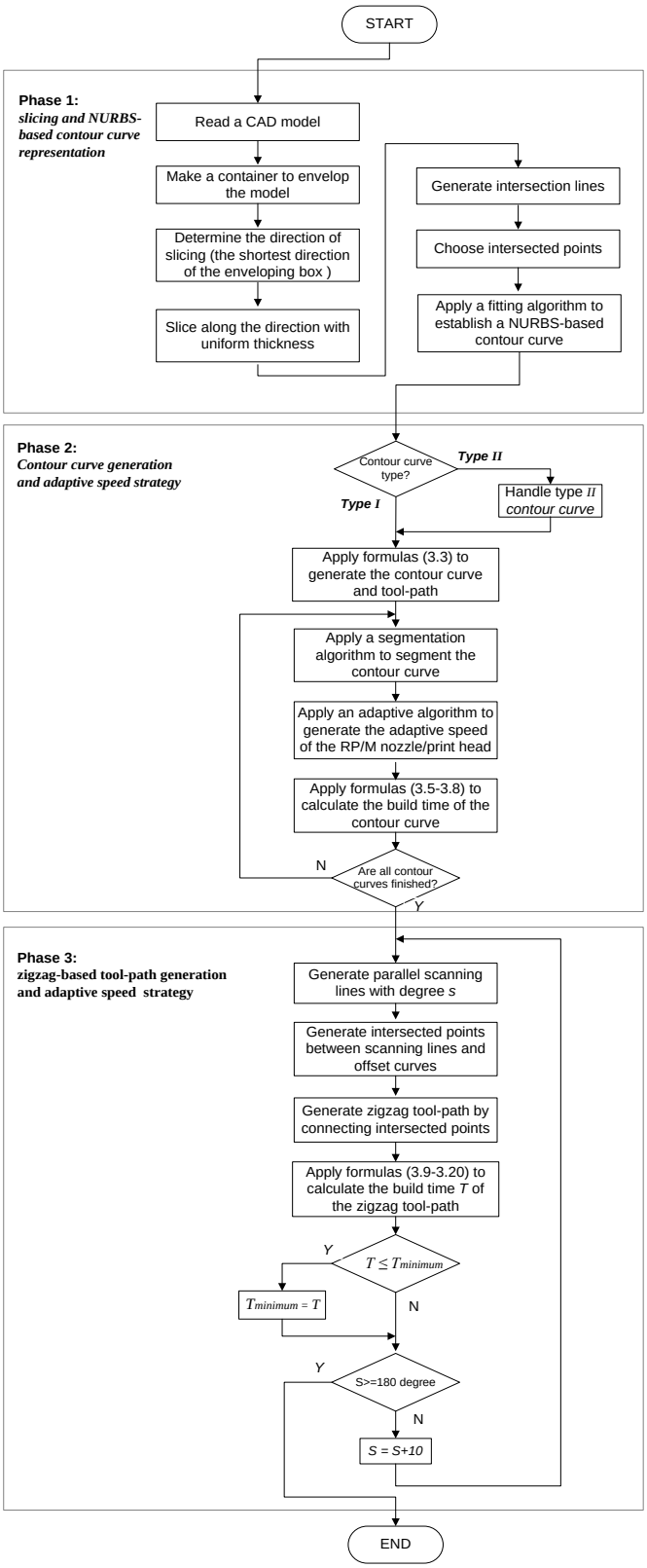


**Figure 3.2** The flowchart of the developed approach.

### 3.2.1 Phase 1 – Directly slicing and NURBS-based contour curve representation

The cloud data from a biomedical model is reconstructed as an Initial Graphics Exchange Specification (IGES) model using the Quick Surface Reconstruction (QSR) and Digitized Shape Editor (DSE) modules in CATIA V5™. The reconstructed model is then read into the developed software platform, which was developed based on the C++ programming language in an open-source CAD kernel system - the Open CASCADE (Open CASCADE, 2012). In the process, a container is created to envelop the model, and the shortest edge of the enveloping box is determined as the orientation direction (Z-axis) to minimize the build time. A series of sliced layers perpendicular to the orientation direction are set. The NURBS-based curve representation is introduced to model the geometrical contour between a sliced layer and the model. In Figure 3.3, a biomedical tibia model is used to illustrate the above process.

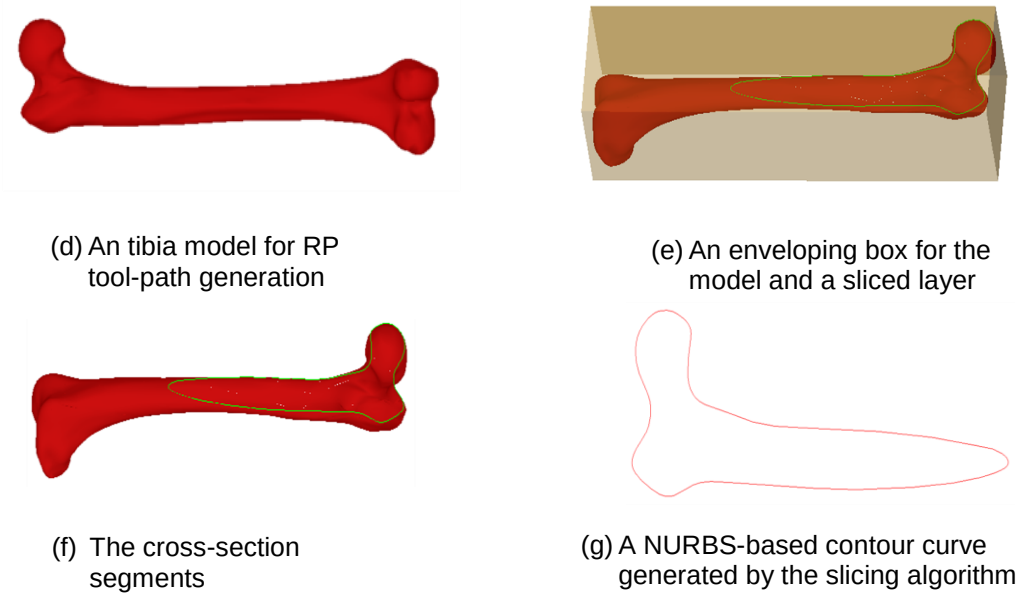

(d) An tibia model for RP tool-path generation

(e) An enveloping box for the model and a sliced layer

(f) The cross-section segments

(g) A NURBS-based contour curve generated by the slicing algorithm

**Figure 3.3** An example to illustrate the developed approach.

In order to establish the NURBS-based contour curve on the boundary between a sliced layer and the model (the boundary will be represented as $C^{i,1}$ in the following), a fitting

algorithm based on the intersected points between the sliced layer and the model is used here (Ma and Hewitt, 2003). A flow of the algorithm is shown in Figure 3.4.

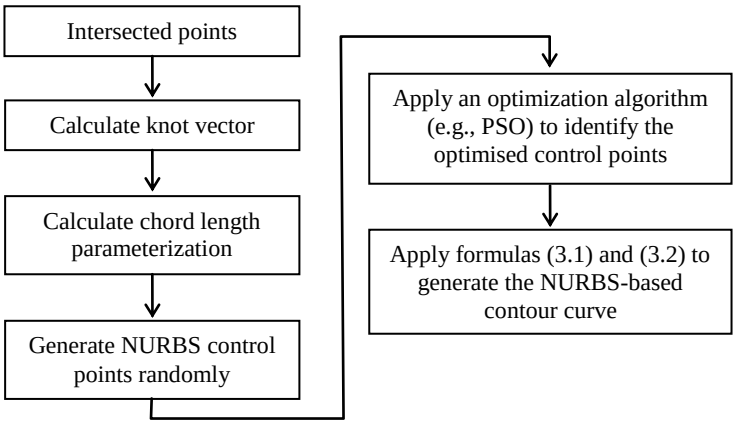


**Figure 3.4** The flow of generating a NURBS-based contour curve of a sliced layer.

A general form of a NURBS-based contour curve is represented below.

$$C^{i,j}(u) = \sum_{i=0}^{n} w_i N_{i,p}(u) C\_P^{i,j} \tag{3.1}$$

where $C^{i,j}$ represents the $j^{th}$ contour curve on the $i^{th}$ RP/M layer; $u$ is the parametric variable ($u = [0,1]$; $w_i$ is the weight associated with control points; $C\_P^{i,j}$ is the control point; $p$ is degree; and

$$N_{i,0}(u) = \begin{cases} 1 & u_i \le u \le u_{i+1} \\ 0 & otherwise \end{cases}, \text{ and } N_{i,p}(u) = \frac{u - u_i}{u_{i+p} - u_i} N_{i,p-1}(u) + \frac{u_{i+p+1} - u}{u_{i+p+1} - u_{i+1}} N_{i+1,p-1}(u) \tag{3.2}$$

The generated contour curves can be further classified into two types defined as follows:

[*Definition 1*] A control point $C\_P^{k+1,1}$ and its two neighbour control points $C\_P^{k,1}$ and $C\_P^{k+2,1}$ form a triangle. Choose a random point $P$ on the boundary or inside of the triangle, and draw a line to pass it. If the line only has two intersected points with the box formed by all the control points (the grey area in Figure 6), and $P$ is between the two intersected points, the control

point $C\_P^{k+1,1}$ is defined as convex; Otherwise, the control point $C\_P^{k+1,1}$ is concave.

[*Definition 2*] If all the control points of a NURBS-based contour curve are convex, the curve is defined as a *Type I* contour curve. Otherwise, the curve is a *Type II* contour curve.

Two examples for a *Type I* contour curve and a *Type II* contour curve respectively are illustrated in Figure 3.5.

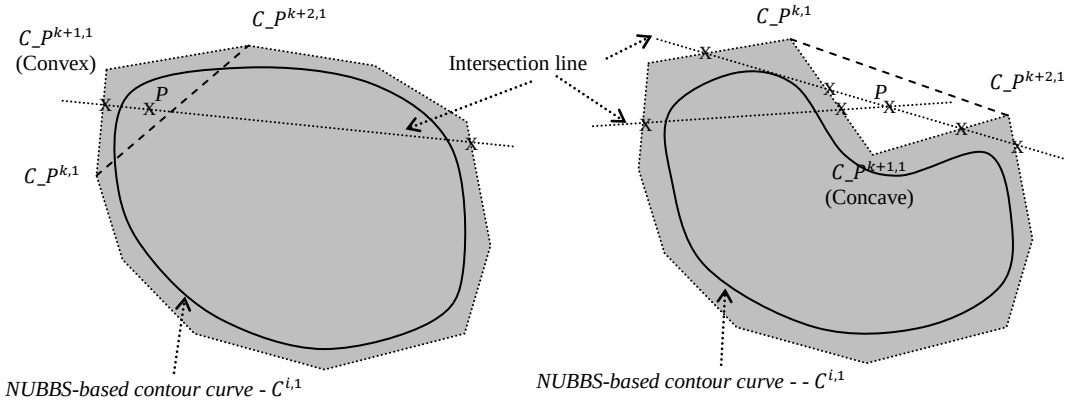


**Figure 3.5** Examples of two types of contour curves.

### 3.2.2 Phase 2 - Offset curve generation and an adaptive speed algorithm along the contour tool-paths

#### 3.2.2.1 Offset curve generation for a Type I or Type II contour curve

***Type I contour curve***

Based on the central point of the control points of the above generated contour curve, each control point for a new NURBS-based curve that offsets the contour curve (i.e., offset contour curve) is computed in the following.

$$C\_P^{k,j} = D + \alpha \cdot (C\_P^{k,1} - D) \tag{3.3}$$

where $C\_P^{i,j}$ represents an offset contour curve in the $i^{th}$ layer; *D* represents the geometric central point of the control points of the contour curve; $\alpha$ is the ratio to generate the new control points of the offset contour curve (e.g., $\alpha$ is set 0.9 in the following example). It is determined by the diameter of the RP/M nozzles/print head and the overlapping rate between two neighbor tool-path lines.

For example, in Figure 3.6, a new control point $C\_P^{k,j}$ of an offset contour curve is computed as follows.

$x\left(C\_P^{k,j}\right) = x(D) + 0.9(x(C\_P^{k,1}) - x(D))$, and

$y\left(C\_P^{k,j}\right) = y(D) + 0.9(y(C\_P^{k,1}) - y(D))$.

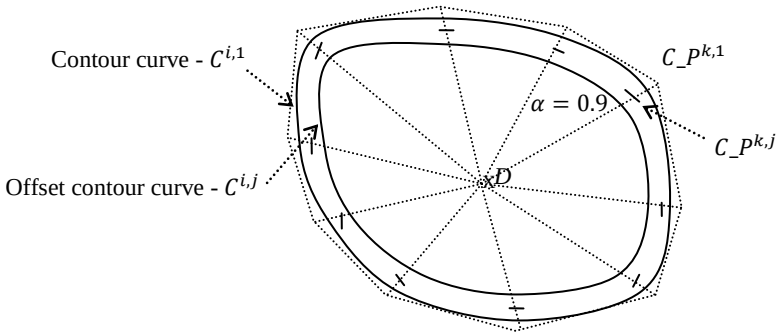


**Figure 3.6** An example for computing the new control points of an offset contour curve.

***Type II contour curve***

Self-intersection could happen if an offset curve for a Type II contour curve is generated by the above procedure. In order to address the issue, the following procedure is adopted.

Each concave point in the box of the control points of a *Type II* contour curve will be connected with another control point in the box to separate the box as two or more control point boxes, in which each control point is convex. An example is shown in Figure 3.7 In each box, new control points for offset contour curves are generated using the above Formula (3.3), and all the control points in a control point box are then used to generate an offset contour curve.

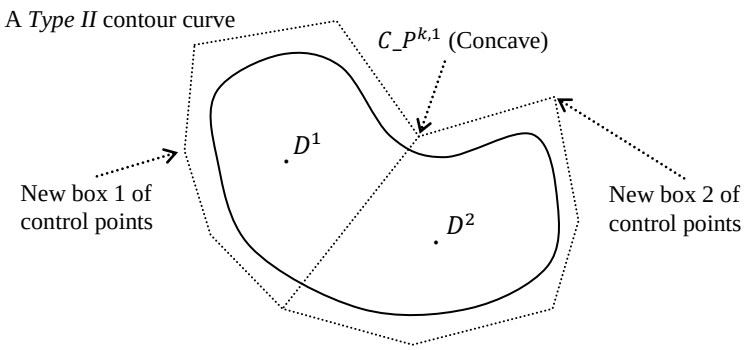


**Figure 3.7** An example for handling a *Type II* contour.

With a series of $\alpha$ for each segmented curve, the control points of offset contour curves and relevant offset contour curves can be generated using Formula (3.3). Figure 3.8 shows the generated contour and offset tool-paths for the tibia model. Along the contour curve and its series of offset contour curves, NURBS-based contour tool-paths can be interpolated.

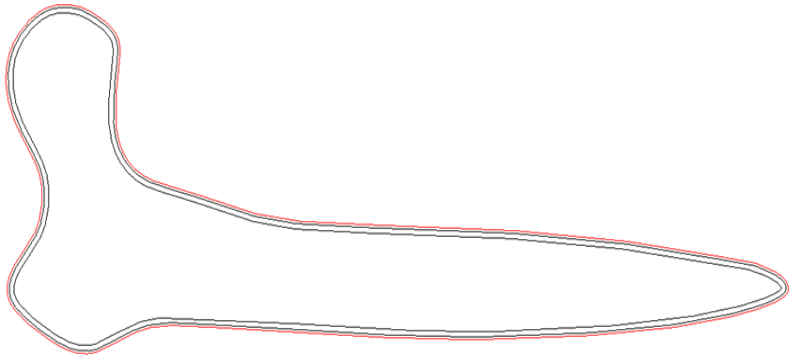

**Figure 3.8** Contour and offset tool-paths generated for the tibia model.

### 3.2.2.2 Adaptive speed algorithm of the RP/M nozzle/print head along the contour tool-paths

In order to further optimise the build time, a contour or offset curve on a sliced layer is segmented according to its geometrical characteristics. For example, the segmented points in Figure 3.9(a) are used to divide the curve as bumpy and smooth segments. According to the smoothness of a segment, an adaptive algorithm is applied to slow down the speed of the RP/M nozzle/print head in the bumpy segments while keeping a higher speed in the smooth segments. With the mechanism, the forming quality can be ensured and the build time can be further minimized. The flow of the segmentation and adaptive algorithm of the RP/M nozzle/print head is shown in Figure 3.10. Explanations are expanded below.

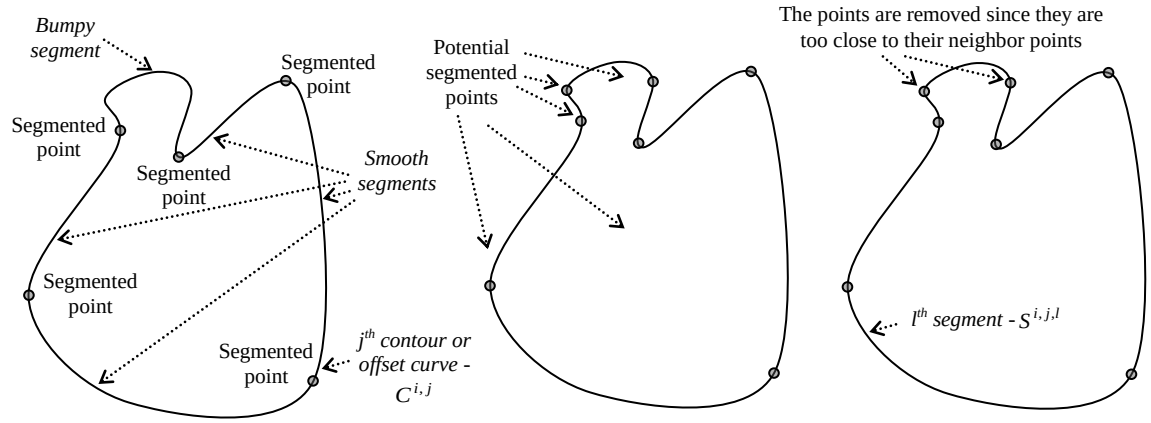


*(a) An example of segmentation (b) Potential segmented points (c) Some removed points*

**Figure 3.9** Example to illustrate the segmentation process for the adaptive speed algorithm.

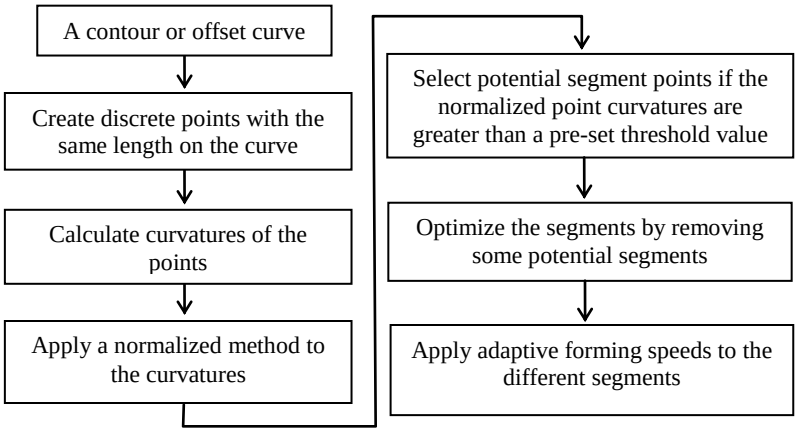


**Figure 3.10** The flow of the segmentation and adaptive speed algorithm.

A series of discrete points with the same length along a contour or offset curve are set. The curvatures of the points are normalized according to the following formula:

$$Normalization(P^t) = \frac{P^t_{curvature} - Min_{curvature}}{Max_{curvature} - Min_{curvature}} \quad (3.4)$$

where $P^t_{curvature}$ represents the curvature of Point $t$ on the curve; $Min_{curvature}$ and $Max_{curvature}$ stand for the minimum and maximum curvatures of all the points.

A threshold is set to filter out the discrete points with low curvatures, and the discrete points passing the threshold are kept as potential segmented points (see the example in Figure 3.9(b)). Another threshold is set to remove those potential segmented points which distance from their neighbor potential segmented points are within this threshold (see the example in Figure 3.9(c)). Based on the segmentation process, the build time of the tool-paths on each contour or offset curve can be defined below.

$$Time(C^{i,j}) = \sum_{l=1}^{m}(Time(S^{i,j,l})) \quad (3.5)$$

where *Time* represents build time; $C^{i,j}$ represents the $j^{th}$ contour or offset curve on the $i^{th}$ layer (a set of tool-paths will be generated along each curve); $S^{i,j,l}$ represents the $l^{th}$ segment in $C^{i,j}$; $m$ is the total number of the segments in $C^{i,j}$.

$Time(S^{i,j,l})$ is further computed in the following. An adaptive speed algorithm for the RP/M nozzle/print head along the tool-paths was developed. An example shown in Figure 3.11 is used to illustrate the concepts in the algorithm and the computation of $Time(S^{i,j,l})$.

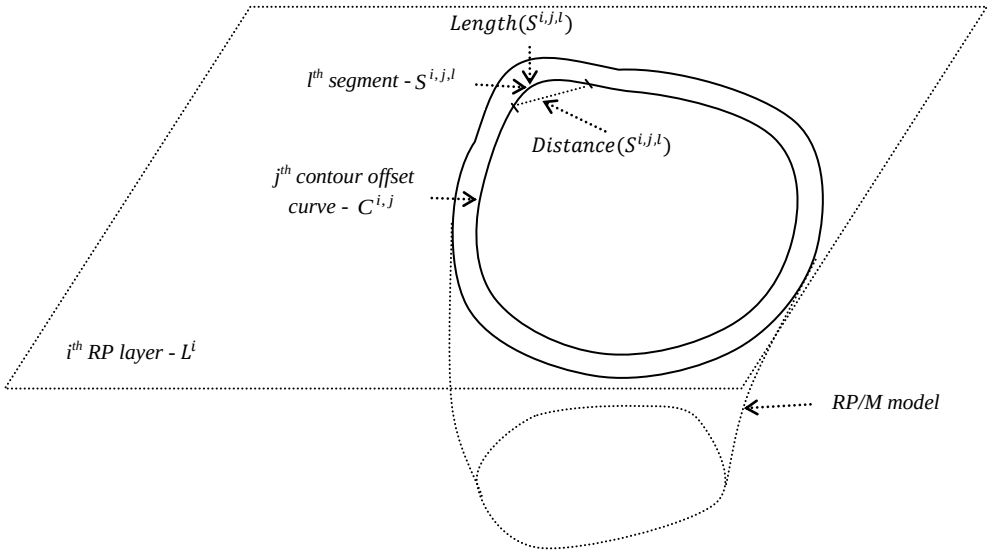


**Figure 3.11** Illustration of the concepts in the contour based curve adaptive speed strategy.

The speed of the RP/M nozzle/print head along a contour-based tool-path can be defined below.

$$V^{i,j,l} = \frac{Distance(S^{i,j,l})}{Length(S^{i,j,l})} \cdot V \tag{3.6}$$

where $V^{i,j,l}$ represents the speed of the RP/M nozzle/print head on the segment $S^{i,j,l}$; $Length(S^{i,j,l})$ represents the curve length of the segment; $Distance(S^{i,j,l})$ represents the straight line length from the start point to the end point of the segment; $V$ is a standard reference speed.

The build time spent on the segment $S^{i,j,l}$ is then computed as the following.

$$Time\left(S^{i,j,l}\right) = \frac{Length(S^{i,j,l})}{V^{i,j,l}} = \frac{(Length(S^{i,j,l}))^2}{Distance(S^{i,j,l})} \cdot \frac{1}{V} \tag{3.7}$$

In the end, the RP/M build time for contour tool-paths based on the boundary of the $i^{th}$ RP/M layer is calculated below:

$$Time(L^i) = \sum_{j=1}^{n} Time(C^{i,j}) \quad (3.8)$$

where *Time* represents build time; $L^i$ represents the $i^{th}$ sliced layer; $C^{i,j}$ represents the $j^{th}$ contour or offset curve on the $i^{th}$ layer (a set of tool-paths will be generated along each curve); $n$ is the total number of the contour and offset curves on the $i^{th}$ layer.

### 3.2.3 Phase 3 - Zigzag-based tool-path generation and adaptive algorithm along the zigzag tool-paths

Once the contour or offset curves and related tool-paths have been generated, zigzag lines and tool-paths will be then generated to fabricate the internal area of the model. The slope of the zigzag lines are first chosen randomly and the overlapping rate between two neighbour zigzag lines can be decided by users (e.g., 50% step-over). In zigzag, there are two types of lines.

[*Definition 3*] A *Type I* zigzag line forms the main tool-paths, and a *Type II* zigzag is the connection line between two neighbouring *Type I* lines.

An example of the two type lines are shown in Figure 3.12.

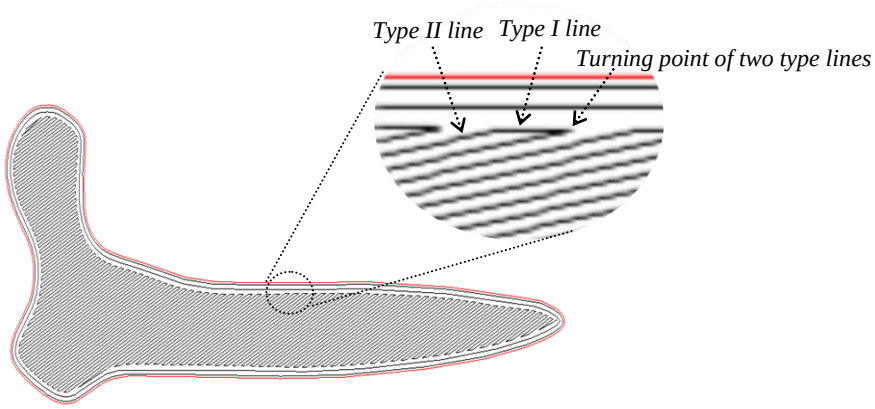


**Figure 3.12** Two type lines in zigzag tool-paths.

An adaptive algorithm developed for the zigzag tool-path generation is the optimisation process of the slope degree of the tool-paths (i.e., the direction of the *Type I* zigzag line). The optimisation objective can be modelled as:

$$Min(\sum_{i=1}^{n} Time(L_I^i) + \sum_{j=1}^{m} Time(L_{II}^j)) \quad (3.9)$$

where $L_I^i$ is the $i^{th}$ of the *Type I* line ($n$ is the total number of the *Type I* lines); $L_{II}^j$ is the $j^{th}$ of the *Type II* line ($m$ is the total number of the *Type II* lines); $Time$ is the build time function of both types of lines.

The variable for the optimisation objective is the slope of the zigzag direction (i.e., the direction of the *Type I* zigzag line), which can be rotated in a scope of $[0^{\circ}, 180^{\circ}]$. In the example of Figure 3.13, the slope degree can be incrementally changed, and the minimum build time can be obtained through the comparison of the computation results for all the degrees.

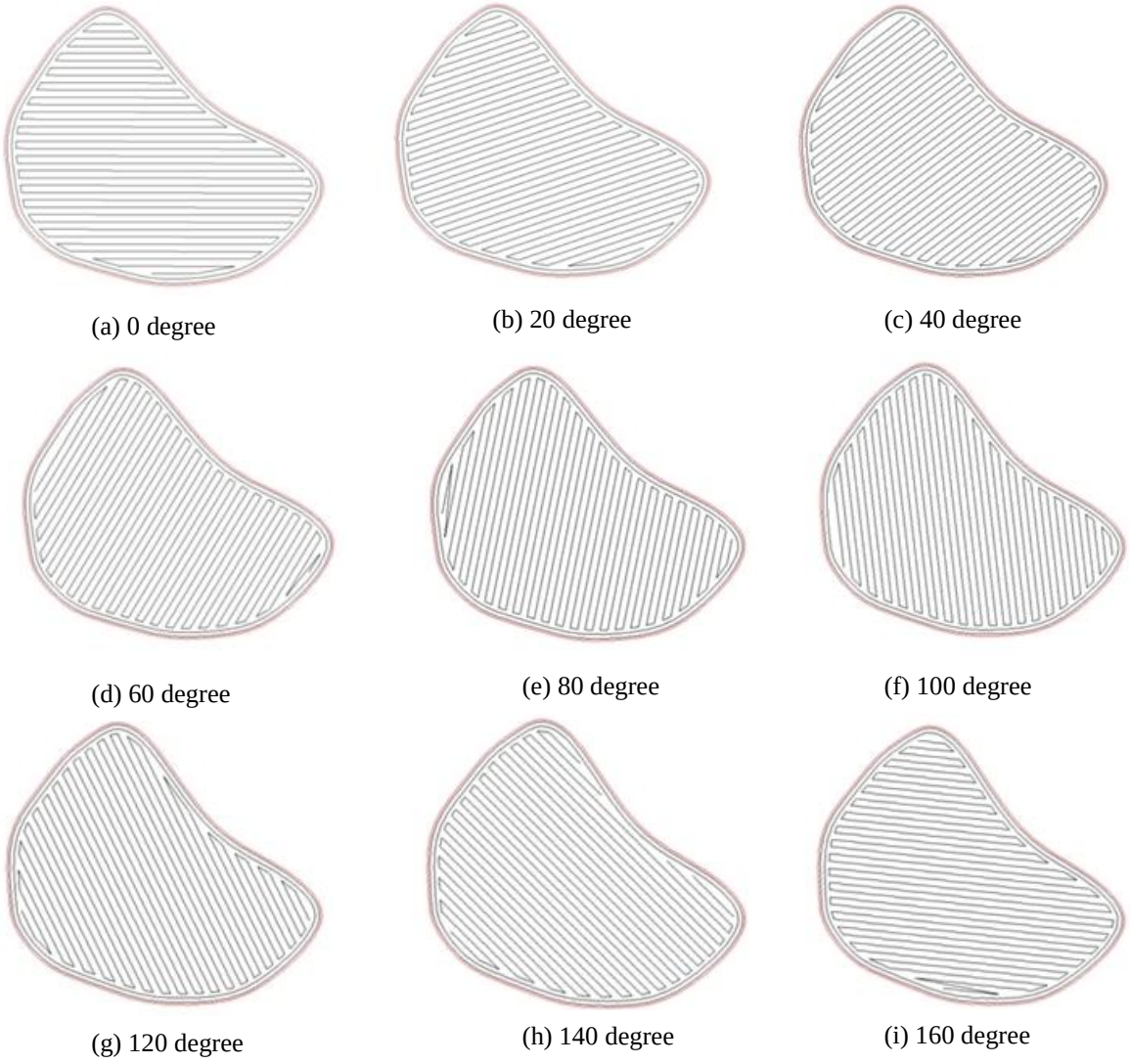

(a) 0 degree (b) 20 degree (c) 40 degree

(d) 60 degree (e) 80 degree (f) 100 degree

(g) 120 degree (h) 140 degree (i) 160 degree

**Figure 3.13** Incremental degrees of slopes for the minimum build time computing.

Each *Type I* or *Type II* line consists of a number of segments. The build time of these segments can be calculated in the following process:

$$Time\left(L_I^i\right) = \sum_{k=1}^{n} Time(S_I^{i,k}) \quad (3.10)$$

$$Time\left(L_{II}^j\right) = \sum_{k=1}^{m} Time(S_{II}^{j,k}) \quad (3.11)$$

where *Time* is the build time function; $L_I^i$ represents the *i*$^{th}$ *Type I* line, and $S_I^{i,k}$ represents the *k*$^{th}$ segment in the line ($n$ is the total number of the segment in the line); $L_{II}^j$ represents the *j*$^{th}$ *Type II* line, and $S_{II}^{j,k}$ represents the *k*$^{th}$ segment in the line ($m$ is the total number of the segment in the line).

In the following, $Time(S_I^{i,k})$ and $Time(S_{II}^{j,k})$ are computed further:

$$Time\left(S_I^{i,k}\right) = \frac{Length(S_I^{i,k})}{Velocity(S_I^{i,k})} \tag{3.12}$$

$$Time\left(S_{II}^{j,k}\right) = \frac{Length(S_{II}^{j,k})}{Velocity(S_{II}^{j,k})} \tag{3.13}$$

where *Length* is the length function; *Velocity* is the speed function of the RP/M nozzles/print heads along the tool-paths.

An adaptive speed algorithm to optimise the movement of the RP/M nozzles/print head along zigzag tool-paths was developed. That is, for a *Type I* or *Type II* line, the RP/M nozzle/print head starts from a minimum speed, accelerates afterwards towards a maximum speed, and then decelerates to the minimum speed at the end of the entire line. The design is aimed to improve the efficiency of the RP/M process by accelerating or decelerating the nozzle/print head in the different stages of zigzag. As thus, the following assumptions are made:

(1) The speed of the RP/M nozzle/print head from all the turning points of the two type lines is the minimum speed (represented as $V_{min}$);

(2) The maximum speed that the RP/M nozzle/print head can achieve is $V_{max}$. The values of $V_{max}$ and $V_{min}$ will be set according to the specification of a RP/M machine. Here an assumption is made to make $V_{max}$ twice of $V_{min}$. Please note the research in this paper is still based on simulation, and the relevant research is ongoing by the same research group, and the parameters are expected to be reported in the future work [36];

(3) The speed of the nozzle/print head in the zigzag tool-paths is either uniformly accelerated or deceleration with an acceleration as $\beta$.

Based on that, the adaptive strategy can be further represented as follows.

$$V_{max} = 2V_{min} \tag{3.14}$$

$$V_{max} = V_{min} + \beta t \tag{3.15}$$

where $t$ is the time used to speed up the RP/M nozzle/print head from the minimum speed to the maximum speed.

From Formulas (3.14) and (3.15), $t$ can be deduced as:

$$t = V_{min}/\beta \tag{3.16}$$

On the other hand,

$$Length = \frac{1}{2}\beta t^2 + V_{min}t \tag{3.17}$$

The following will be obtained if Formulas (3.16) and (3.17) are combined:

$$Length = \frac{3V_{min}^2}{2\beta} \tag{3.18}$$

Based on the above analysis, there are three cases for the RP/M nozzle/print head to move on a segment:

(1) If the length of the segment is less than $\frac{3V_{min}^2}{\beta}$, the nozzle/print head's speed could not reach the maximum speed $V_{max}$ (shown in Figure 3.14(a));

(2) If the length of the segment is equals to $\frac{3V_{min}^2}{\beta}$, the nozzle/print head's speed just reach the maximum speed $V_{max}$ in the middle of the segment (shown in Figure 3.14(b));

(3) If the length of the segment is less than $\frac{3V_{min}^2}{\beta}$, the nozzle/print head's speed reach the maximum speed $V_{max}$ before the middle of the segment (shown in Figure 3.14(c)).

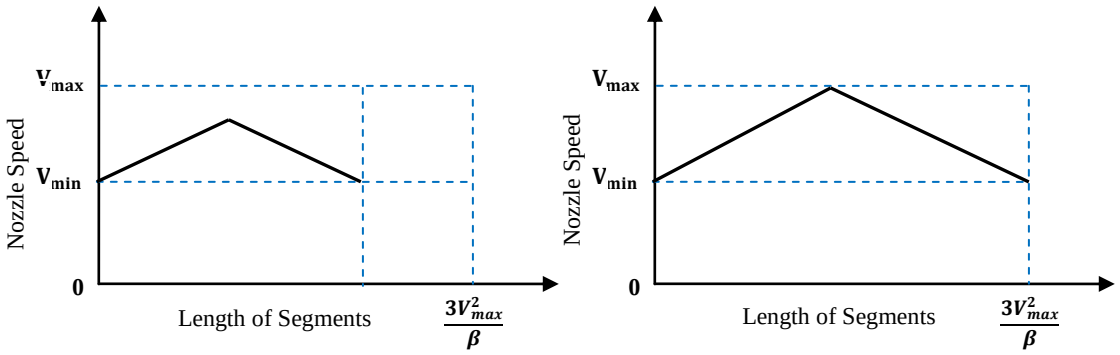


*(a) The length of a segment is less than* $\frac{3V_{min}^2}{\beta}$




*(b) The length of a segment equals* $\frac{3V_{min}^2}{\beta}$

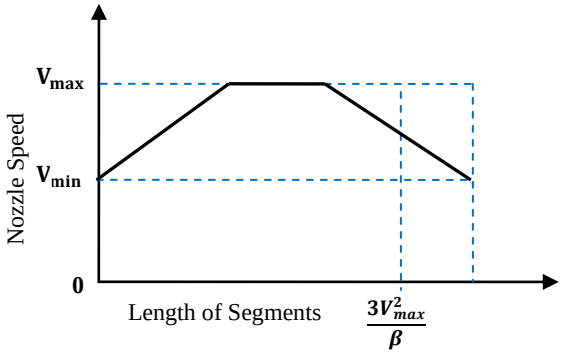


*(c) The length of a segment is more than* $\frac{3V_{min}^2}{\beta}$

**Figure 3.14** Three cases of a segment and the speed of the RP/M nozzle/print head.

To summarize the above Formulas (3.10)-(3.18), the time of a *Type I* or *Type II* line of zigzag will be computed as follows:

$$Time(L_I^{i,k}) = \begin{cases} \frac{2V_{min}}{\beta} & if\ \ Length(L_I^{i,k}) = \frac{3V_{min}^2}{\beta} \\ \frac{-2V_{min}}{\beta} + \sqrt{\left(\frac{2V_{min}}{\beta}\right)^2 + \frac{4Length(L_I^{j,k})}{\beta}} & if\ \ 0 < Length(L_I^{i,k}) < \frac{3V_{min}^2}{\beta} \\ \frac{2V_{min}}{\beta} + \frac{\beta * Length(L_I^{j,k}) - 3V_{min}^2}{2\beta * V_{min}} & if\ \ \frac{3V_{min}^2}{\beta} < Length(L_I^{i,k}) \end{cases} \quad (3.19)$$

$$Time(L_{II}^{j,k}) = \begin{cases} \frac{2V_{min}}{\beta} & if\ \ Length(L_{II}^{j,k}) = \frac{3V_{min}^2}{\beta} \\ \frac{-2V_{min}}{\beta} + \sqrt{\left(\frac{2V_{min}}{\beta}\right)^2 + \frac{4Length(L_{II}^{j,k})}{\beta}} & if\ \ 0 < Length(L_{II}^{i,k}) < \frac{3V_{min}^2}{\beta} \\ \frac{2V_{min}}{\beta} + \frac{\beta * Length(L_{II}^{j,k}) - 3V_{min}^2}{2\beta * V_{min}} & if\ \ \frac{3V_{min}^2}{\beta} < Length(L_{II}^{j,k}) \end{cases} \quad (3.20)$$

## 3.3 The geometrical accuracy analysis model

The tolerance distribution of RP/M can be defined as three scenarios: (1) negative, (2) positive, (3) a combination of both (showed in Figure 3.15). In this research, the negative tolerance distribution is used for geometrical accuracy analysis of RP/M models.



(a) Negative tolerance (b) Positive tolerance (c) Mixed tolerance

**Figure 3.15** Different tolerance distribution methods of RP/M (Ma et al., 2004).

The geometrical accuracy of a RP/M model can be calculated below:

$$Accuracy\ (R) = (G_{model} - G_{error})/G_{model}\ * 100\% \quad (3.21)$$

where *Accuracy(R)* represents the geometrical accuracy; $G_{model}$ is the whole volume of the model; $G_{error}$ is the whole volume error of the RP/M model.

$G_{error}$ can be computed below:

$$G_{error} = \sum_{i=1}^{n} G_{error}^{i} \quad (3.22)$$

where $i \in [1, n]$ is the index of a sliced layer; $n$ is the total number of the layers; $G^i_{error}$ is the geometrical error on the $i^{th}$ layer of the model.

$G^i_{error}$ is comprised of a type *I* error $G^i_{error\_type1}$ and a type *II* error $G^i_{error\_type2}$ (showed in Figure 3.16). The two errors are defined as follows:

[*Definition 4*] A type *I* error $G^i_{error\_type1}$ is accumulated between consecutive layers, and it is the principle error of RP/M. It is affected by the thickness of the layer: the thicker of the layer, the greater of the type *I* error.

[*Definition 5*] A type *II* error $G^i_{error\_type2}$ is accumulated along the boundary of every layer. It is in the boundary area which is not filled during the RP/M process.

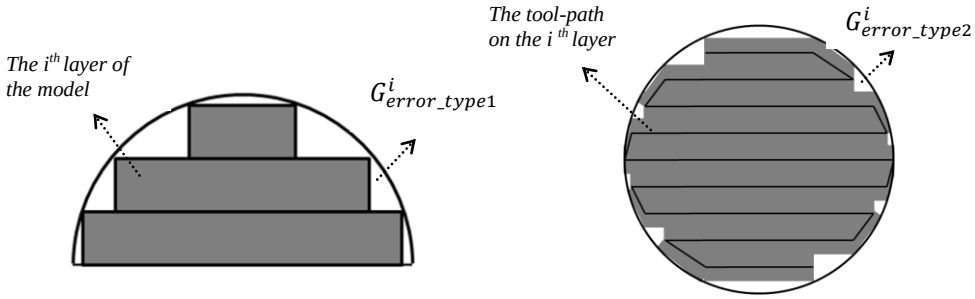


(a) A Type I error (b) A Type II error

**Figure 3.16** Geometrical errors of RP/M.

$G^i_{error}$ is computed below:

$$G^i_{error} = f\left(G^i_{error\_type1}, G^i_{error\_type2}\right) = V^i_{model} - S^i_{RP/M} * H^i_{thickness} \quad (3.23)$$

where $V^i_{model}$ is the volume of the $i^{th}$ layer; $S^i_{RP/M}$ is the area covered by the tool-paths of RP/M on the $i^{th}$ layer; $H^i_{thickness}$ is the thickness of the $i^{th}$ layer.

## 3.4 Case studies and algorithm validation

Five complex biomedical models, which were first created by CMMs scanning to obtain the point cloud data and then reconstructed as IGES/IGS format models in CATIA V5™ with QSR and DSE modules, were tested to validate the effectiveness and robustness of the developed algorithms and strategies. The minimum and maximum speeds of the RP/M nozzle/print head were defined as 10mm/s and 20mm/s respectively, and the acceleration of the nozzle/print head was $20\mathrm{mm/s^2}$ ($\mathrm{V_{min}} = 10\mathrm{mm/s}; \mathrm{V_{max}} = 20\mathrm{mm/s};\ \mathrm{a} = 20\mathrm{mm/s^2}$). All results were obtained in a Pentium Dual-Core CPU 2.10GHz, 2GB RAM system.

### 3.4.1 Case study 1 – a tibia model

A tibia model was used to validate the research. The length, width, height and volume of the tibia model are 405.29mm, 106.96mm, 98.249mm and 471600mm$^3$ respectively. The process for the NURBS-based contour curve generation, and the generation of contour-based tool-paths and zigzag tool-paths are shown in Figure 3.17. The result of the build time in the contour-based tool-paths is shown in Table 3.1. For the zigzag tool-paths, different slope degrees were used for each layer (shown in Figure 3.13). Table 3.2 shows the results of each build time with an incremental 10 degree for the slope from 0 degree until 170 degree. It can be observed that in 20 degree the build time is the shortest. The total build time for the shown layer of the tibia model = 33.401+78.638 = **112.039 seconds** (contour tool-paths + zigzag tool-paths).

(a) The tibia model

(b) The slicing layer

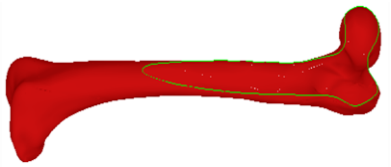

(c) The sliced model

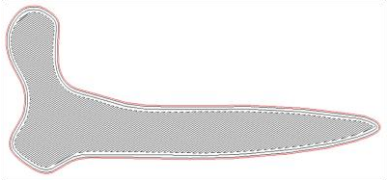

(d) The generated tool-paths for one layer

**Figure 3.17** Model 1 - a tibia model.

**Table 3.1** The RP/M nozzle/print head speed of the contour tool-paths for the tibia model.

| Segment no. | 1 | 2 | 3 | 4 | 5 | 6 |
|---|---|---|---|---|---|---|
| Distance (mm) | 172.677 | 255.355 | 79.108 | 23.214 | 32.942 | 49.230 |
| Length (mm) | 175.994 | 265.461 | 89.365 | 24.523 | 33.692 | 50.262 |
| Average speed (mm/s) | 19.624 | 19.238 | 17.704 | 18.932 | 19.554 | 19.590 |
| Build time (s) | 8.969 | 13.799 | 5.048 | 1.296 | 1.723 | 2.566 |
| ***Total build time for contour tool-path = 33.401 (s)*** | | | | | | |

**Table 3.2** Comparisons of the different slope degrees of zigzag tool-paths for the tibia model.

| Degree | 0 | 10 | **20** | 30 | 40 | 50 | 60 | 70 | 80 |
|---|---|---|---|---|---|---|---|---|---|
| Length (mm) | 1465.97 | 1463.74 | **1425.84** | 1419.55 | 1424.22 | 1439.13 | 1461.97 | 1466.97 | 1465.95 |
| Time (s) | 82.086 | 82.987 | **78.638** | 79.749 | 80.880 | 82.647 | 83.866 | 82.885 | 86.601 |
| | | | | | | | | | |
| Degree | 90 | 100 | 110 | 120 | 130 | 140 | 150 | 160 | 170 |
| Length (mm) | 1485.41 | 1522.77 | 1516.44 | 1502.71 | 1497.11 | 1478.73 | 1511.41 | 1475.74 | 1481.44 |
| Time (s) | 85.035 | 87.498 | 84.945 | 86.604 | 85.719 | 85.588 | 83.631 | 82.890 | 86.523 |

### 3.4.2 Case study 2 – an iliac model

The second model is an iliac model. The main slicing and tool-path generation is shown in Figure 3.18. The length, width, height and volume of the talus model are 207.24mm, 153.47mm, 128.26mm and 282260mm$^3$ respectively. Table 3.3 and Table 3.4 show the results of the each build time of contour and zigzag tool-paths for this model.

(a) The iliac model

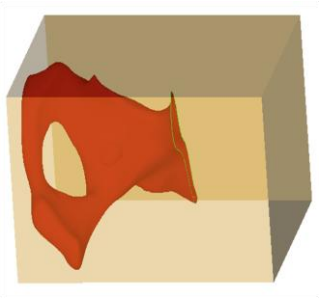

(b) The slicing layer

(c) The sliced model

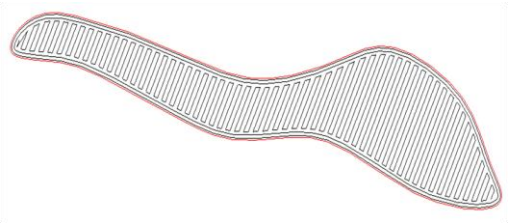

(d) The generated tool-paths for one layer

**Figure 3.18** Model 2 - an iliac model.

**Table 3.3** The RP/M nozzle/print head speed of the contour tool-paths for the iliac model.

| Segment no. | 1 | 2 | 3 | 4 | 5 | 6 | 7 | 8 | 9 |
|---|---|---|---|---|---|---|---|---|---|
| Distance (mm) | 16.149 | 24.855 | 19.917 | 17.309 | 26.110 | 30.508 | 56.001 | 13.324 | 46.417 |
| Length (mm) | 16.196 | 24.903 | 20.548 | 17.663 | 27.155 | 30.742 | 61.411 | 13.435 | 46.726 |
| Average speed (mm/s) | 19.942 | 19.962 | 19.386 | 19.598 | 19.230 | 19.848 | 18.238 | 19.834 | 19.868 |
| Build time (s) | 0.812 | 1.248 | 1.060 | 0.901 | 1.412 | 1.549 | 3.367 | 0.678 | 2.352 |
| ***Total build time for contour tool-path = 13.379 (s)*** | | | | | | | | | |

**Table 3.4** Comparisons of the different slope degrees of zigzag tool-paths for the iliac model.

| Degree | 0 | 10 | 20 | 30 | 40 | 50 | 60 | 70 | 80 |
|---|---|---|---|---|---|---|---|---|---|
| Length (mm) | 757.026 | 731.640 | 744.506 | 746.196 | 740.218 | 744.870 | 747.118 | 745.944 | 746.88 |
| Time (s) | 45.367 | 43.213 | 43.061 | 44.054 | 45.039 | 45.669 | 45.741 | 45.402 | 45.756 |
| | | | | | | | | | |
| Degree | 90 | 100 | 110 | 120 | 130 | 140 | **150** | 160 | 170 |
| Length (mm) | 744.842 | 753.832 | 757.572 | 753.300 | 739.734 | 745.568 | **731.892** | 707.372 | 722.810 |
| Time (s) | 45.162 | 45.603 | 45.195 | 44.274 | 42.852 | 41.424 | **39.567** | 39.883 | 41.577 |

In 150 degree the build time of the zigzag tool-paths is the shortest. The total build time for the shown layer of the iliac model = 13.379+39.567 = **52.946 seconds**.

### 3.4.3 Case study 3 – an ear model

The fourth model is an ear model. The length, width, height and volume of the human ear model are 61.056mm, 37.932mm, 18.302mm and 4730mm$^3$ respectively. The main slicing process and the generation of mixed tool-paths are shown in Figure 3.20. Table 3.5 and Table 3.6 show the results of each build time for contour and zigzag tool-path for this model.

(a) The ear model

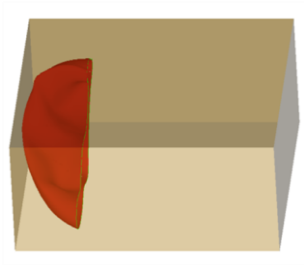

(b) The slicing layer

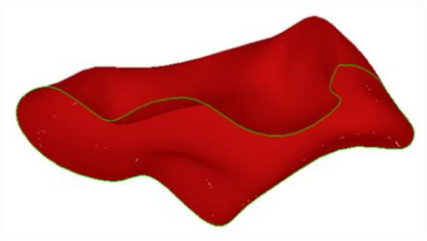

(c) The sliced model

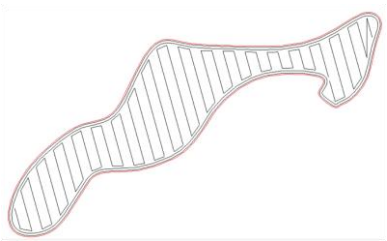

(d) The generated tool-paths for one layer

**Figure 3.19** Model 3 – an ear model.

**Table 3.5** The RP/M nozzle/print head speed of the contour tool-paths for the ear model.

| Segment no. | 1 | 2 | 3 | 4 | 5 | 6 |
|---|---|---|---|---|---|---|
| Distance (mm) | 16.278 | 20.092 | 8.662 | 20.290 | 6.918 | 2.393 |
| Length (mm) | 16.762 | 21.645 | 9.921 | 21.804 | 12.099 | 3.096 |
| Average speed (mm/s) | 19.422 | 18.564 | 17.462 | 18.610 | 11.436 | 15.460 |
| Build time (s) | 0.863 | 1.166 | 0.568 | 1.172 | 1.058 | 0.201 |
| ***Total build time for contour tool-path = 5.027 (s)*** | | | | | | |

**Table 3.6** Comparisons of the different slope degrees of zigzag tool-paths for the ear model.

| Degree | 0 | 10 | 20 | 30 | 40 | 50 | 60 | 70 | 80 |
|---|---|---|---|---|---|---|---|---|---|
| Length (mm) | 150.916 | 158.119 | 156.179 | 152.094 | 153.061 | 156.923 | 155.442 | 154.884 | 148.398 |
| Time (s) | 11.700 | 12.640 | 12.630 | 12.416 | 12.404 | 12.858 | 12.646 | 12.536 | 11.942 |
| | | | | | | | | | |
| Degree | 90 | 100 | **110** | 120 | 130 | 140 | 150 | 160 | 170 |
| Length (mm) | 147.599 | 144.954 | **146.976** | 167.510 | 161.265 | 159.627 | 166.244 | 163.230 | 160.695 |
| Time (s) | 11.790 | 11.390 | **10.872** | 12.14 | 12.270 | 12.822 | 14.278 | 13.082 | 12.784 |

From the results of the above table, it can be observed that in 110 degree the build time is the shortest. The total build time for the shown layer of the ear model = 5.027+10.872 = **15.899 seconds**.

### 3.4.4 Case study 4 – a calcaueus model

The fifth model is a calcaueus model. The length, width, height and volume are 71.94mm, 53.463mm, 52.444mm and 62761mm$^3$ respectively. Figure 3.20 shows the main slicing process and tool-path generation process for this model. Table 3.7 and Table 3.8 show the results of each build time for contour and zigzag tool-path for this calcaueus model.

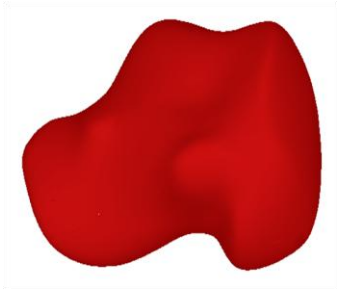

(b) The calcaueus model

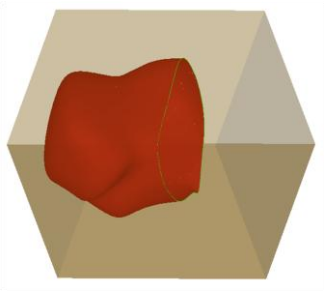

(b) The slicing layer

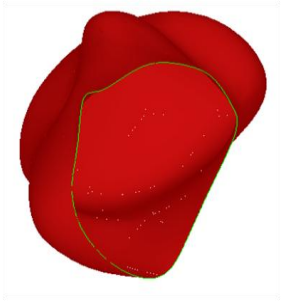

(c) The sliced model

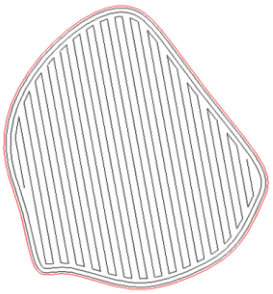

(d) The generated tool-paths for one layer

**Figure 3.20** Model 4 - a calcaueus model.

**Table 3.7** The RP/M nozzle/print head speed of the contour tool-paths for the calcaueus model.

| Segment no. | 1 | 2 | 3 | 4 | 5 |
|---|---|---|---|---|---|
| Distance (mm) | 19.904 | 29.876 | 3.073 | 39.503 | 10.303 |
| Length (mm) | 20.117 | 34.738 | 3.091 | 48.531 | 10.415 |
| Average speed (mm/s) | 19.788 | 17.200 | 19.882 | 16.280 | 19.784 |
| Build time (s) | 1.017 | 2.020 | 0.156 | 2.981 | 0.527 |
| ***Total build time for contour tool-path = 6.701 (s)*** | | | | | |

**Table 3.8** Comparisons of the different slope degrees of zigzag tool-paths for the calcaueus model.

| Degree | 0 | 10 | 20 | 30 | 40 | 50 | 60 | 70 | 80 |
|---|---|---|---|---|---|---|---|---|---|
| Length (mm) | 933.95 | 927.58 | 918.10 | 921.07 | 914.47 | 909.67 | 908.87 | 908.72 | 910.00 |
| Time (s) | 62.448 | 61.512 | 60.962 | 61.278 | 59.722 | 57.716 | 57.010 | 56.042 | 57.266 |
| | | | | | | | | | |
| Degree | 90 | 100 | 110 | 120 | **130** | 140 | 150 | 160 | 170 |
| Length (mm) | 926.23 | 921.84 | 920.91 | 904.09 | **899.76** | 901.03 | 914.16 | 911.47 | 909.42 |
| Time (s) | 62.156 | 63.178 | 60.290 | 58.340 | **55.022** | 56.324 | 57.232 | 58.586 | 60.554 |

In 130 degree the build time of the zigzag tool-paths is the shortest. The total build time for the shown layer of the calcaueus model = 6.701 +55.022 = **61.723 seconds**.

## 3.5 Build efficiency and geometrical accuracy comparisons

### 3.5.1 Build efficiency comparisons

The four biomedical models (shown in Figure 3.17-3.20) were also used for build efficiency comparisons. Figure 3.21-3.24 shows the comparison results between this developed approach (i.e., the developed approach) and typical zigzag tool-path generation approaches in a layer with an incremental 10 degree of tool-path slope from 0 degree until 180 degree. The zigzag tool-path generation approaches include an approach in uniform speed and an approach in adaptive speed of the RP/M nozzle/print head. All results were obtained in a Pentium Dual-Core CPU 2.10GHz, 2GB RAM system.

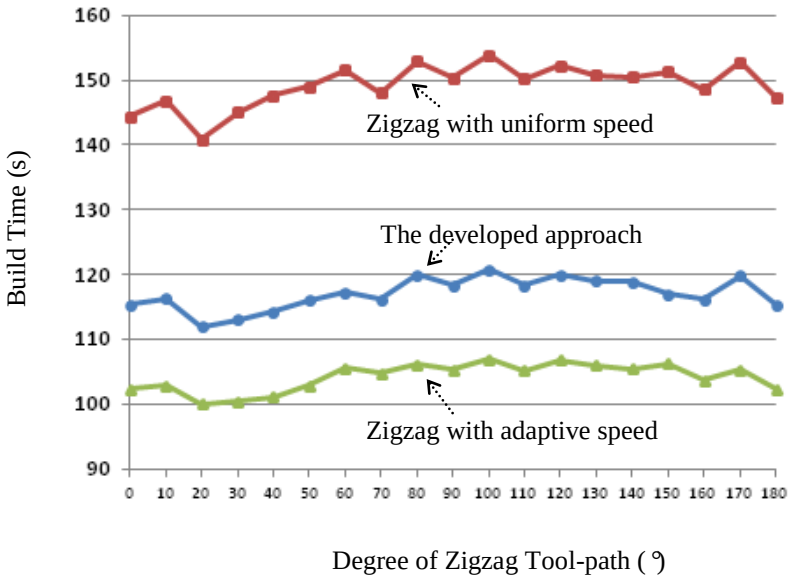


**Figure 3.21** Build time comparisons - Model 1.

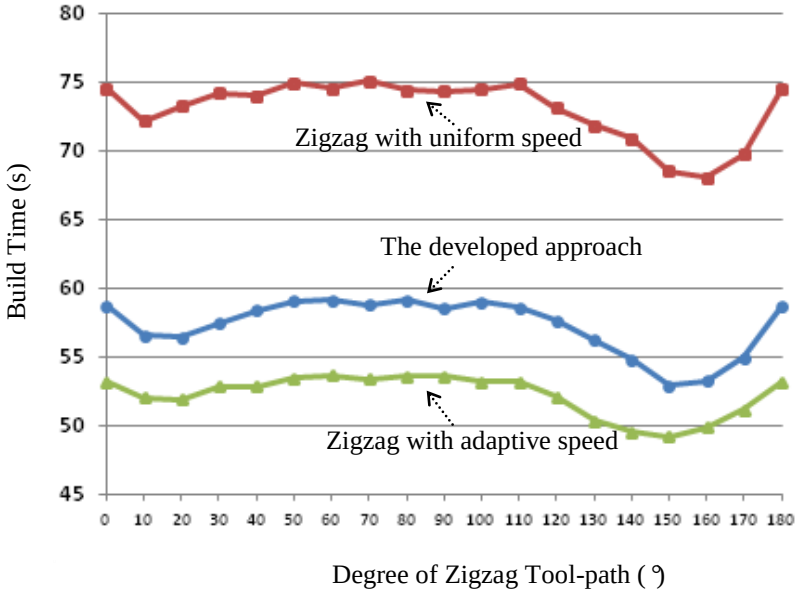


**Figure 3.22** Build time comparisons - Model 2.

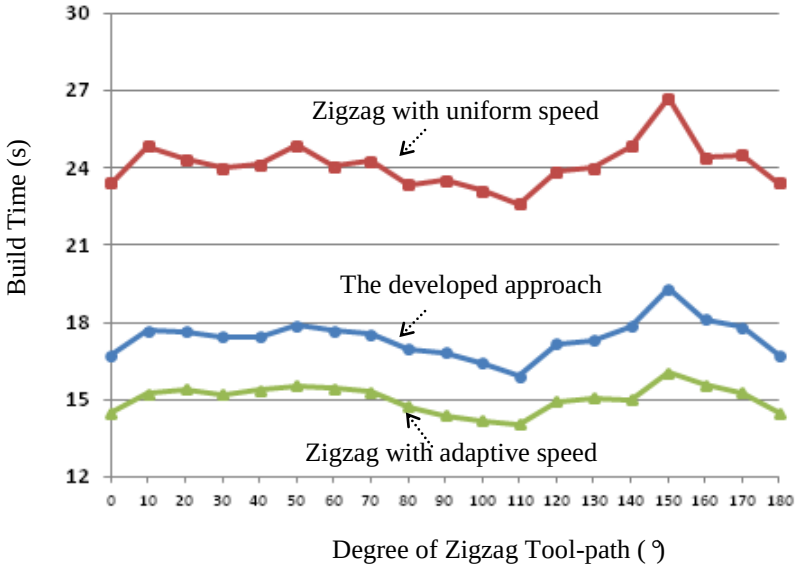


**Figure 3.23** Build time comparisons - Model 3.

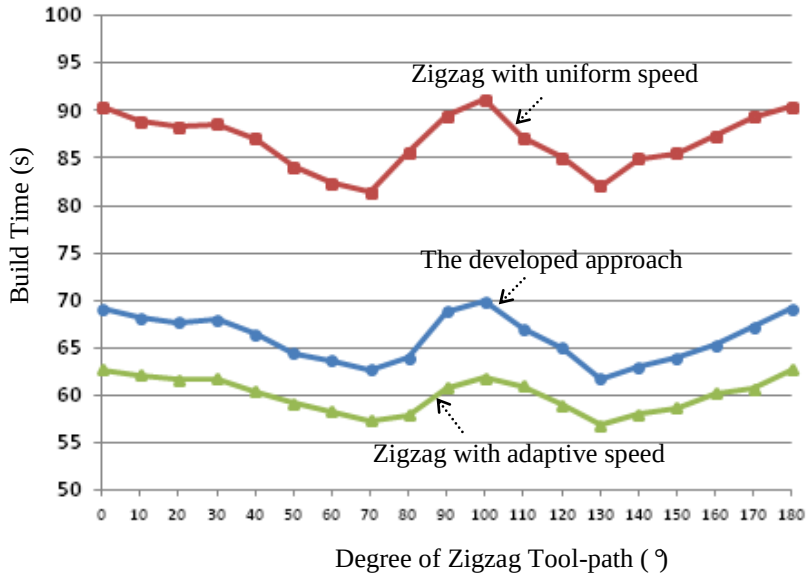


**Figure 3.24** Build time comparisons - Model 4.

From the above data, it can be observed that the build time of this developed approach can be reduced about 35% compared to that of the zigzag tool-path generation approach in uniform speed. Meanwhile, the developed zigzag tool-path optimisation strategy to obtain the best slope degree of the RP/M nozzle/print head can further reduce approximated 10% of RP/M build time. The build time of this developed approach is about 10% more than that of the zigzag tool-path generation approach in adaptive speed. However, the geometrical accuracy of this developed mixed tool-paths algorithm will be much better than that of the zigzag tool-path generation approaches. The geometrical accuracy comparisons are explained below.

### 3.5.2 Geometrical accuracy comparisons

Figure 3.25-3.28 shows the comparisons of geometrical accuracy between this developed approach and typical zigzag tool-path generation approaches. The series of comparisons are based on an incremental 0.1mm of the diameter of RP/M nozzle/print head each time from 0mm until 1.9mm. All results were obtained in a Pentium Dual-Core CPU 2.10GHz, 2GB RAM system.

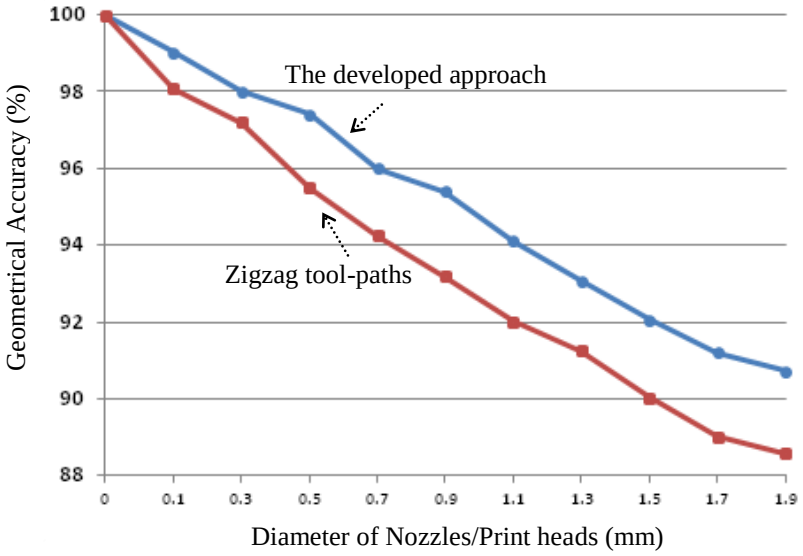


**Figure 3.25** Geometrical accuracy comparisons - Model 1.

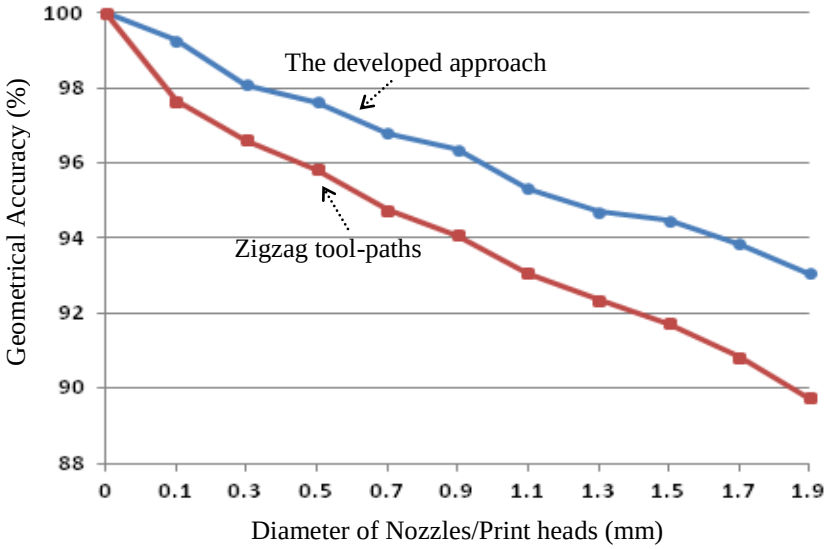


**Figure 3.26** Geometrical accuracy comparisons - Model 2.

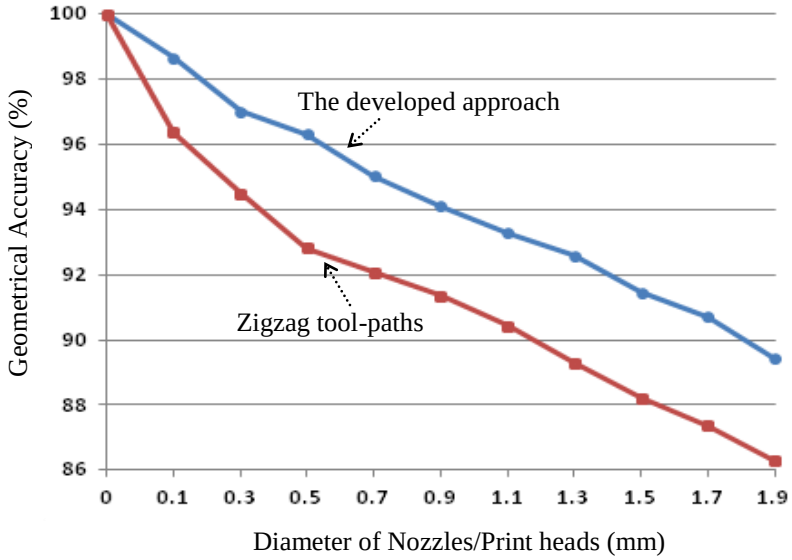


**Figure 3.27** Geometrical accuracy comparisons - Model 3.

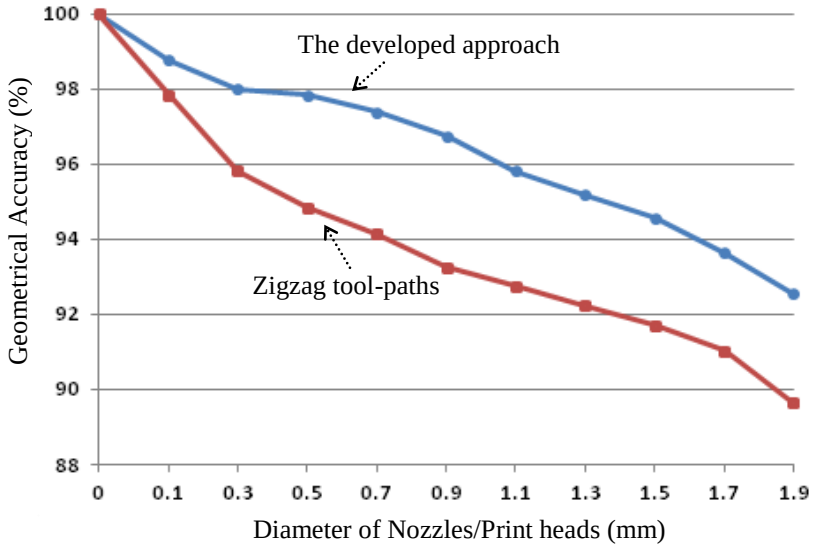


**Figure 3.28** Geometrical accuracy comparisons - Model 4.

It can be observed that this developed approach achieved much better in terms of geometrical accuracy and geometrical quality compared to that of the typical zigzag tool-path generation approaches of RP/M. Therefore, this approach can achieve an overall improvement and a better balance of build efficiency and geometrical accuracy.

## 3.6 Summary

This chapter has presented adaptive tool-path generation algorithms and strategies to improve geometrical accuracy and to reduce build time for biomedical model fabrication in RP/M. A series of optimisation algorithms and strategies have been developed to optimise the tool-path generation in RP/M process planning. They include a slicing algorithm and NURBS-based representation, the zigzag and contour tool-path generation, adaptive speed algorithms, and the build time and geometrical accuracy analysis modules of RP/M systems. The major features of the research are as follows:

(1) The geometrical accuracy of original biomedical CAD model is maintained through introducing NURBS to represent the contours of sliced layers of biomedical CAD models to keep high-fidelity information. It establishes a good original data source for further RP/M tool-path generation;
(2) The developed mixed tool-path generation algorithms can effectively balance RP/M geometrical accuracy and build efficiency. The developed adaptive speed strategies of and contour and zigzag tool-paths for RP/M nozzle/print head can be used to further optimise build time towards a minimum target;
(3) The developed build time and geometrical accuracy mathematical model can be used to analyse the build time and the geometrical accuracy of models with different parameters. It provides an effective guideline for parameter setting of a RP/M system for reducing build time and improving geometrical accuracy;
(4) Four biomedical models were used to demonstrate that the developed approach has achieved significantly improved performance in terms of effectiveness and robustness.

# CHAPTER 4

# ADAPTIVE SLICING APPROACH OF RP/M FOR COMPLEX BIOMEDICAL MODELS

## 4.1 Introduction

The slicing strategy is to transfer a digital 3D model (e.g., a 3D biomedical CAD model) into a series of 2.5D sliced layers perpendicular to the orientation direction with a certain layer thickness. The strategy is normally classified as uniform slicing and adaptive slicing (Ma et al., 2004). Uniform slicing maintains the same thickness between two consecutive layers along the entire model. It has been widely used in commercial RP/M systems today. However, uniform slicing is difficult to achieve an optimised balance of build efficiency and geometrical accuracy. For instance, for some models, if a layer is too thick, the build time is reduced but the geometrical accuracy of the models could be relatively poor, or the geometrical accuracy is improved but the build time is also extended significantly (Singhal et al., 2008). To solve the above problem, adaptive slicing has been recently proposed by some researchers. It can effectively reduce the staircase effect of RP/M for some crucial areas in models to improve geometrical accuracy and minimize build time considering varied thickness of layers would address the different geometrical characteristics of models' surfaces. However, the models used to demonstrate the effectiveness of the developed research works of adaptive slicing are still relatively simple. A research gap still exists between the adaptive slicing thickness determination, and an analysis and control solution to balance and optimise the geometrical accuracy and build time for complex biomedical models in the RP/M process.

In this chapter, a novel adaptive slicing approach for RP/M has been developed with a bid to balance the build efficiency and geometrical accuracy of complex biomedical models. The approach is capable and robust to control the layer thickness of models adaptively according to their characteristics.

Firstly, directly slicing on a CAD-represented biomedical model and NURBS-based curves for the sliced boundaries in layers are introduced to preserve the geometrical accuracy of the biomedical model. Secondly, rotating cutting and two controlling thresholds are then designed to extract the surface feature of the biomedical model. Thirdly, adaptive slicing algorithm is developed to decide the thickness for each layer based on the number of feature points passing the two controlling thresholds. Fourthly, geometrical accuracy and build time analysis strategies are used to calculate and analyze the geometrical accuracy and build time during RP/M processing with the different values of the controlling thresholds. Finally, two case studies of complex biomedical models are used to demonstrate and verify the performance of the developed strategies and algorithms in this chapter.

## 4.2 The developed adaptive slicing approach for biomedical models in RP/M

The developed adaptive slicing approach in the RP/M process planning consists of three phases as follows (shown in Figure 4.1). The details of the each phase are depicted in Table 4.1.

Phase 1: The adaptive slicing thickness determination algorithms and strategies
Phase 2: The geometrical accuracy and build time analysis modules
Phase 3: The geometrical accuracy and build time control strategy

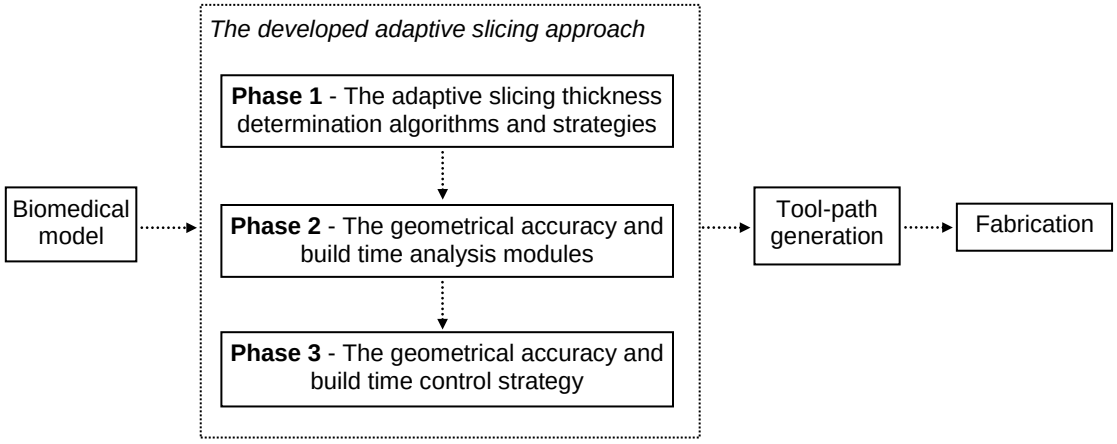


**Figure 4.1** The developed adaptive slicing approach for biomedical models.

**Table 4.1** The characteristics of the three phases of the developed adaptive slicing approach.

| ***Phase1:*** *Adaptive slicing thickness algorithms and strategies* | ***Phase2:*** *Geometrical accuracy and build time analysis modules* | ***Phase3:*** *Geometrical accuracy and build time control strategy* |
|---|---|---|
| Rotating slicing was used to extract the surface feature of the biomedical model<br><br>Two thresholds were introduced to filter out the feature point based on the surface complexity of biomedical model<br><br>The slicing thickness is determined by the number of feature points pass the two thresholds | Analyze the relationship between geometrical accuracy, build time and various slicing thickness | Find out the relationship between the thresholds, geometrical accuracy and build time of fabrication<br><br>Control geometrical accuracy and build time of fabrication by various the value of the two thresholds |
| *Advantage*<br>To balance the geometrical accuracy and build time | *Advantage*<br>To calculate and analyze the geometrical accuracy and build time | *Advantage*<br>To control and optimise the geometrical accuracy and build time |

*The software platform which is integrated with the above functional modules were developed based on the C++ language in an open-source CAD kernel system - the Open CASCADE (Open CASCADE, 2012)*

### 4.2.1 Phase 1 – Adaptive slicing algorithms and strategies

Firstly, the cloud point data of a biomedical model are generated from CT or MRI by biomedical software such as Mimic packages, and are reconstructed as an IGES/IGS

surface model using the QSR and DSE modules in CATIA V5™. The reconstructed biomedical model is then processed by the adaptive slicing approach developed based on the C++ programming language and an open-source CAD kernel system - the Open CASCADE (Open CASCADE, 2012). The developed adaptive slicing algorithms and strategies consist of three parts:

Part 1: The slicing process with the minimum slicing thickness and NURBS-based representation for the slicing contours

Part 2: The rotating slicing process to extract the surface feature of the biomedical model and two controlling thresholds definition

Part 3: Adaptive slicing thickness determination for each slicing layer of the biomedical model

#### 4.2.1.1 Part 1 – NURBS-based representation of slicing boundary

The directly slicing process and NURBS-based curve representation of biomedical model has been detailed introduced in chapter 3. After the directly slicing algorithm and strategy, a closed NURBS curve can be generated to represent the contour of each sliced layer of biomedical model. In Figure 4.2, a biomedical bone model is used to illustrate the process. Firstly, a container is created to envelop the model, and the shortest edge of the enveloping box is determined as the orientation direction (Z axis) to minimize the build time of RP/M. Then, a series of slicing surfaces with a pre-set minimum slicing thickness (represented as $Thickness(T_{min})$) are first generated along the Z axis for later adaptive processing.

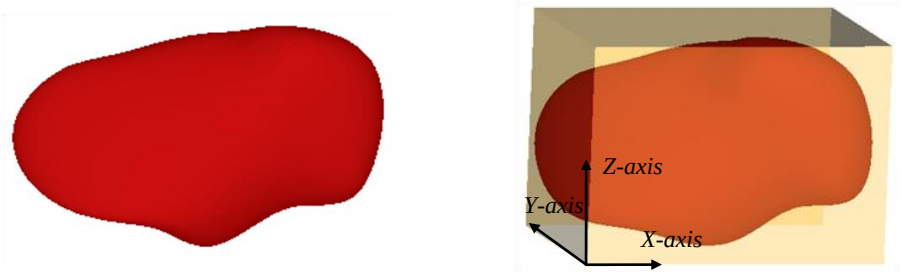


(a) A biomedical model to be sliced

(b) An enveloping box for the biomedical

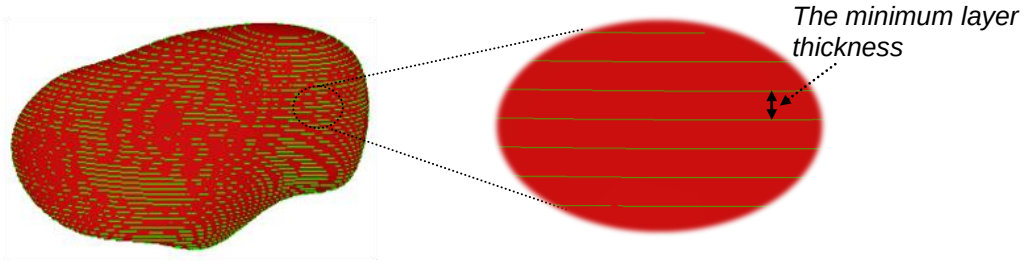


(c) Sliced layers with a pre-set minimum layer thickness

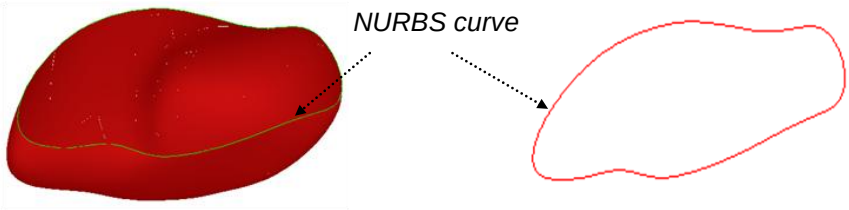


(d) A NURBS-based contour curve generated for each slicing layer

**Figure 4.2** An example to illustrate the directly slicing and NURBS representation.

#### 4.2.1.2 Part 2 – Rotating slicing and two controlling thresholds

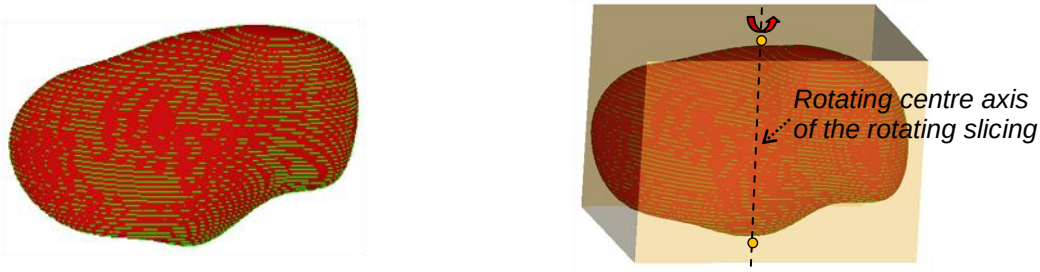


(a) The minimum thickness slicing of the biomedical model

(b) An enveloping box and rotating axis of the rotating slicing

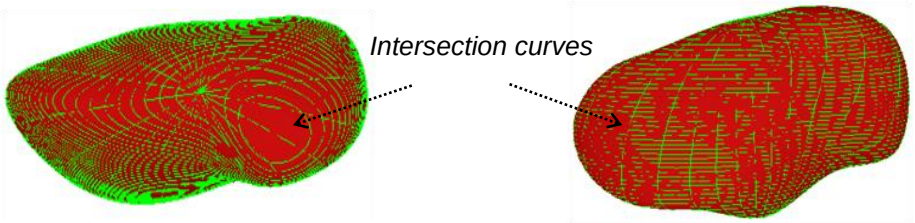


(1) Overlook

(2) Side face

(c) The generated intersection curves between rotating slicing surface and the biomedical model

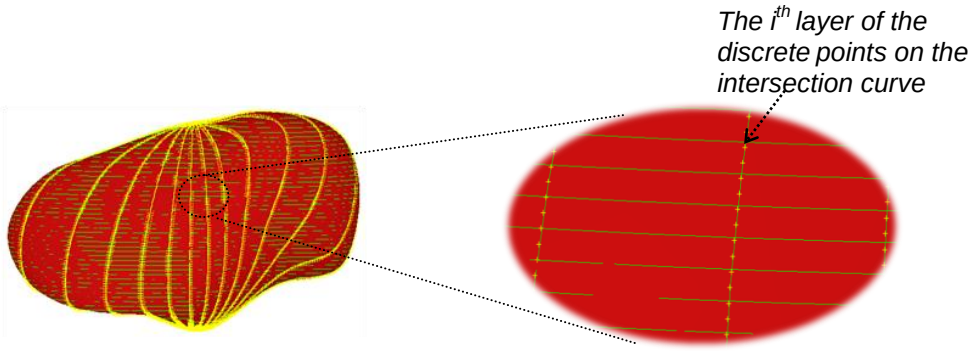


(d) Discrete points with same distance on the intersection curves

**Figure 4.3** An example to illustrate the rotating slicing strategy.

In order to extract the surface feature of a biomedical model and get the original data for the adaptive slicing algorithm in next section, a rotating cutting process and two controlling thresholds are used here.

In the rotating cutting process, a series of cutting planes rotating evenly along the Z-axis (orientation direction) of the model are generated (such a plane is denoted as a cutting plane in the following). Meanwhile, the model is also sliced with a series of planes with the minimum thickness along the Z direction (such a plane is denoted as a slicing plane in the following). Intersection curves are generated between the cutting plane and the slicing plane of the biomedical model Figure 4.3 shows the main process of the above process.

The intersected points of the biomedical model can be used to represent the surface complexity and further the adaptive thickness strategy. Two thresholds are defined here.

**(1) Threshold one – $\boldsymbol{Threshold(D^{1}_{threshold})}$**

The surface complexity of the intersected contour between the cutting plane and the model can be presented by the curvature of the contour. However, curvature computation is time consuming. Here, a relatively simplified formula is introduced for surface complexity computation.

Discrete points are generated in the contour curve evenly. Two distances for each pair of adjacent discrete points, i.e., one is along the curve (denoted as D1), and another is along their connected line (denoted as D2), are computed. Qualitively, the larger the two distances, the more complexity of the contour in the model (shown in Figure 4.4(a)). Quantitively, Formula (4.1) is used to represent:

$$D^{i,j,k}_{change} = Distance\left(Point^{i}, Point^{i+1}\right) - Length(Point^{i}, Point^{i+1}) \quad (4.1)$$

$i \in (0,1,2,\dots,N);\ j \in (1,2,\dots,M)$

$N = \ Point\ number\ on\ \ curve\ C^{j}\ of\ Thickness(T^{k}_{min})\ part$

$M = 180°/(Rotated\ slicing\ degree)$

Threshold one is set to filter out the discrete points with pre-set distance change between two adjacent points on the rotated intersection curve, and the two points passing the threshold are kept as feature points.

**(2) Threshold two -** $\boldsymbol{Threshold(D^2_{threshold})}$

The angle between the normal of a discrete point along the contour curve and the Z direction can influence the stair effect in RP/M. Formula (4.2) is used to calculate the angle:

$$A^{i,j,k}_{change} = Arccos\left(\frac{Projection\ Length(\mathrm{Point^i},\mathrm{Point^{i+1}})}{Length(\mathrm{Point^i},\mathrm{Point^{i+1}})}\right) \quad (4.2)$$

$i \in (0,1,2,\dots,N);\ j \in (1,2,\dots,M)$

$N = Point\ number\ on\ curve\ C^j of\ Thickness(T^k_{min})\ part$

$M = 180°/(Rotated\ slicing\ degree)$

Threshold two is set to filter out the discrete points with pre-set angle between the line, which connecting two adjacent points on the rotated intersection curve, and the Z direction. If the angle value passes the pre-setting threshold, the two adjacent points are kept as feature points. The angle value shows the slope between the line which by connecting two adjacent points on the intersection curve and the manufacturing direction, the larger the angle value is, the more complexity of the outside surface of the biomedical within these two adjacent points along the manufacturing direction (shown in Figure 4.4(b)).

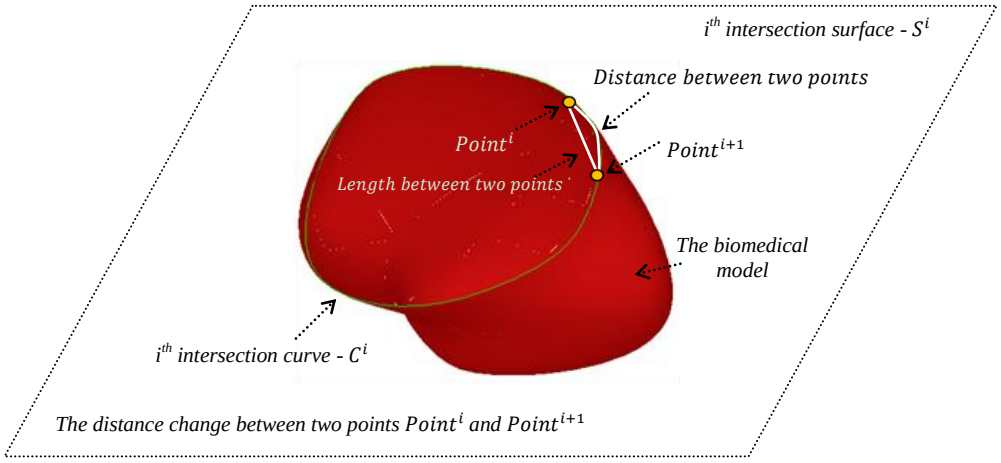


(a) Threshold one – Threshold ($D^1_{threshold}$)

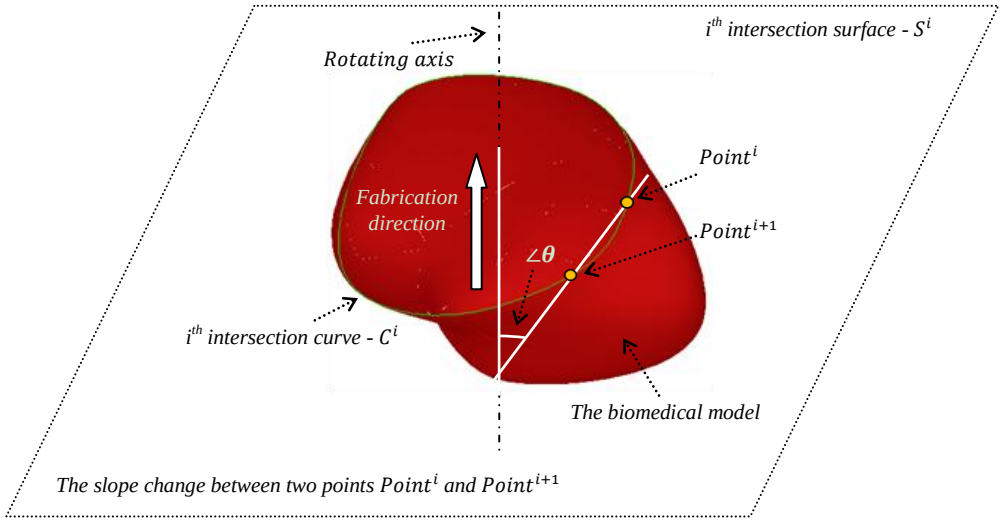


(b) Threshold two – Threshold ($D^2_{threshold}$)

**Figure 4.4** An example to illustrate the two thresholds.

#### 4.2.1.3 Part 3 – Adaptive slicing thickness determination

The thickness of a slicing layer is a very important parameter related to the build time and the geometrical accuracy during biomedical model fabrication in a RP/M system. An adaptive slicing approach provides a better solution to balance the build time and the

geometrical accuracy of RP/M fabrication as the slicing thickness of each layer can be varied based on the geometric complexity of the model. In this section, a novel adaptive slicing thickness determination algorithm has been developed based on the number of feature points in each minimum layer (i.e.,$Thickness(T_{min})$) of the biomedical model. If number of feature points in $Thickness(T_{min}^{k})$ is large, then the surface of $Thickness(T_{min})$ is complex, and so the slicing thickness should be smaller to protect feature characteristics and to improve geometrical accuracy during fabrication; if the feature point number in $Thickness(T_{min}^{k})$ is small, the surface of $Thickness(T_{min}^{k})$ is simple, and so slicing thickness should be set bigger to reduce the build time of fabrication.

In the adaptive slicing process, the number of the feature points in each $Thickness(T_{min})$ of the biomedical model can be calculated, and two thresholds have been used to judge whether to filter out the feature points. The thickness of each slicing layer can be determined based on the number of feature points in each $Thickness(T_{min})$ of the biomedical model (shown in Figure 4.5). The main flow of the developed algorithm of the complex biomedical model is shown in Figure 4.6. Explanations are expanded below.

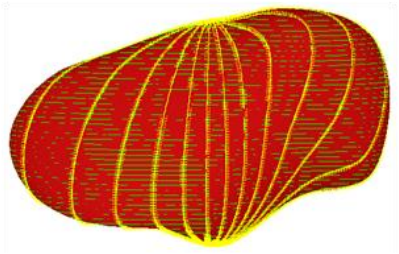

(a) The discrete points on the intersection curves

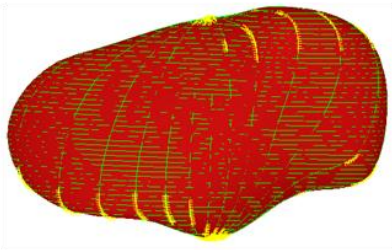

(b) Feature points pass the threshold one

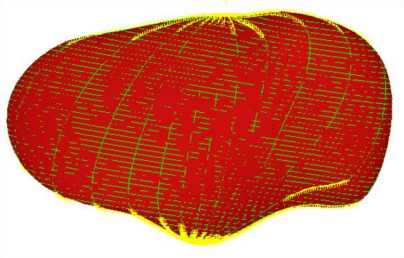

(c) Feature points pass the threshold two

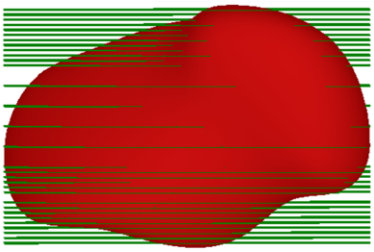

(d) Adaptive slicing the biomedical model

**Figure 4.5** The main process of the developed adaptive slicing thickness determination algorithm.

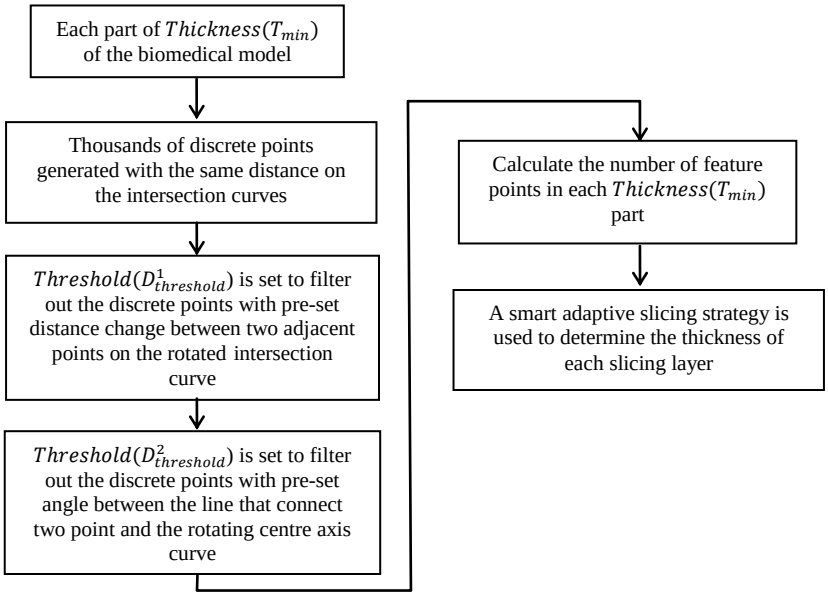


**Figure 4.6** The main flow of the developed adaptive slicing thickness determination algorithm.

In order to determine the thickness of each slicing layer, the minimum and the maximum slicing thickness were set based on the characteristics of the used RP/M system.

$$Thickness(T_{min}) \leq T^t_{thickness} \leq Thickness(T_{max}) \tag{4.3}$$

where $T^t_{thickness}$ represents the thickness of the number $t$ slicing layer for the biomedical model; $Thickness(T_{min})$ and $Thickness(T_{max})$ represent for the minimum and maximum slicing thickness of the used RP/M system respectively.

The whole feature point passing each $Thickness(T_{min})$ part can be calculated below:

$$Whole\left(Num^k_{point}\right) = Threshold1\left(Num^k_{point}\right) + Threshold2(Num^k_{point}) \tag{4.4}$$

where $Whole\left(Num^k_{point}\right)$ represents the number of whole feature points for the $k^{th}$ minimum slicing layer part $Thickness(T^k_{min})$ ; $Threshold1\left(Num^k_{point}\right)$ and $Threshold2(Num^k_{point})$ represent the feature point number pass the threshold one and the threshold two respectively. They can be calculated as follows:

**(1) The feature point number pass the threshold one - $Threshold(D^1_{threshold})$**

The feature point number in $Thickness(T^k_{min})$ can be computed below:

$$\begin{cases} Threshold1(Num^k_{point}) = 0 & Initialization \\ Threshold1(Num^k_{point}) = Threshold1(Num^k_{point}) + 0 & if\ D^1_{threshold} > D^{i,j,k}_{change} \\ Threshold1(Num^k_{point}) = Threshold1(Num^k_{point}) + 2 & if\ D^1_{threshold} \leq D^{i,j,k}_{change} \end{cases} \quad (4.5)$$

where $D^1_{threshold}$ represents the pre-setting value of the threshold one; $D^{i,j,k}_{change}$ represents the distance change between points $Point^i$ and $Point^{i+1}$ on the intersection curve $C^j$ for $Thickness(T^k_{min})$ part. It can be calculated by Formula (4.1) as shown in 4.2.1.2 section.

**(2) The feature point number for the threshold two - $Threshold(D^2_{threshold})$**

The feature point number in $Thickness(T^k_{min})$ is computed as follows:

$$\begin{cases} Threshold2(Num^k_{point}) = 0 & Initialization \\ Threshold2(Num^k_{point}) = Threshold2(Num^k_{point}) + 0 & if\ D^2_{threshold} > A^{i,j,k}_{change} \\ Threshold2(Num^k_{point}) = Threshold2(Num^k_{point}) + 2 & if\ D^2_{threshold} \leq S^{i,j,k}_{change} \end{cases} \quad (4.6)$$

where $D^2_{threshold}$ represents the pre-setting value of the threshold two; $A^{i,j,k}_{change}$ represents the angle change between the line, which connecting two adjacent points $Point^i$ and $Point^{i+1}$ on the intersection curve $C^j$ for $Thickness(T^k_{min})$, and the rotating centre axis. It can be calculated by Formula (4.2) as shown in 4.2.1.2 section.

In order to get the adaptive slicing thickness for each slicing layer of the complex biomedical model, a flow of the smart adaptive slicing strategy is shown in Figure 4.7

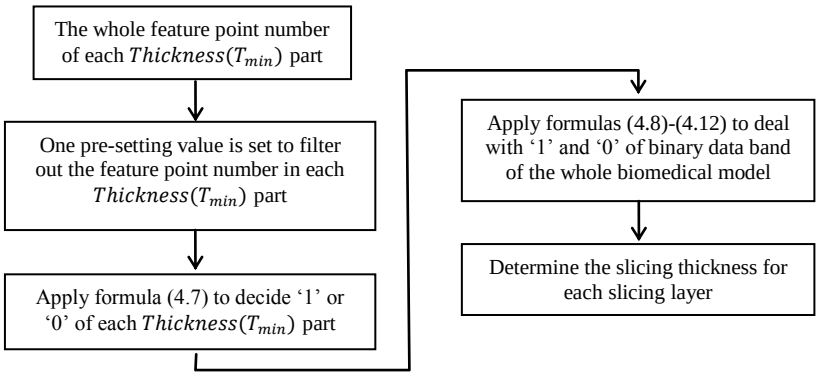


**Figure 4.7** The main flow of the smart adaptive slicing strategy.

The value of '1' and '0' for each $Thickness(T_{min})$ part of the biomedical model can be calculated below:

$$\begin{cases} Layer_{min}^{k} = 0 & if\ Threshold\left(Num_{point}^{k}\right) > Whole\left(Num_{point}^{k}\right) \\ Layer_{min}^{k} = 1 & if\ Threshold\left(Num_{point}^{k}\right) \leq Whole\left(Num_{point}^{k}\right) \end{cases} \quad (4.7)$$

where $Layer_{min}^{k}$ represents the number $k$ $Thickness(T_{min})$ part; $Threshold\left(Num_{point}^{k}\right)$ represents the setting value to filter out the feature point number.

Based on the above research, one binary data band can be obtained for the whole biomedical model such as: "11100010…0001010". Each "0" and "1" in this binary data band represents for one $Thickness(T_{min})$ part. If $Layer_{min}^{k} = 1$, which means the outside surface of the number $k$ $Thickness(T_{min})$ is of more complexity, the thickness of slicing layer should be smaller to protect feature characteristics and to improve geometrical accuracy of fabrication; If $Layer_{min}^{k} = 0$, which means the outside surface of the number $k$ $Thickness(T_{min})$ is of less complexity, the thickness of slicing layer should be bigger to reduce build time of fabrication. The following formula was used to deal with the binary data band. The adaptive slicing thickness of each slicing layer can be calculated below:

$$Q = \frac{Thickness(T_{max})}{Thickness(T_{min})},\ and\ V \leq Q \quad (V\ and\ Q\ are\ postive\ integer) \quad (4.8)$$

(1) if the value of the number $k$ $Thickness(T_{min})$ part is '1', the slicing thickness of the layer can be calculated as follows:

$$T_{thickness}^{t} = Thickness(T_{min}), \qquad if\ Layer_{min}^{k} = 1 \tag{4.9}$$

(2) if the value of the number k $\mathrm{Thickness}(\mathrm{T_{min}})$ part is '0', and the values of next '$\mathrm{Q-1}$' $\mathrm{Thickness}(\mathrm{T_{min}})$ part are all '0', the slicing thickness of the layer can be calculated as follows:

$$T_{thickness}^{t} = Q * Thickness(T_{min}), \quad if\ Layer_{min}^{k+i} = 0\ , and\ \mathrm{i} \in 0,1,\dots,Q-1 \tag{4.10}$$

(3) if the value of the number k $\mathrm{Thickness}(\mathrm{T_{min}})$ part is '0', and the values of next '$\mathrm{V-2}$' $\mathrm{Thickness}(\mathrm{T_{min}})$ part are all '0', and the value of the number '$\mathrm{V-1}$' $\mathrm{Thickness}(\mathrm{T_{min}})$ part is '1', the slicing thickness of the layer can be calculated as follows:

$$T_{thickness}^{t} = V * Thickness(T_{min}),$$
$$if\ Layer_{min}^{k+i} = 0 \cap Layer_{min}^{k+V-1} = 1, and\ \mathrm{i} \in 0,1,\dots,V-2 \tag{4.11}$$

(4) if the value of the number k $\mathrm{Thickness}(\mathrm{T_{min}})$ part is '0', and the values of next '$\mathrm{V-2}$' $\mathrm{Thickness}(\mathrm{T_{min}})$ part are all '0', and the value of the number '$\mathrm{V-1}$' $\mathrm{Thickness}(\mathrm{T_{min}})$ part is not exist, the slicing thickness of the layer can be calculated as follows:

$$T_{thickness}^{t} = V * Thickness(T_{min})$$
$$if\ Layer_{min}^{k+i} = 0 \cap Layer_{min}^{k+V-1} = "N/A"\ , and\ \mathrm{i} \in 0,1,\dots,V-2 \tag{4.12}$$

### 4.2.2 Phase 3 – Geometrical accuracy and build time control strategies

Based on the above research and the developed geometrical accuracy and build time analysis modules, a user can balance the geometrical accuracy and build time of

fabricating for biomedical model in RP/M by control the value of the two thresholds. Figure 4.8 shows the relationship between the two thresholds, geometrical accuracy and build time. By changing the value of the two thresholds, the results of the geometrical accuracy and the build time will be changed. By choosing the right threshold values the performance in terms of geometrical accuracy and effectiveness can be improved significantly. In the example of Figure 4.9, the value of the threshold one ($D^1_{threshold}$) is incrementally changed, and the balance of the build time and geometrical accuracy can be obtained through the comparison of the all computation results. In the following section, some discussions have been made to analyze the relationship with data from two case studies of complex biomedical models.

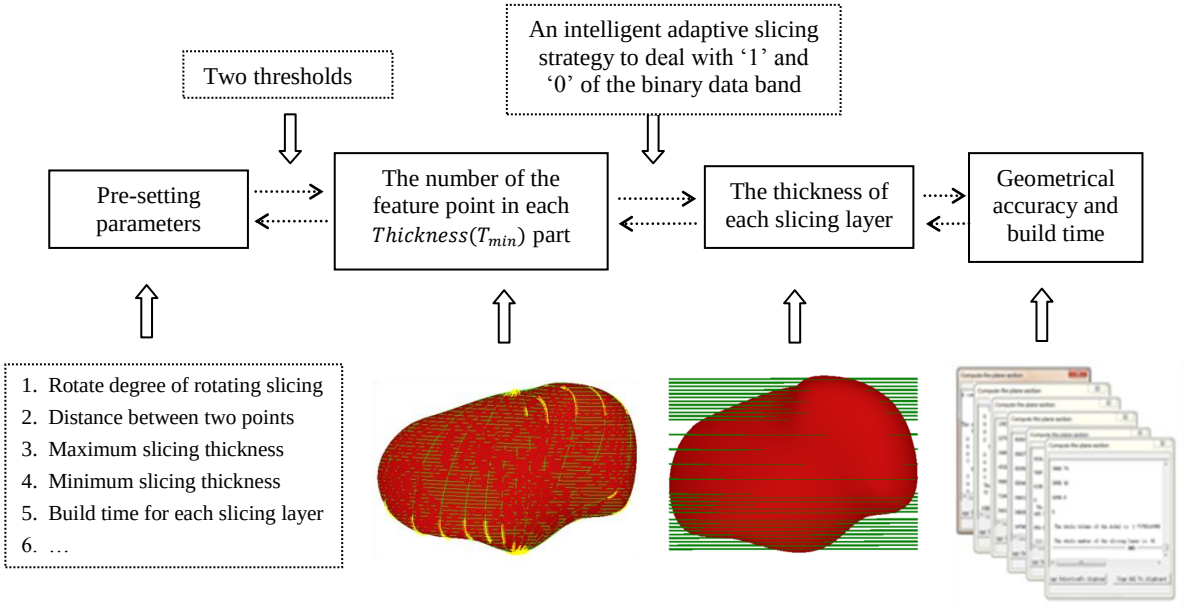


**Figure 4.8** The relationship between the thresholds and geometrical accuracy and build time.

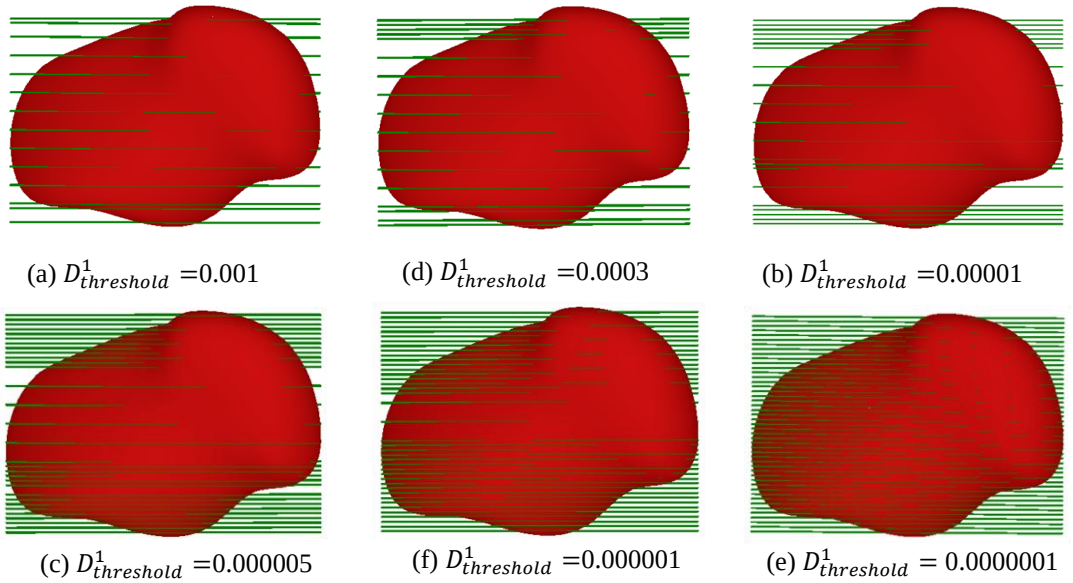


**Figure 4.9** The adaptive slicing of the biomedical model with the different value of the threshold one ($D^1_{threshold}$).

## 4.3 Case studies

Two biomedical bone models were tested to validate the effectiveness and robustness of the developed adaptive slicing approaches. The minimum and maximum thickness of the slicing was defined as 1.0mm and 4.0mm respectively, and the rotated angle of the intersection surface is set as 30 degree. The distance between two points is set as 0.5mm. The build time of each slicing layer is supposed as one minute. ($Thickness(T_{min}) = 1.0\text{mm}$; $Thickness(T_{max}) = 4.0\text{mm}$; $R_{angle} = 30°$; $Distance(Point^i, Point^{i+1}) = 0.5mm$). All results were obtained in a Pentium Dual-Core CPU 2.10GHz, 2GB RAM system.

### 4.3.1 Case study 1 – a navicular bone model

A navicular bone model was used to validate the research. The length, width, height and volume of the model are 67.1379mm, 52.7243mm, 48.0909mm and 54487.2mm$^3$ respectively. The process for the directly slicing with the minimum slicing thickness,

rotating slicing, discrete points generation with same distance and feature points pass the two thresholds, and finial determine the slicing thickness for each layer are shown in Figure 4.10 The threshold two is set as 78.46 degree; The value of threshold one is incrementally changed (shown in Figure 4.9). The result of the volume for the each slicing layer, and the whole fabrication volume and build time of the biomedical model are shown in Table 4.2. Table 4.3 shows the results of build time and geometrical accuracy for the threshold one from 0.001mm until 0.0000001mm. The geometrical accuracy percentages can be calculated based on the formula 3.21 in Section 3.3. It can be observed that the smaller the $Threshold(D^1_{threshold})$ is, the more slicing layers of the biomedical model, and the higher the geometrical accuracy is, and the more build time is.

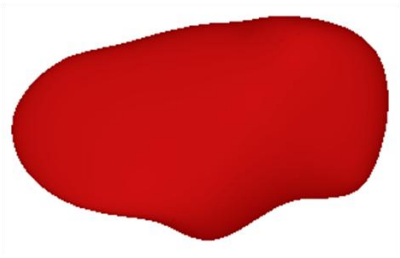

(a) A navicular bone model

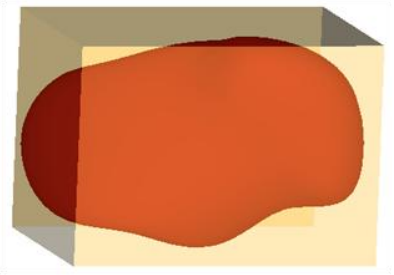

(b) An enveloping box

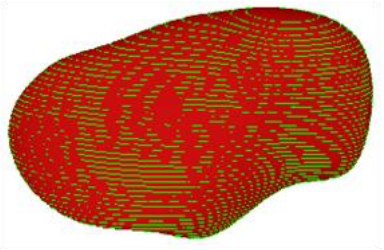

(c) Slicing with minimum thickness slicing

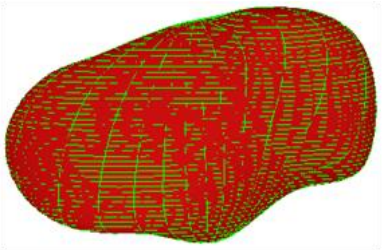

(d) Rotating slicing and intersection curves

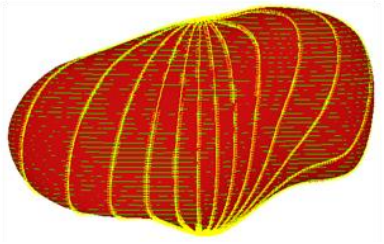

(e) The generated discrete points on the intersection curves

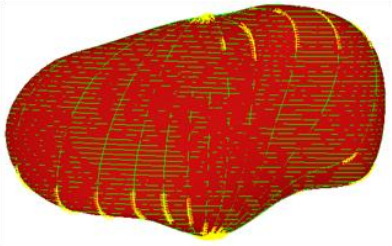

(f) Feature points passing the threshold one

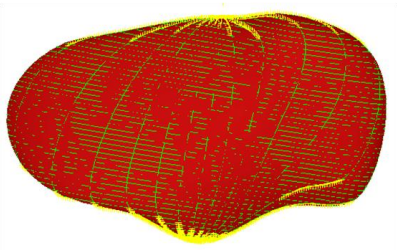

(g) Feature points passing the threshold two

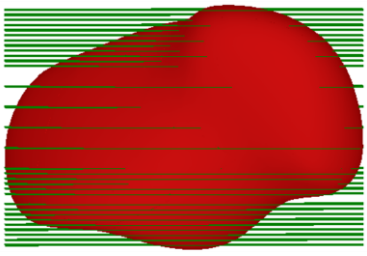

(h) Adaptive slicing the navicular model

**Figure 4.10** The process of the developed approach for the navicular model.

**Table 4.2** The volume and bi-data for each layer of the navicular model.

| No. | Volume | Bi- data | No. | Volume | Bi- data | No. | Volume | Bi- data | No. | Volume | Bi- data |
|---|---|---|---|---|---|---|---|---|---|---|---|
| 1 | 0 | 1 | 16 | 1562.03 | 0 | 31 | 1577.31 | 0 | 46 | 370.757 | 0 |
| 2 | 84.993 | 1 | 17 | 1621.55 | 0 | 32 | 1538.46 | 0 | 47 | 251.482 | 1 |
| 3 | 176.014 | 1 | 18 | 1677.73 | 0 | 33 | 1486.81 | 0 | | | |
| 4 | 268.823 | 1 | 19 | 1697.96 | 0 | 34 | 1429.57 | 0 | | | |
| 5 | 373.661 | 1 | 20 | 1716.76 | 0 | 35 | 1378.29 | 0 | | | |
| 6 | 556.321 | 1 | 21 | 1739.17 | 0 | 36 | 1322.54 | 1 | | | |
| 7 | 650.804 | 1 | 22 | 1744.06 | 0 | 37 | 1247.38 | 1 | | | |
| 8 | 760.737 | 1 | 23 | 1750.81 | 0 | 38 | 1169.15 | 1 | | | |
| 9 | 862.305 | 1 | 24 | 1740.54 | 0 | 39 | 1085.27 | 1 | | | |
| 10 | 960.71 | 1 | 25 | 1732.59 | 0 | 40 | 1001.82 | 1 | | | |
| 11 | 1063.38 | 1 | 26 | 1710.10 | 0 | 41 | 913.459 | 1 | | | |
| 12 | 1185.01 | 1 | 27 | 1705.41 | 0 | 42 | 820.185 | 1 | | | |
| 13 | 1308.19 | 1 | 28 | 1679.86 | 0 | 43 | 721.095 | 1 | | | |
| 14 | 1414.3 | 1 | 29 | 1643.30 | 0 | 44 | 614.369 | 1 | | | |
| 15 | 1502.13 | 1 | 30 | 1607.94 | 0 | 45 | 498.676 | 1 | | | |

The totally volume of fabrication is: ***51238.1mm$^3$***

The build time of fabrication is : ***33minutes***

**Table 4.3** Comparison of computational results of different threshold one for the navicular model.

| Threshold one -$D^1_{threshold}$(mm) | 0.001 | 0.0005 | 0.0001 | 0.00005 | 0.00001 | **0.000005** | 0.000003 | 0.000001 | 0.0000001 |
|---|---|---|---|---|---|---|---|---|---|
| Build time (mint) | 19 | 20 | 22 | 23 | 28 | **33** | 36 | 45 | 46 |
| Volume(mm$^3$) | 48900.1 | 49175.2 | 49450.1 | 49831.6 | 50947.2 | **51238.1** | 51582.7 | 52282.9 | 52302.6 |
| Geometrical accuracy (%) | 89.75 | 90.25 | 90.76 | 91.46 | 93.50 | **94.04** | 94.67 | 95.95 | 95.99 |

### 4.3.2 Case study 2 – a calcaneus bone model

The second biomedical model is a calcaneus model. The length, width, height and volume of the model are 71.9052mm, 51.9091mm, 45.6315mm and 62649.8mm$^3$ respectively. Figure 4.11 shows the process and geometrical results with the developed approach. The results of the volume for the each slicing layer, and the whole fabrication volume and build time of the model are shown in Table 4.4 Build time and geometrical accuracy of the fabrication with different value of threshold one is shown in Table 4.5.

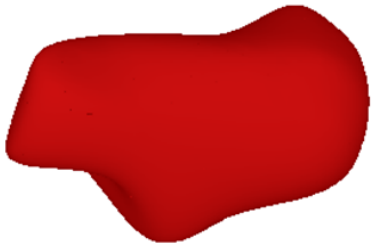

(a) A biomedical model

(b) An enveloping box

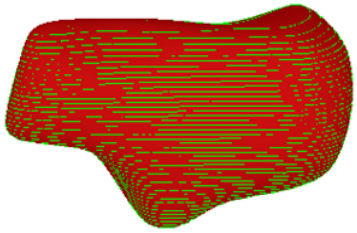

(c) Directly slicing with minimum thickness slicing

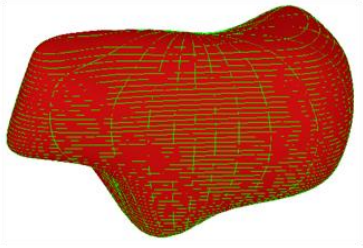

(d) Rotating slicing and intersection curves

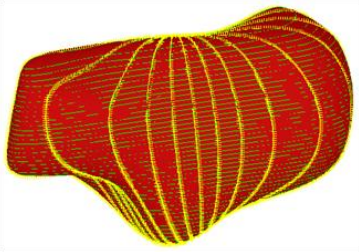

(e) The generated discrete points on the intersection curves

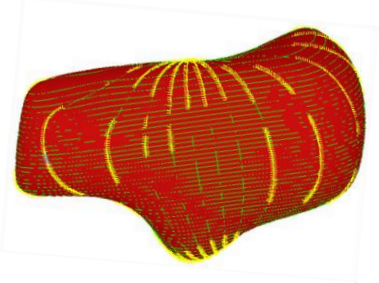

(f) Feature points pass the threshold one

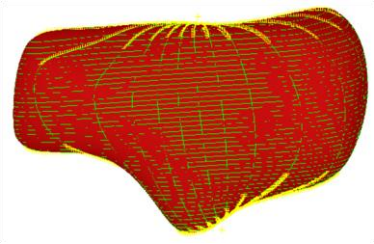

(g) Feature points passing the threshold two

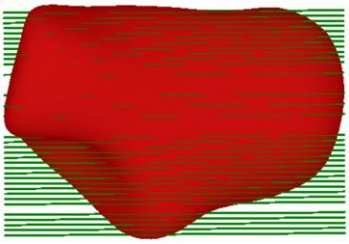

(h) Adaptive slicing the model

**Figure 4.11** The process of the developed approach for the calcaneus model.

**Table 4.4** The volume and bi-data for each layer of the calcaneus model.

| No. | Volume | Bi- data | No. | Volume | Bi- data | No. | Volume | Bi- data | No. | Volume | Bi- data |
|---|---|---|---|---|---|---|---|---|---|---|---|
| 1 | 0 | 1 | 12 | 1064.75 | 1 | 23 | 2102.52 | 0 | 34 | 1963.11 | 1 |
| 2 | 50.83 | 1 | 13 | 1171.52 | 1 | 24 | 2124.39 | 0 | 35 | 1912.65 | 1 |
| 3 | 104.56 | 1 | 14 | 1268.76 | 1 | 25 | 2138.96 | 0 | 36 | 1853.78 | 1 |
| 4 | 160.13 | 1 | 15 | 1359.47 | 1 | 26 | 2145.86 | 0 | 37 | 1782.24 | 1 |
| 5 | 221.25 | 1 | 16 | 1444.04 | 1 | 27 | 2144.18 | 0 | 38 | 1693.65 | 1 |
| 6 | 294.34 | 1 | 17 | 1522.94 | 1 | 28 | 2139.19 | 0 | 39 | 1601.33 | 1 |
| 7 | 393.02 | 1 | 18 | 1597.66 | 1 | 29 | 2125.61 | 0 | 40 | 1507.03 | 1 |
| 8 | 532.48 | 1 | 19 | 1670.48 | 0 | 30 | 2104.92 | 0 | 41 | 1395.87 | 1 |
| 9 | 684.27 | 1 | 20 | 1751.47 | 0 | 31 | 2078.45 | 0 | 42 | 1244.48 | 1 |
| 10 | 824.58 | 1 | 21 | 1976.05 | 0 | 32 | 2043.71 | 1 | 43 | 1074.55 | 1 |
| 11 | 951.17 | 1 | 22 | 2059.03 | 0 | 33 | 2002.57 | 1 | 44 | 859.173 | 1 |

The totally volume of fabrication is: ***58914.6mm3***
The build time of fabrication is : ***36minutes***

**Table 4.5** Comparison of computational results of different threshold one for the calcaneus model.

| Threshold one - $D^1_{threshold}$(mm) | 0.001 | 0.00005 | 0.00003 | **0.00001** | 0.000003 | 0.000001 | 0.0000005 | 0.0000003 | 0.0000001 |
|---|---|---|---|---|---|---|---|---|---|
| Build time (mint) | 24 | 26 | 29 | **36** | 39 | 41 | 42 | 43 | 45 |
| Volume($mm^3$) | 56416.2 | 56921.5 | 57588.8 | **58914.6** | 59147.5 | 59461.6 | 59488.1 | 59502.9 | 59537.2 |
| Geometrical accuracy (%) | 90.05 | 90.86 | 91.92 | **94.04** | 94.41 | 94.91 | 94.95 | 94.98 | 95.03 |

## 4.4 Geometrical Accuracy and Build Time Analysis and Control

The two biomedical bone models (shown above in Figure 4.10-4.11) were also used for geometrical accuracy and build time analysis with different value of the thresholds. Figure 4.12 shows the results between various change with an incremental from 0.0000001mm until 0.001mm of threshold one. Table 4.6 shows the change results between the build time and geometrical accuracy with different value of the threshold one. All results were obtained in a Pentium Dual-Core CPU 2.10GHz, 2GB RAM system.

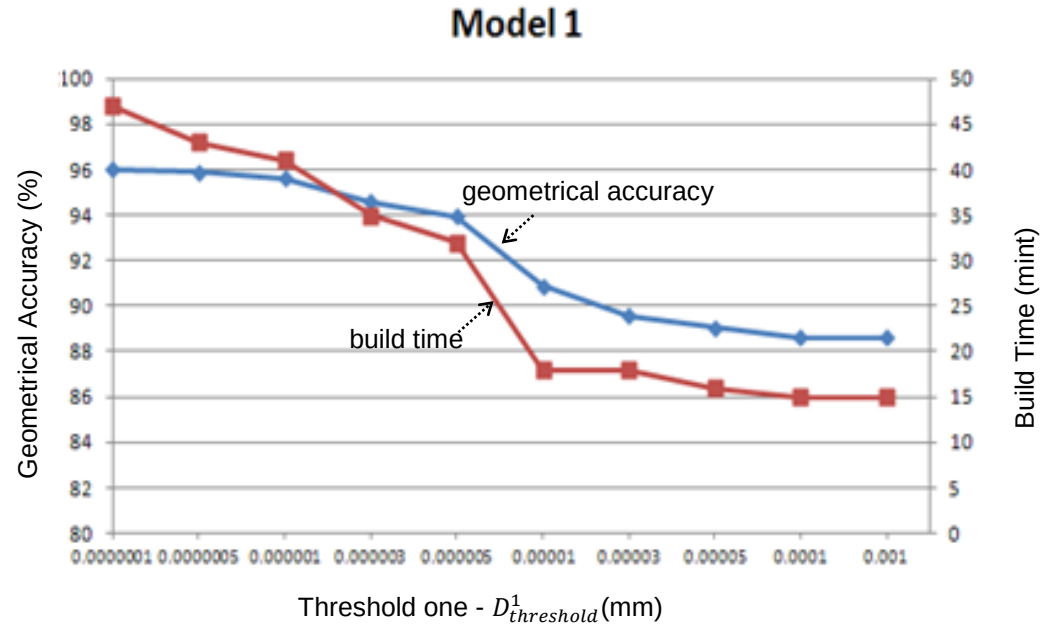


(a) a navicular bone model

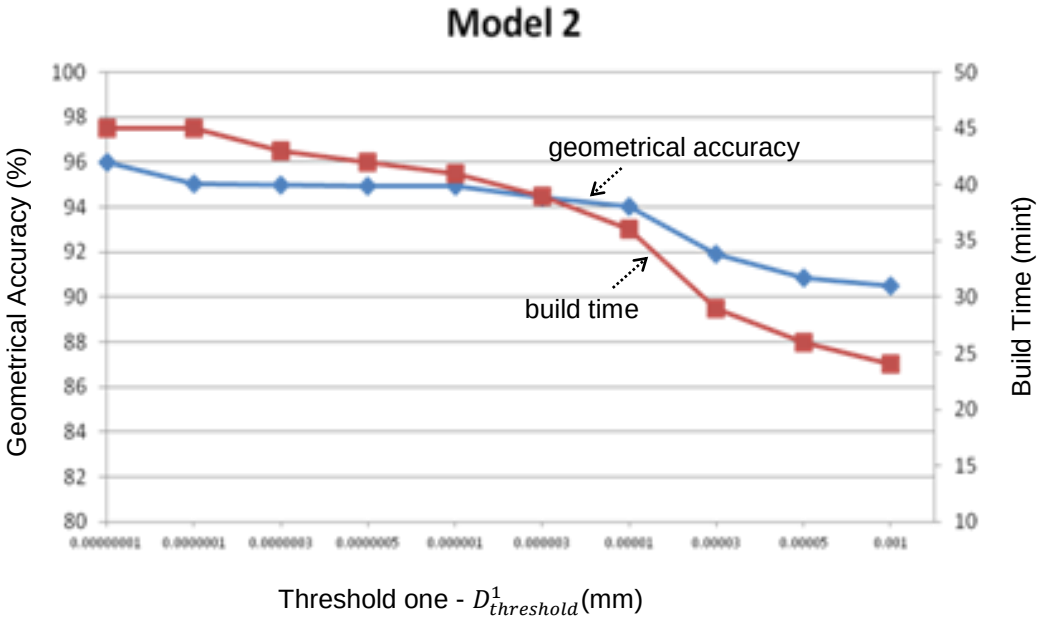


(b) a calcaneus bone model

**Figure 4.12** The results of geometrical accuracy and build time with different value of threshold one.

**Table 4.6** The change results of the different value of threshold one.

| Model | $D^1_{threshold}$ (mm) | Added build time (minutes) | Change of geometrical accuracy (%) |
|---|---|---|---|
| Model one | 0.001 ~ 0.000005 | 14 | 4.29 |
| | 0.000005 ~ 0.0000001 | 13 | 1.95 |
| Model two | 0.001 ~ 0.00001 | 12 | 3.99 |
| | 0.00001 ~ 0.00000001 | 9 | 0.99 |

From the above data, it can be observed that there are linear relationships between the geometrical accuracy, build time and the value of two thresholds. For instances, based on the Figure 4.12, if a user would like to fabricate the model one (shown in Figure 4.10) with about 94% geometrical accuracy, the values of two thresholds can be set as 0.000005mm and 78.46 degree ($D^1_{threshold} = 0.000005mm;\ D^2_{threshold} = 78.46\ \text{degree}$) to obtain each slicing thickness of the whole model. Meanwhile, if a user would like to fabricate the model with about 29 minutes, the values of two thresholds can be set as 0.00003mm and 78.46 degree ( $D^1_{threshold} = 0.00035mm;\ D^2_{threshold} = 78.46\ \text{degree}$ ) to obtain each slicing thickness. In addition, based on the Table 4.6, a user can improve the geometrical accuracy about 4.29% (the build time added about 14 minutes) by changing the value of threshold one from 0.001mm to 0.000005mm for model one. Furthermore, by changing the value of threshold one from 0.000005mm to 0.0000001mm, the geometrical accuracy only improve 1.95%, which is about half of 4.29% as above (but the build time still need added about 13 minutes, which is almost the same of 14 minutes as above).

Based on the above analysis, it is obvious that the developed approach provides an effective guideline for a user to balance the geometrical accuracy and build efficiency for complex biomedical model fabrication of RP/M, and can achieve significant improvement of geometrical accuracy and build efficiency by choosing the right threshold values.

## 4.5 Summary

In this chapter, a novel adaptive slicing approach has been developed with a series of algorithms and strategies to balance the geometrical accuracy and build efficiency of fabrication in RP/M. The major features of this research are as follows:

(5) The developed adaptive slicing thickness determination algorithms and strategies can be used to decide the thickness of each slicing layer to balance geometrical accuracy and build efficiency of fabrication of complex biomedical models in RP/M system.

(6) The developed geometrical accuracy and build time control strategy can used to control the geometrical accuracy and build time by verifying the value of the two thresholds. It provides an effective guideline for a user to control and optimise the geometrical accuracy and build efficiency during RP/M processing by choosing the right threshold values.

(7) Two complex biomedical models were used to illustrate the developed adaptive slicing approach, which can achieve significantly improved performance in terms of geometrical accuracy and effectiveness of fabrication for complex biomedical models in RP/M.

# CHAPTER 5

# ADAPTIVE RP/M FOR FGM-BASED BIOMEDICAL MODELS

## 5.1 Introduction

Recent advances in material engineering and manufacturing technologies have brought enormous innovation opportunities in product development. A forefront research and development issue is to rapidly fabricate heterogeneous material-based products with varied material compositions and distributions. A typical example is FGM-based products, which have shown broad potentials in various applications such as biomedical, automotive, aerospace, energy, civil, nuclear and naval engineering (Miyamoto et al., 1999; Pompe et al., 2003; Kieback et al., 2003; Watari et al., 2004; Cannillo et al., 2007). Different from homogenous materials, FGM objects contain spatial and gradual variations in composition from two or more materials for stress concentration avoidance and a better local control of thermal, structural, electrical or functional properties. An example of FGM-based model is illustrated in Figure 5.1**.**

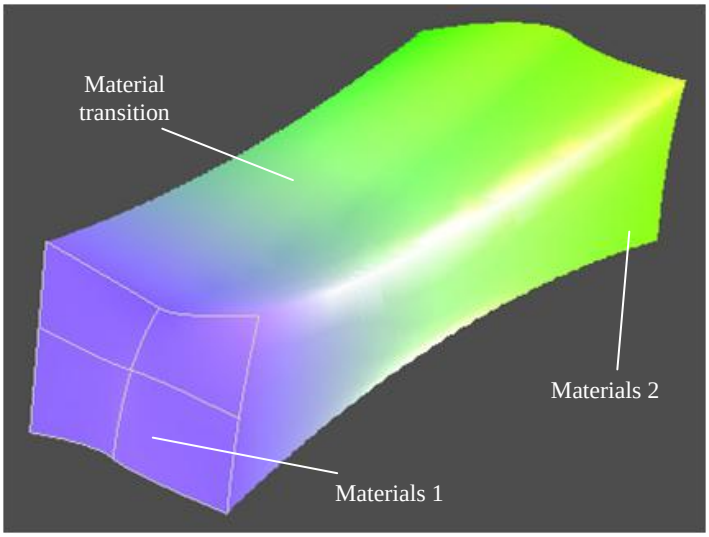


**Figure 5.1** An example of FGM-based model.

The concept of FGM was initially proposed in 1984-85 when Japanese researchers developed advanced materials in an aerospace project (Miyamoto et al., 1999). Owing to the requirement to meet the significant temperature difference between inside and outside of a space plane, in which the body of the space plane will be exposed to the environment with approximately 1700°C and the inside temperature is gradient to approximately 1000°C, there was no uniform and homogeneous material able to endure such conditions. The researchers designed FGM objects by gradually changing the material composition, and in this way both thermal resistance and mechanical properties were improved. Therefore, by adopting such heterogeneities, the advantages of various materials can be fully exploited and some conflicting functional requirements can be alleviated. Meanwhile, functional gradation is an important characteristic of living organisms, and FGM objects can mimic such gradient so that the concept of FGM brings potentials to new biomedical product development (Pompe et al., 2003; Kieback et al., 2003; Watari et al., 2004). For instance, a natural bone has been evolved as a FGM-based structure consisting of various materials (e.g., principle proteins, collagen, glycoproteins, protein-polysacchrides, calcium phosphate, etc.) to meet multiple mechanical and biological requirements, such as structural integrity, strength, transport, and ideal micro-environment for cell and tissue in-growth (Burstein and Wright, 1994; Fang, 2005). As thus, it becomes more important to apply the concept of FGM in bone implant design.

More than 2500 surgical operations to incorporate graded hip implants have been successfully performed in Japan over 20 years. The graded implants enable a strong bond between Titinium (Ti) implants, bone cement, Hydroxyapatite (HAp) and bone. Another example is the development of FGM Ti/HAp-based artificial teeth, in which pure Ti is at one end achieving excellent mechanical properties, increasing the composition concentration of HAp towards 100% at the other end to be more appetitive for the lower part implanted inside the jaw bone.

However, the extraordinary characteristics of FGM objects have not been fully leveraged in new biomedical product development. Some major technical barriers include:

- The current CAD systems have been developed mainly for homogenous material-based product modelling. It is desired to develop FGM-based design features and

data structures compatible and integrative to the current CAD systems so as to take advantage of the knowledge, best practices and simulation methods developed in the CAD systems. Apart from the representation of regular product shapes, the new design features are also expected to be extensible and adaptive to represent more complex shapes such as biomedical models and products.

- Manufacturing technologies of FGM objects are essential because FGM-based biomedical models need to be not only theoretically correct in design but also realizable in manufacturing. In recent years, the RP/M technology has been increasingly used in FGM applications. The driver is that RP/M is based on a layer-based additive process so that it is flexible to prototype or rapidly fabricate products with complex material and structural heterogeneities such as some biomedical models and products. Considering the characteristics of FGM-based products, an important research issue is how to develop more efficient and adaptive RP/M algorithms and strategies to support the realizable, customized and free-form FGM-based biomedical models fabrication in RP/M systems.

In this chapter, research results to address the above challenges are presented. Firstly, directly slicing and closed NURBS curve was used to represent the outside contour curve of the sliced layer of FGM-based biomedical model. Secondly, FGM-based features have been proposed to present each sliced layer of FGM-based biomedical model. Thirdly, mixed tool-path generation and speed optimisation algorithms, which were introduced in the chapter 3, have been applied to generate contour/offset and zigzag tool-paths for the different materials of the biomedical model and balance the build time and geometrical accuracy of fabrication. Finally, based on the developed geometrical accuracy and build time analysis modules, several case studies of FGM-based biomedical models have been used to verify and demonstrate the performance of this research in terms of algorithm effectiveness and robustness.

## 5.2 Developed adaptive RP/M approach for FGM-based biomedical models

The developed algorithms and strategies for the FGM-based biomedical models in the RP/M process planning are shown in Figure 5.2, which consists of three phases:

Phase 1: The directly slicing process and NURBS-based contour curve representation of each sliced layer of FGM-based biomedical model

Phase 2: The FGM features representation of each sliced layer of FGM-based biomedical model

Phase 3: The mixed tool-path generation and adaptive speed algorithm of the RP/M nozzle/print head for FGM-based biomedical models

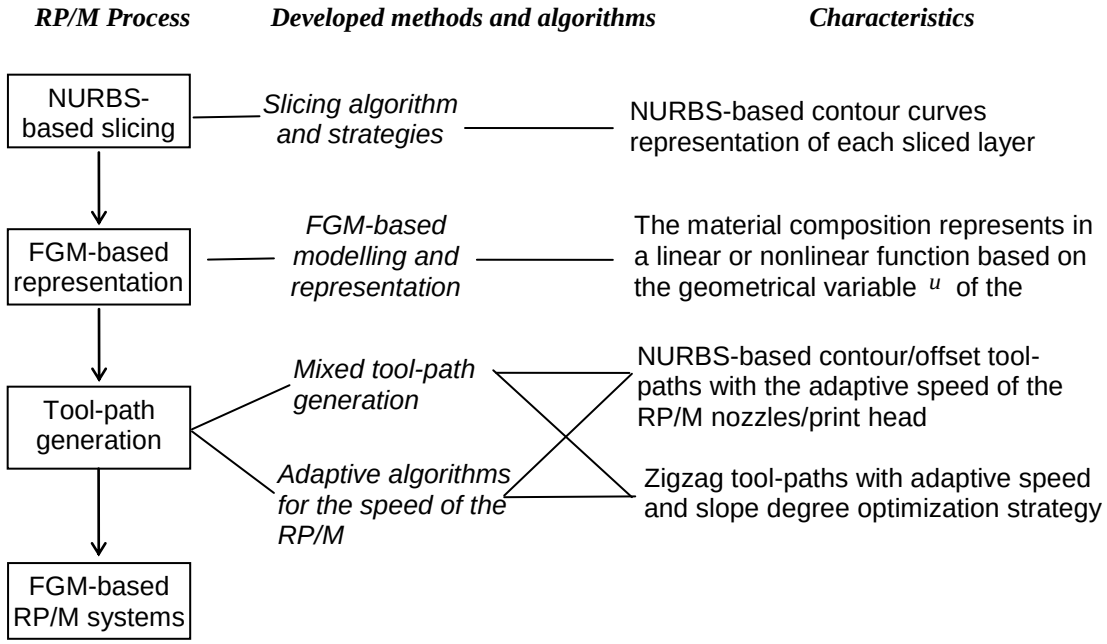


**Figure 5.2** The algorithms and strategies for RP/M processing of FGM-based biomedical models.

## 5.3 FGM-based representation of sliced layer

NURBS is effective to represent regular and non-regular (e.g., free-form) geometrical shapes so that it has been popularly used in modern CAD systems. The directly slicing

process and NURBS-based curve representation of biomedical model has been detailed introduced in chapter 3. After the directly slicing algorithm and strategy, a closed NURBS curve can be generated to represent the contour of each sliced layer of biomedical model (shown in Figure 5.3).

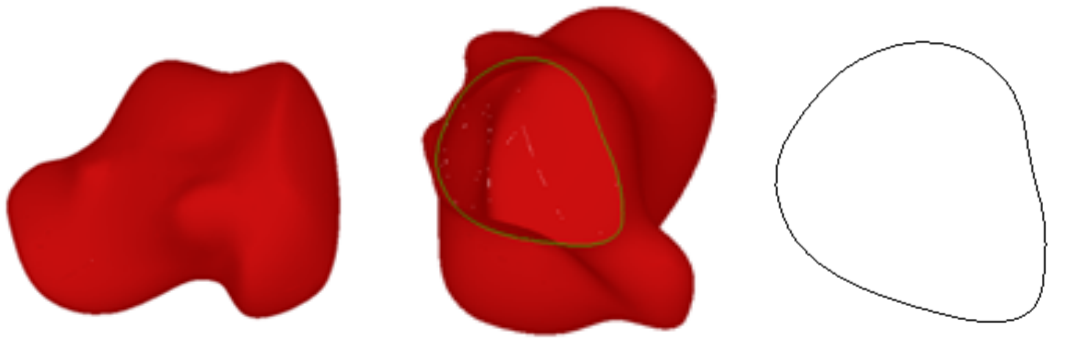

(a) A calcaneus model (b) Directly slicing (c) NURBS representation of the sliced layer

**Figure 5.3** Direct slicing and NURBS representation for one layer.

In this chapter, the NURBS geometrical representation is introduced to represent FGM-based biomedical models of each sliced layer (shown in Figure 5.4). In the RP/M technology, a FGM-based layer $F$ can be symbolically described as:

$$F = (P_g, P_m) \tag{5.1}$$

where $P_g$ is the geometrical domain of the layer; $P_m$ is the material domain of the layer.

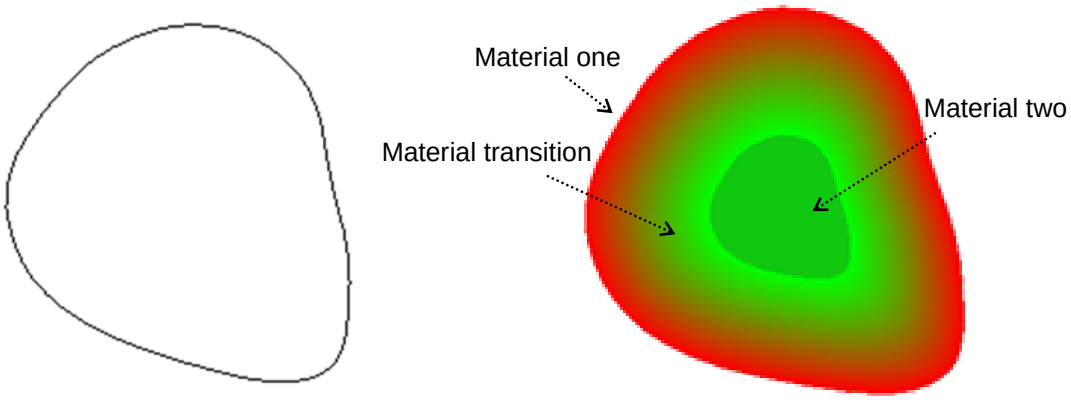


(a) NURBS representation of one layer

(b) FGM-based feature representation of the sliced layer

**Figure 5.4** FGM-based feature representation of the sliced layer.

The most widely used FGM representation method for a layer is the inverse distance-based weighting function (Siu and Tan, 2002; Biswas et al., 2004). In the method, the concept of a "material grading source" has been introduced as the origin of a single material. The material composition from several FGM grading sources at a specific point $P$ can be computed using the following formulas. A specific case is that a FGM could be from the same material but with different densities.

$$P_m(P) = \sum_{i=1}^{n} w(d_i) S_i \qquad i = 1,2,...n \tag{5.2}$$

$$d_i = distance(P, S_i) \tag{5.3}$$

$$w(d_i) = \frac{\prod_{l=1, l\neq i}^{n} d_l}{\sum_{j=1}^{n} \prod_{l=1, l\neq j}^{n} d_l} \tag{5.4}$$

where $P_m(P)$ is the FGM composition associated with a point $P$; $S_i$ is the $i^{th}$ material grading source; $w(d_i)$ is the interpolation weight to the contribution of the $i^{th}$ material grading source according to the distance $d_i$; $d_i$ is the distance between a point $P$ and the $i^{th}$ material grading source.

The formulas are illustrated in Figure 5.5. There are two material grading sources $S_1$ and $S_2$; The distances between an internal point $P$ and $S_1$ / $S_2$ are $d_1$ / $d_2$ respectively; Two weights to $S_1$ and $S_2$ are $w(d_1)$ and $w(d_2)$ respectively, which are computed to be $\frac{d_2}{d_1+d_2}$ and $\frac{d_1}{d_1+d_2}$ respectively according to Formulas (5.3)-(5.4); $P_m(P)=\frac{d_2}{d_1+d_2}M(S_1)+\frac{d_1}{d_1+d_2}M(S_2)$ according to Formula (5.2).

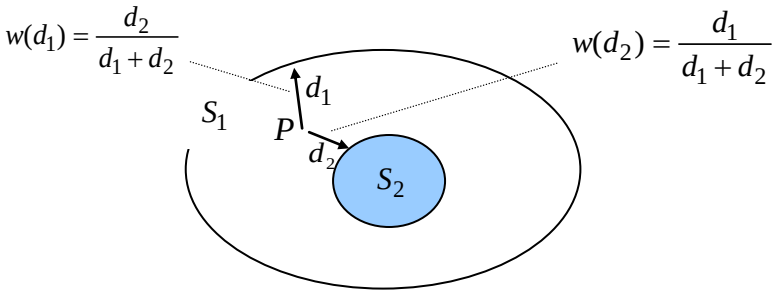


**Figure 5.5** An example of material composition from two material grading sources.

However, it is not efficient and flexible to use the distance function defined above to compute the material composition for each geometrical point. It is desirable to establish the relationship of the geometrical domain $P_g$ and the material domain $P_m$ to improve the computation processes of geometries and materials. With the purpose, the variables over the geometrical domain can be used to develop a material mathematical function so as to facilitate the computation of the material domain. For instance, the geometry of an internal curve interpolated based on the boundaries of $S_1$ and $S_2$ in Figure 5.6 is defined as: $P_g = f_g(u)$, where $u$ is the geometrical variable from the centre $C_1$ of $S_1$ to the centre $C_2$ of $S_2$. As thus, a curve having the same value of $u$ will have the same material composition generated from its material function $P_m$, and the computation efficiency will be improved. Based on the concept, a set of NURBS material features have been developed.

In this research, the material composition functions in the above Formulas (5.2)-(5.4) are refined here in a linear or non-linear means. In a case for a linear change with two material grading sources (it can be extended to more grading sources), the material composition functions have been redefined in the following Formulas (5.5)-(5.7). Based on a geometrical variable $u$ , a linear $P_m$ of the material domain across the geometrical domain is illustrated in Figure 5.7(a).

$$P_m = f_m(r_1(u), r_2(u)) \ , \ u \in [0,1] \tag{5.5}$$

$$r_1(u) = 1 - u \tag{5.6}$$

$$r_2(u) = u \tag{5.7}$$

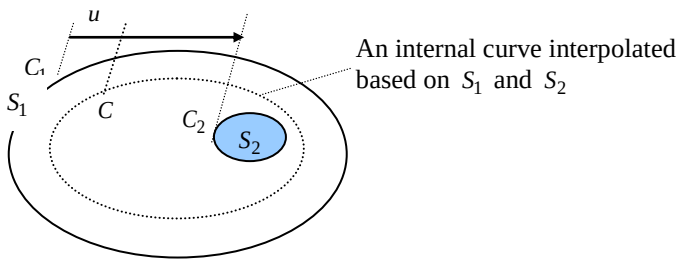


**Figure 5.6** The computation of the material composition based on geometrical variable.

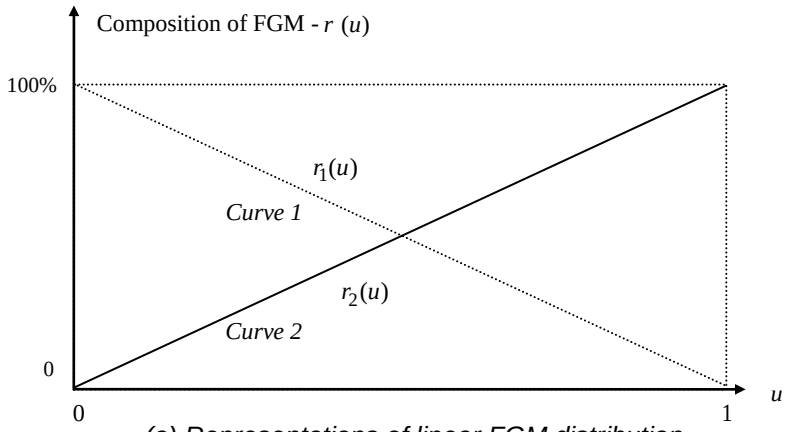


*(a) Representations of linear FGM distribution*

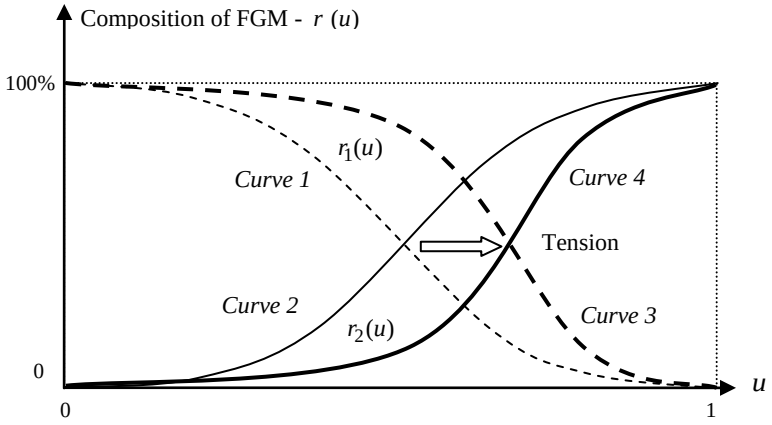


*(b) Representations of non-linear FGM distribution*

**Figure 5.7** Representations of linear and non-linear FGM distribution.

Sigmoid functions (S-Curves) have been developed here to represent the non-linear heterogeneity of the material composition and the distance from material grading sources. The functions are illustrated using Figure 5.7(b), in which it assumes there are two material grading sources 1 and 2 to build up the overall material composition and distribution of a product (it can be extended to more grading sources similarly). Curve 1 is a "standard" sigmoid function to represent the composition contribution of the material 1 $r_1(u)$ (from 100% to 0% from its source), and Curve 2 is mirrored from Curve 1 to represent the composition of the material 2. To develop a more flexible representation, a "tension" is incorporated to adjust the trend of the compositions of the materials 1 and 2 according to

users' design requirements (e.g., Curves 3 and 4). The following formulas have been developed for the above representation.

$$r_1(u) = 1 - \frac{1}{1 + e^{-C(-u+0.5+T)/Norm}} \tag{5.8}$$

$$r_2(u) = \frac{1}{1 + e^{C(-u+0.5+T)/Norm}} \tag{5.9}$$

where $C$ is an adjustable constant (for instance, it can be set as 5 here as a best practice); $T$ is an adjustable constant for the tension control; $Norm$ is the normalization value computed below:

$$Norm = 0.5 + T \tag{5.10}$$

Examples with several tension controlling parameters for $r_1(u)$ are plotted in Figure 5.8.

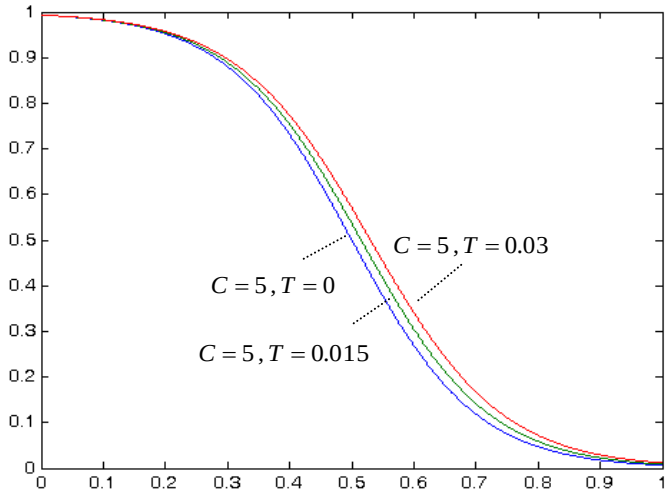


**Figure 5.8** $r_1(u)$ with different tensions is plotted.

A sliced layer of biomedical model can be defined as a surface with a pre-setting slicing thickness which can be formed along the manufacturing direction of RP/M process. The material composition and distribution of the sliced layer is characterized as interpolation gradation from one material grading source to another. For instance, Figure 5.9 represents a simple FGM feature of a sliced layer.

A NURBS surface defined in the following formula (5.11) is a relatively effective and ubiquitous means to represent regular and non-regular surface geometries.

$$S(u,v)=\sum_{i=0}^{n}\sum_{j=0}^{m}w_{j,i}N_{i,p}(u)N_{j,q}(v)P_{j,i} \tag{5.11}$$

where $u,v=[0,1]$; $w_{j,i}$ is the weight associated with control points $P_{j,i}$; $p,q$ are degrees in the $u$ and $v$ directions; $N_{i,p}$ and $N_{j,q}$ are defined similarly as above.

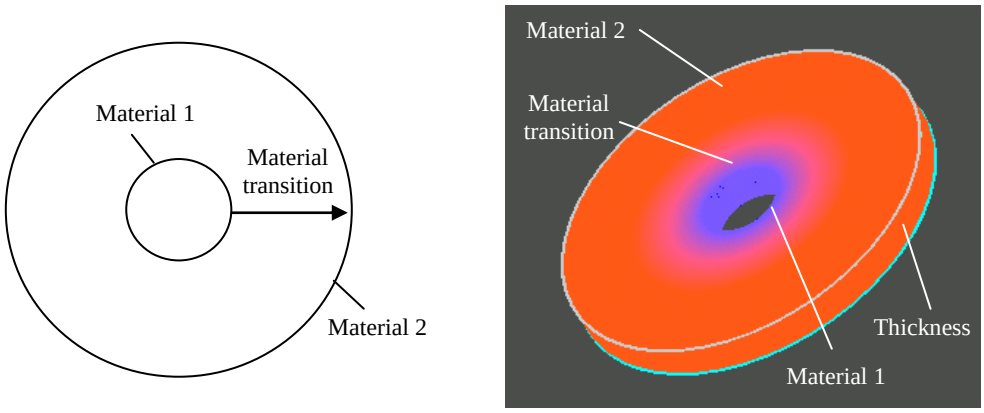


(a) A base sketch with FGM (b) A FGM-based sketch feature

**Figure 5.9** The example of a FGM-based sliced layer.

In Figure 5.10, the NURBS surface (e.g., a planar surface as a base sketch) has two material grading sources in its geometrical boundary curves along the $u$ direction. The material composition $P_m$ of each geometrical point in the surface can be computed using a linear or non-linear function in the formulas (5.5)-(5.10) based on the variable $u$ (the material gradual change is along the $u$ direction), and then the material composition is associated with the geometry of the point computed in the formula (5.11). A more efficient method has been developed with two assumptions that the NURBS curves in the $u$ direction to form the NURBS surface have the same number of control points and the weights associated with the corresponding control points are the same (i.e.,

$w_{0,i} = ... = w_{j,i} = ... = w_{m,i} = w_i$ (In fact, many NURBS surfaces use 1 for all their weights to simplify the computation). Therefore, the formula (5.11) will be re-defined below:

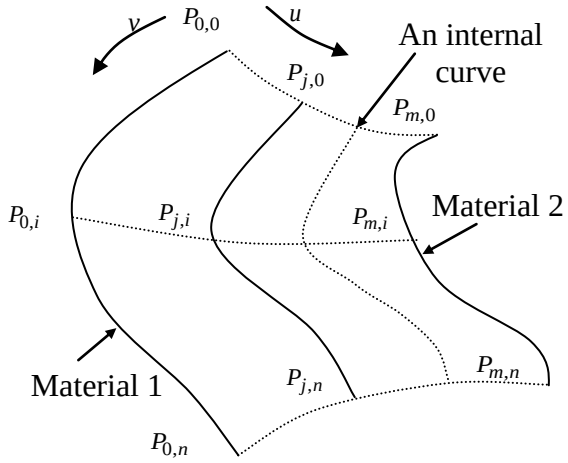


**Figure 5.10** A FGM-based NURBS surface.

$$C(u,v) = \sum_{i=0}^{n} w_i N_{i,p}(u)(\sum_{j=0}^{m} N_{j,q}(v) P_{j,i}) = \sum_{i=0}^{n} w_i N_{i,p}(u) P_i^{'} \tag{5.12}$$

For a value for the variable $u$ , it will therefore generate an internal curve with the same material composition. The geometry of an internal curve can be defined as a set of new control points $P_i^{'}$ according to (5.12). That is, material compositions will be associated with individual curves and further new control points. The efficiency of the method comes from avoiding point-based association between geometrical and material information, and the optimisation of the storage of data by introducing new control points to set up a parametric formula for internal curves in the same material composition.

## 5.4 Contour/offset and zigzag FGM-based tool-path generation

In the Chapter 3, there is a detailed description about contour/offset and zigzag tool-path generation for single material biomedical models. As FGM-based biomedical model is

consisted by more than one material, the materials distribution is a critical parameter for tool-path generation of FGM-based biomedical model.

The material composition and distribution of each sliced layer that introduced in the above section brings convenience to RP/M tool-path generation for FGM-based biomedical model. Each internal curve with the same material composition can be used as contour/offset tool-paths of the nozzle/print head of the RP/M system. In here, a mixed tool-path algorithm has been developed to generate contour/offset and zigzag tool-paths to meet both the geometrical and material requirements. The contour/offset tool-paths are used to fabricate the area along the boundary of each sliced layer to represent varying material composition and improve the geometrical accuracy of a model. The zigzag tool-paths are used to fabricate the interior area of a single material in the model to improve the efficiency of computing and processing (Shown in Figure 5.11).

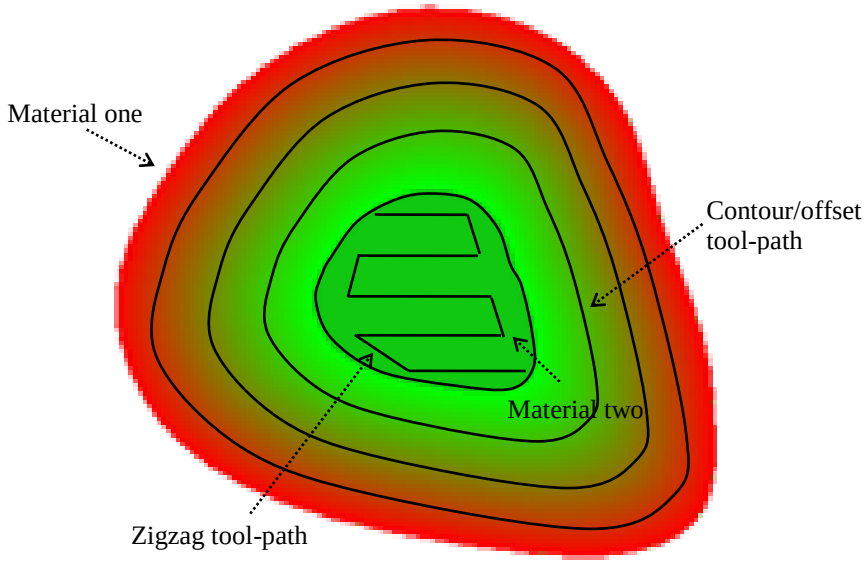


**Figure 5.11** Contour/offset and zigzag tool-paths generation for a FGM-based sliced layer.

Based on the central point of the control points of the generated NURBS contour curve in the above directly slicing algorithm, each control point for a new NURBS-based curve that offsets the contour curve (i.e., offset contour curve) is computed in the following:

$$C\_P^{k,j} = D + u \cdot (C\_P^{k,1} - D) \tag{5.13}$$

where $C\_P^{i,j}$ represents an offset contour curve in the $i^{th}$ layer; $D$ represents the geometric central point of the control points of the contour curve; $u$ is the variable to generate the new control points of the offset contour curve and used to calculate the material composition on the curve according to Formulas (5.5)-(5.12).

Once the contour or offset curves and related tool-paths have been generated, zigzag lines and tool-paths will be then generated to fabricate the internal area of a single material in the model to simplify computing and processing.

Then, based on the adaptive speed algorithms which include an algorithm to optimise the speed of the RP/M nozzle/print head along the contour/offset tool-paths, and an algorithm to obtain the best slope degree of the zigzag tool-paths to achieve the minimum build time of the tool-paths and developed geometrical accuracy and build time analysis modules, which has been introduced in Chapter 3, the build time and geometrical accuracy of FGM-based biomedical model can also be calculated and optimised.

## 5.5 Case studies and analysis

### *5.5.1 Case study I: Demonstration of the algorithms and the flow*

The algorithms in this research have been implemented in an Open CASCADE modelling and C++ programming environment (Open CASCADE, 2012). A bone model, created by CT scanning to obtain the cloud data and reconstructed as an IGES/IGS format model in CATIA V5™ with the QSR and DSE modules, has been tested to verify and validate the effectiveness and robustness of the developed research. The minimum and maximum speeds of the RP/M nozzle/print head have been set 10mm/s and 20mm/s respectively, and the acceleration of the nozzle/print head $20\mathrm{mm/s^2}$ ($\mathrm{V_{min}} = 10\mathrm{mm/s}; \mathrm{V_{max}} = 20\mathrm{mm/s}; \mathrm{a} = 20\mathrm{mm/s^2}$). Please note that the parameter setting in this research here is based on

simulation and the obtained results are preliminary. Optimised parameters need to be found out by more physical experiments and will be reported in future.

All results have been obtained in a system with a Pentium Dual-Core CPU 2.10GHz and 2GB RAM. The length, width, height and volume of the bone model are 108.76mm, 80.63mm, 68.342mm and 122432mm$^3$ respectively. The process for the NURBS-based contour/offset curve generation, FGM-based representation and the generation of contour/offset and zigzag tool-paths are shown in Figure 5.12. The result of the build time for the contour/offset tool-paths is shown in Table 5.1. For the zigzag tool-paths, different slope degrees in a layer can lead to different build times of tool-paths based on the developed adaptive speed algorithm in Chapter 3**.** Figure 5.13 shows the interpolated curve built based on different slope degrees. From the curve, it can be obtained that at 149.0 degree the build time of the zigzag tool-paths is the minimum (52.356 seconds). The total build time for the shown layer of the bone model is 158.852 seconds (build times of the contour/offset tool-paths + zigzag tool-paths = 106.456 seconds +52.356 seconds).

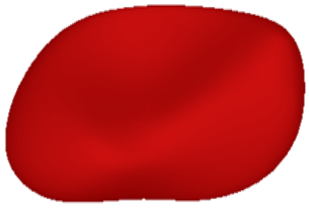

(c) The bone model

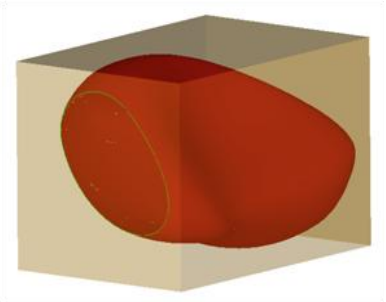

(b) The slicing layer

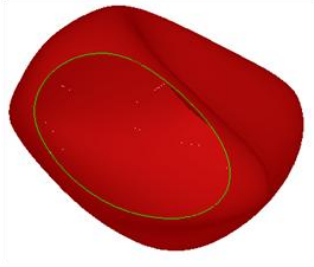

(c) The sliced model

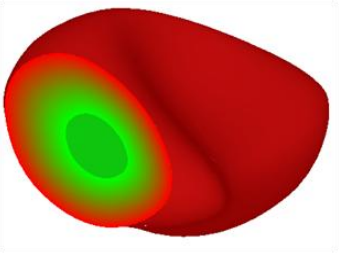

(d) The FGM representation for one layer

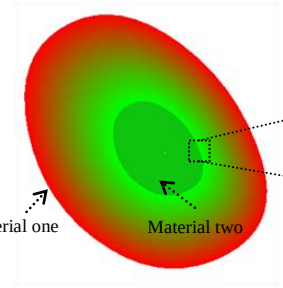


(e) The material distribution

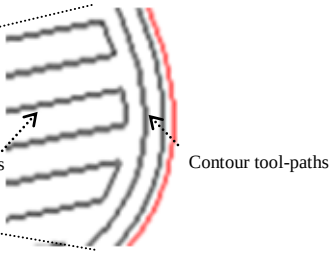


(f) The generated tool-paths for one layer

**Figure 5.12** Case Study I for a bone model.

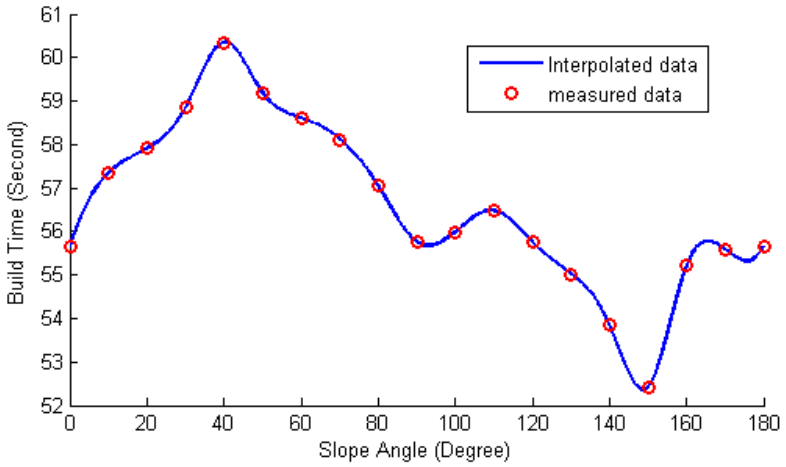


**Figure 5.13** The interpolated curve for the relation between the build times and slope degrees of zigzag tool-paths.

**Table 5.1** Build time of the contour/offset tool-paths for the bone model.

| Contour/offset tool-paths no. | 1 | 2 | 3 | 4 | 5 | 6 | 7 | 8 |
|---|---|---|---|---|---|---|---|---|
| Length (mm) | 295.394 | 269.260 | 245.521 | 224.203 | 209.291 | 196.762 | 184.311 | 174.970 |
| Build time (seconds) | 17.219 | 15.899 | 14.648 | 13.590 | 12.503 | 11.696 | 10.858 | 10.143 |

***Total build time for contour tool-paths = 106.456 (seconds)***

### *5.5.2 Case Study II: Benchmarking the efficiency and geometrical quality*

Three biomedical models have been used for this case study (shown in Figures 5.14-5.16). First, the build time of the adaptive speed algorithms developed in this research with a slope degree of $0^{\circ}$ for each model in five different layers has been calculated and the results are shown in Table 5.2. Then, the results of the build time for the comparison between our developed adaptive speed algorithms and a uniform speed algorithm of zigzag tool-path for each model in the same layer (layer 13) are shown in Table 5.3. From the above data, it can be observed that the build time of this developed approach can be reduced about 30% compared to that of the zigzag tool-path generation approach in a uniform speed. Second, the surface accuracy from the developed mixed tool-path generation algorithm and a typical zigzag tool-path generation algorithm for each model in the same layer has been compared (the diameter of the RP/M nozzles/print head has been set as 1.0 mm) and the results are shown in Table 5.4. It can be observed that this

developed approach has achieved better geometrical accuracy compared to that of the typical zigzag tool-path generation approaches of RP/M. Therefore, this approach can achieve an overall improvement.

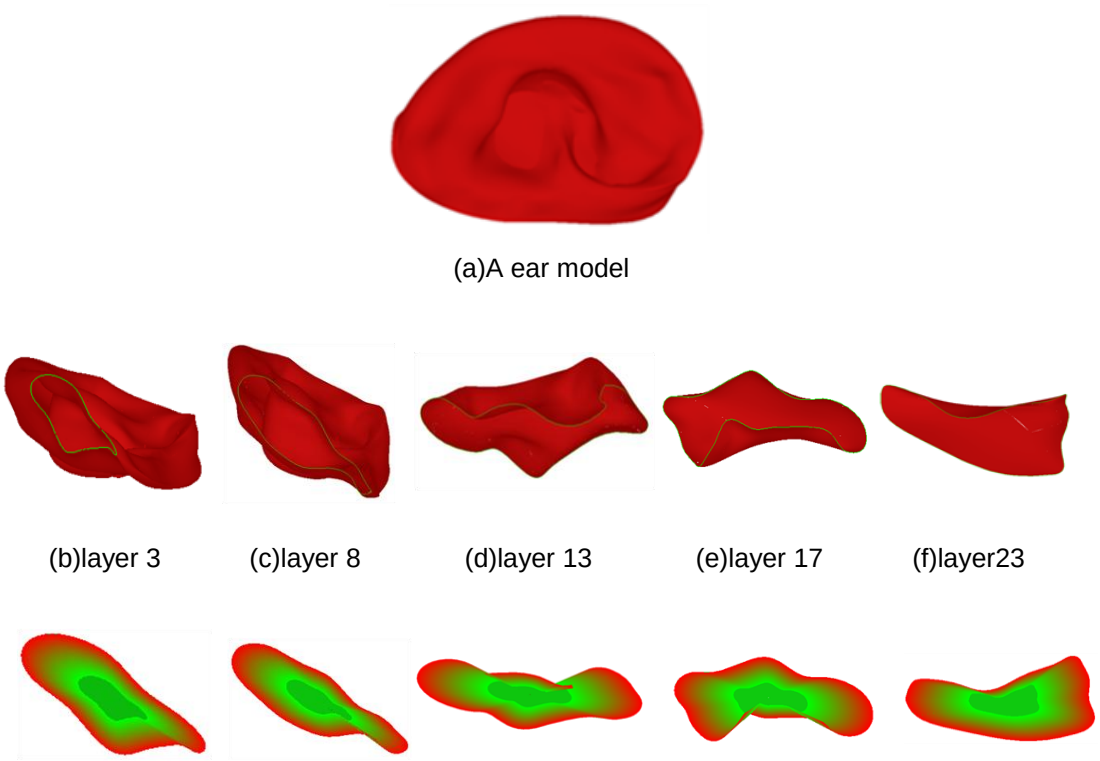

(a)A ear model

(b)layer 3 (c)layer 8 (d)layer 13 (e)layer 17 (f)layer23

(g)The materials distribution of the corresponding sliced layers

**Figure 5.14** Case Study II – Model one: an ear model.

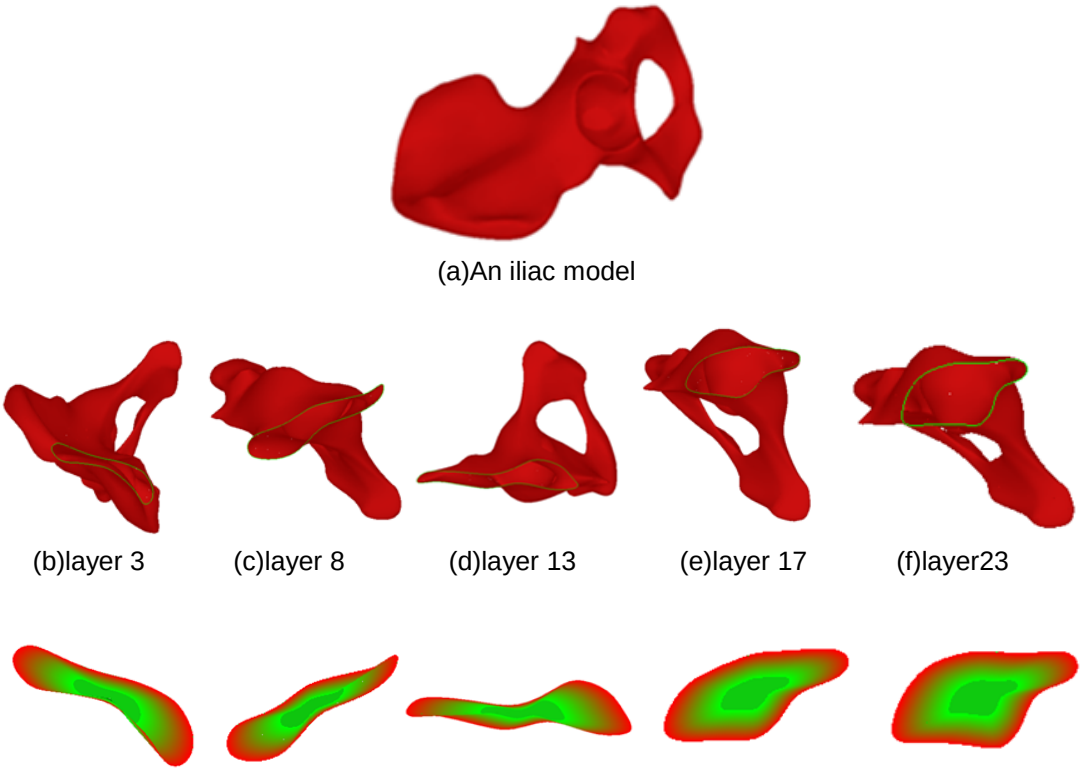

(a)An iliac model

(b)layer 3 (c)layer 8 (d)layer 13 (e)layer 17 (f)layer23

(g)The materials distribution of the corresponding sliced layers

**Figure 5.15** Case Study II – Model two: an iliac bone model.

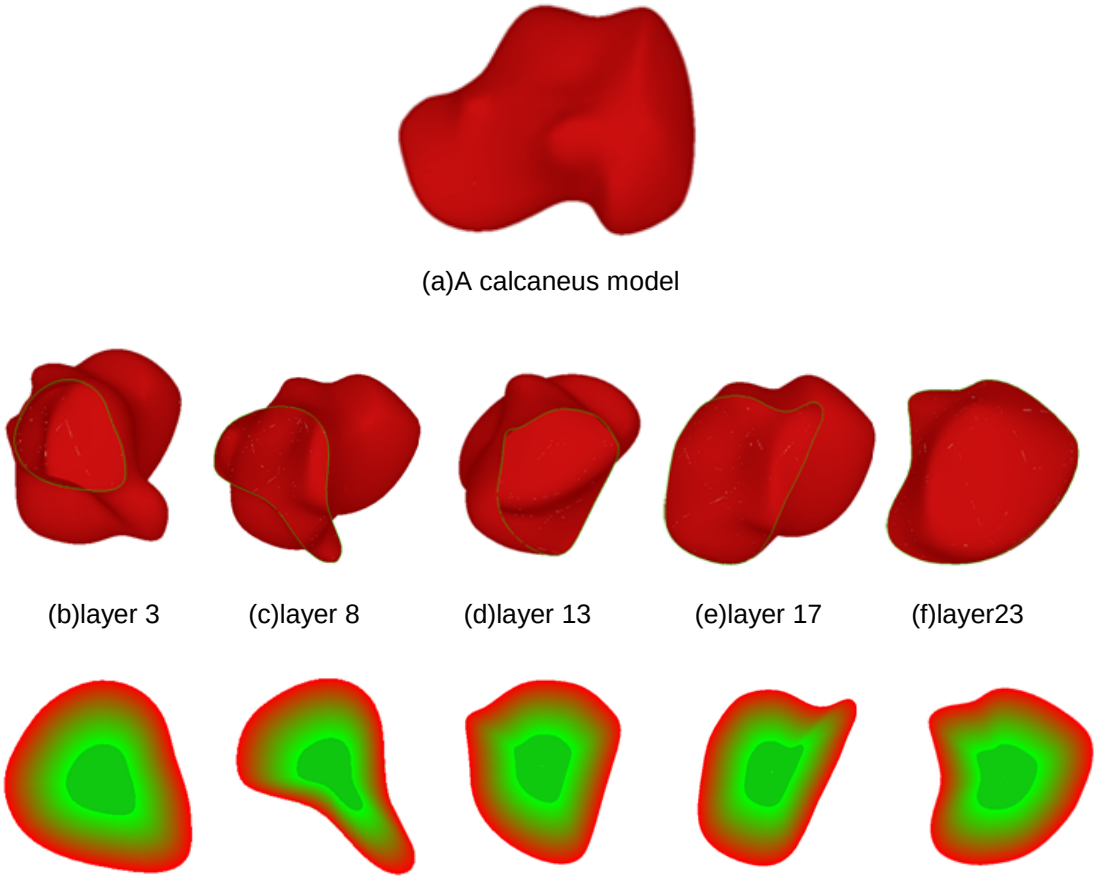

(a)A calcaneus model

(b)layer 3 (c)layer 8 (d)layer 13 (e)layer 17 (f)layer23

(g)The materials distribution of the corresponding sliced layers

**Figure 5.16** Case Study II – Model three: an calcaneus model.

**Table 5.2** Results of the build time with different sliced layers in the developed approach.

| **Model no.** | | Model 1 | Model 2 | Model 3 |
|---|---|---|---|---|
| **The build time of the developed approach (s).** | Layer 3 | 10.579 | 46.220 | 50.263 |
| | Layer 8 | 13.880 | 54.301 | 58.960 |
| | Layer 13 | 15.891 | 52.946 | 61.723 |
| | Layer 17 | 16.071 | 66.573 | 67.891 |
| | Layer 23 | 13.820 | 76.365 | 66.505 |

**Table 5.3** Results of the build time comparison in the same layer (layer 13).

| **Model no.** | Model 1 | Model 2 | Model 3 |
|---|---|---|---|
| **The build time of uniform speed approach (s)** | 23.672 | 74.327 | 90.021 |
| **The build time of the developed approach (s).** | 15.891 | 52.946 | 61.723 |
| **Reduced build time (%)** | 32.87 | 28.77 | 31.43 |

**Table 5.4** Comparison of the geometrical accuracy of the models (layer 13).

| **Model no.** | Model 1 | Model 2 | Model 3 |
|---|---|---|---|
| **The geometrical accuracy of the typical zigzag tool-paths (%)** | 93.124 | 94.290 | 96.382 |
| **The geometrical accuracy of this developed approach (%)** | 96.273 | 96.846 | 98.821 |

## 5.6 Summary

This chapter has presented an adaptive RP/M approach to support the realizable and customized FGM-based biomedical models fabrication in RP/M systems. The contributions of this research are summarized as follows:

(1) The geometrical accuracy of original biomedical models is maintained through introducing NURBS to represent the contours of sliced layers of FGM-based biomedical models to keep high-fidelity information. It establishes a good original data source for the further tool-path generation of the FGM-based biomedical models;

(2) The developed FGM-based modelling features can represent typical FGM-based biomedical models effectively. The linear and non-linear control parameters for FGM composition and distributions can enable users to address their specific functional needs;

(3) A mixed tool-path algorithm has been devised to generate a series of contour/offset tool-paths to represent the material composition and to ensure the surface quality of the model, and zigzag tool-paths for the internal area of a single material in the model to simplify computing and processing;

(4) In the end, case studies of FGM-based product models have been used to demonstrate the effectiveness and robustness of the developed algorithms and strategies.

# CHAPTER 6
# SYSTEMATIC APPLICATION OF THE DEVELOPED ADAPTIVE APPROACH AND CONCEPT DESIGN OF MULTI-MATERIAL RP/M SYSTEM

## 6.1 Introduction

Previous chapters described specific topics in adaptive RP/M process planning technologies of complex biomedical models in detail, for example, adaptive mixed tool-path generation, adaptive slicing, and adaptive approach for FGM-based biomedical model. In this chapter, the systematic application of the developed adaptive RP/M process planning for a biomedical talus bone model is studied. Firstly, the model is directly adaptive sliced with the developed adaptive slicing algorithms. It can be used to obtain the thickness of each slicing layer to balance the build time and geometrical accuracy of the biomedical model. Secondly, the mixed tool-path generation algorithms are used to generate contour and zigzag tool-path for the sliced layer to improve the geometrical accuracy and speed up fabrication, and the adaptive speed algorithm is also used to reduce build time based on the developed geometrical accuracy and build time analysis modules. Thirdly, based on the information of the sliced layer, a FGM-based feature is used to present the material gradual change of each sliced layer of the model. Finally, the mixed tool-path algorithms are applied to generated contour and zigzag tool-path for the different material requirement of the model for FGM-based biomedical model fabrication in RP/M.

In addition, a concept design of multi-material RP/M system is also introduced in this chapter. It consists of four major system assemblies: (1) nozzle deposition apparatus, (2) z-axis, (3) feeding apparatus, (4) material pipe and pipe hanger. The designed multi-material RP/M system can be used to fabricate multi-material objects such as FGM-based biomedical models.

## 6.2 Systematic application of the developed adaptive process planning approach

The systematic application of the developed adaptive process planning approach for complex biomedical models in the RP/M consists of three parts as follows (shown in Figure 6.1). The details of the each part are depicted in the following sections.

Part 1: The adaptive slicing algorithms and strategies
Part 2: The adaptive tool-path generation algorithms and strategies
Part 3: The adaptive approach for FGM-based model

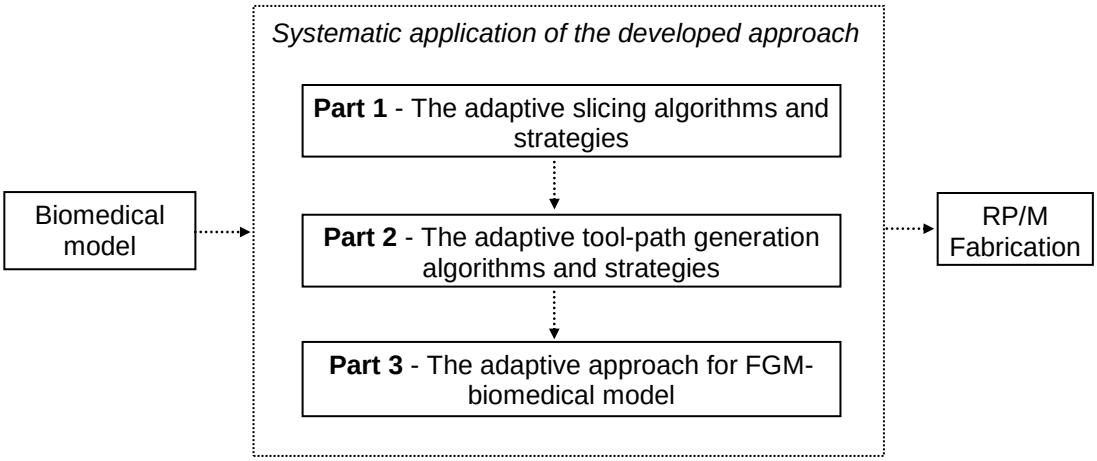


**Figure 6.1** Systematic application of the developed approach.

### 6.2.1 Part 1 (systematic application) - The adaptive slicing algorithms and strategies

A biomedical talus bone model of human being left feet (shown in Figure 6.2), which was first created by CMMs scanning to obtain the point cloud data and then reconstructed as IGES/IGS format models in CATIA V5™ with QSR and DSE modules, was tested to validate the effectiveness and robustness of the developed adaptive process planning in

RP/M. The minimum and maximum thickness of the slicing was defined as 1.0mm and 4.0mm respectively, and the rotated angle of the intersection surface is set as 30 degree. The distance between two points is set as 0.5mm. The minimum and maximum speeds of the RP/M nozzle/print head were defined as 10mm/s and 20mm/s respectively, and the acceleration of the nozzle/print head was 20mm/s ($V_{min} = 10mm/s; V_{max} = 20mm/s; a = 20mm/s^2$ ; $Thickness(T_{min}) = 1.0mm$ ; $Thickness(T_{max}) = 4.0mm$ ; $R_{angle} = 30°$; $Distance(Point^i, Point^{i+1}) = 0.5mm$). All results were obtained in a Pentium Dual-Core CPU 2.10GHz, 2GB RAM system.

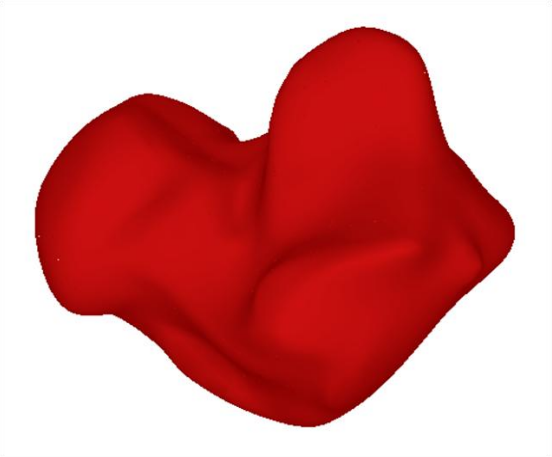

**Figure 6.2** A biomedical talus bone model.

The length, width, height and volume of the talus model are 58.087mm, 42.849mm, 35.433mm and 34170mm$^3$ respectively. The reconstructed model is first read into the developed software platform, which was developed based on the C++ programming language in an open-source CAD kernel system - the Open CASCADE (Open CASCADE, 2012).

The process for generating an enveloping box for the model, slicing with minimum thickness, rotating slicing and intersection curves generation, discrete points generation on the intersection curves and feature points pass the two thresholds, and finial determine the slicing thickness for each layer are shown in Figure. 6.3.

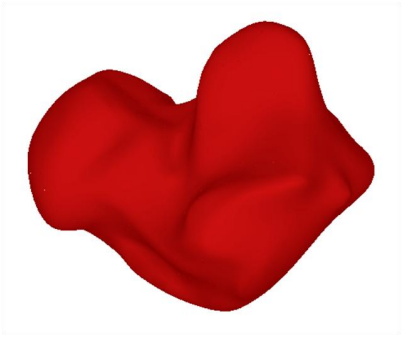

(a) A talus bone model

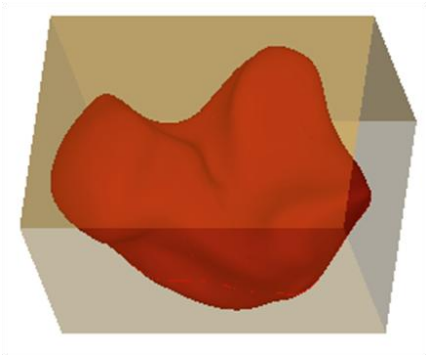

(b) An enveloping box

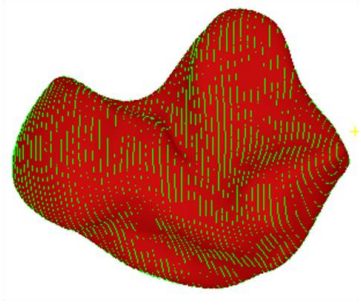

(c) Slicing with minimum thickness slicing

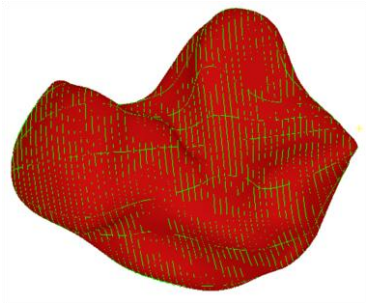

(d) Rotating slicing and intersection curves

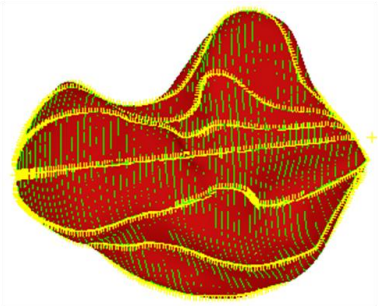

(e) Discrete points on the intersection curves

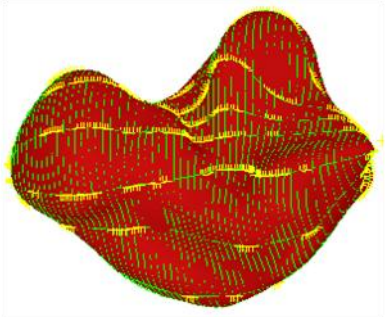

(f) Feature points passing the threshold one

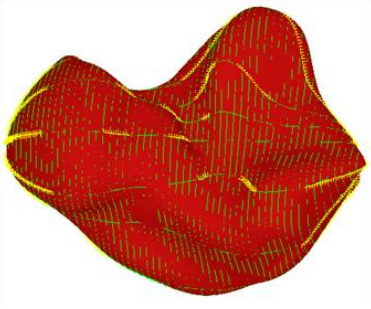

(g) Feature points passing the threshold two

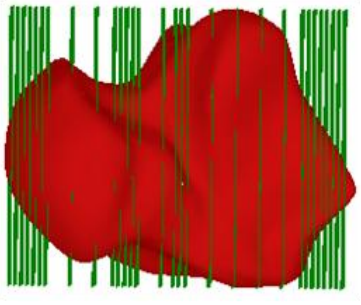

(h) Adaptive slicing the talus model

**Figure 6.3** The developed adaptive slicing process for the talus model.

Here, the threshold two is set as 78.46 degree; the value of threshold one is incrementally changed from 0.0000001mm until 0.001mm. The build time of each slicing layer is supposed as one minute. The precious build time of each layer can be calculated based on the developed build time analysis module in the next section. The results of the volume for the each slicing layer, the whole fabrication volume and build time of the model are shown in Table 6.1. Table 6.2 shows the results of build time and geometrical accuracy for the incrementally changed threshold one - $D^1_{threshold}$.

**Table 6.1** The volume and bi-data for each layer of the talus model.

| No. | Volume | Bi- data | No. | Volume | Bi- data | No. | Volume | Bi- data | No. | Volume | Bi- data |
|---|---|---|---|---|---|---|---|---|---|---|---|
| 1 | 0 | 1 | 16 | 622.019 | 0 | 31 | 860.047 | 0 | 46 | 694.928 | 0 |
| 2 | 70.9304 | 1 | 17 | 625.463 | 0 | 32 | 879.465 | 0 | 47 | 637.941 | 0 |
| 3 | 142.737 | 1 | 18 | 628.59 | 1 | 33 | 910.317 | 0 | 48 | 575.185 | 0 |
| 4 | 208.246 | 1 | 19 | 633.419 | 1 | 34 | 940.991 | 0 | 49 | 507.733 | 1 |
| 5 | 269.927 | 1 | 20 | 636.215 | 1 | 35 | 969.016 | 0 | 50 | 442.292 | 1 |
| 6 | 329.26 | 1 | 21 | 638.034 | 1 | 36 | 981.54 | 0 | 51 | 365.836 | 1 |
| 7 | 386.91 | 0 | 22 | 639.566 | 0 | 37 | 982.549 | 0 | 52 | 288.595 | 1 |
| 8 | 440.96 | 0 | 23 | 658.213 | 0 | 38 | 971.91 | 0 | 53 | 223.084 | 1 |
| 9 | 491.58 | 0 | 24 | 690.494 | 0 | 39 | 956.266 | 0 | 54 | 172.264 | 1 |
| 10 | 535.365 | 0 | 25 | 731.539 | 0 | 40 | 929.881 | 0 | 55 | 128.362 | 1 |
| 11 | 571.219 | 0 | 26 | 767.516 | 1 | 41 | 900.774 | 0 | 56 | 81.5368 | 0 |
| 12 | 595.693 | 0 | 27 | 801.361 | 1 | 42 | 870.444 | 0 | 57 | 32.8987 | 0 |
| 13 | 609.706 | 0 | 28 | 823.025 | 0 | 43 | 827.322 | 0 | | | |
| 14 | 616.128 | 0 | 29 | 839.146 | 1 | 44 | 786.025 | 0 | | | |
| 15 | 619.324 | 0 | 30 | 847.548 | 0 | 45 | 743.34 | 0 | | | |

The totally volume of fabrication is: ***31683.8mm$^3$***
The build time of fabrication is : ***32minutes***

**Table 6.2** Comparison of computational results of different threshold one for the talus model.

| Threshold one -$D^1_{threshold}$(mm) | 0.001 | 0.0003 | 0.0001 | 0.00005 | **0.00003** | 0.00001 | 0.000005 | 0.000001 | 0.0000001 |
|---|---|---|---|---|---|---|---|---|---|
| Build time (mint) | 24 | 25 | 28 | 31 | **32** | 46 | 51 | 54 | 57 |
| Volume(mm$^3$) | 31261.1 | 31270.6 | 31486.4 | 31667.7 | **31683.8** | 32700.6 | 33028.6 | 33054.3 | 33154.3 |
| Geometrical accuracy (%) | 91.49 | 91.51 | 92.15 | 92.66 | **92.72** | 95.70 | 96.66 | 96.73 | 97.03 |

Figure 6.4 shows the results between various change of the number of slicing layer and geometrical accuracy with an incremental from 0.0000001mm until 0.001mm of threshold one. Table 6.3 shows the change results between the build time and geometrical accuracy with different value of the threshold one.

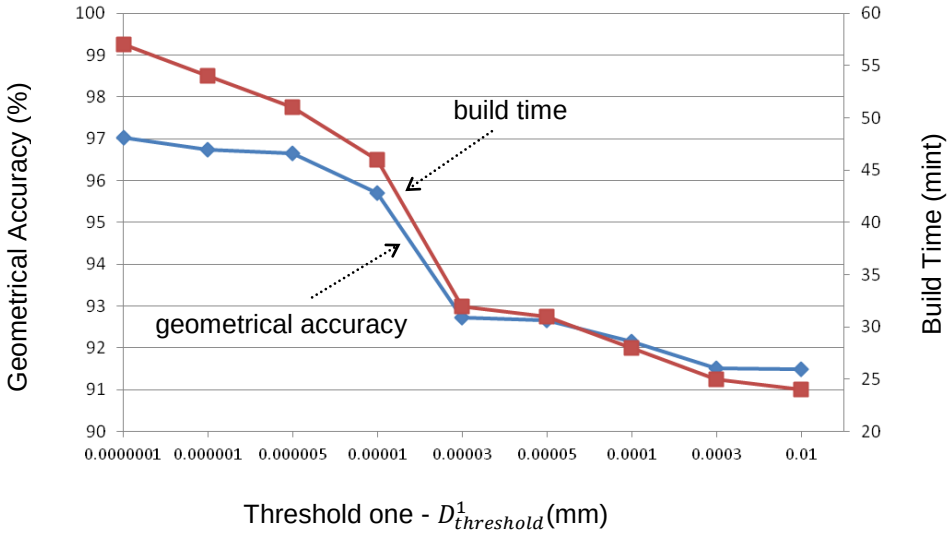


**Figure 6.4** The results of geometrical accuracy and build time with changed threshold one.

**Table 6.3** The results of the build time and geometrical accuracy of changed threshold one

| Model - talus | $D^1_{threshold}$ (mm) | Added build time (minutes) | Changed geometrical accuracy (%) |
|---|---|---|---|
| Talus model | 0.001 ~ 0.00003 | 12 | 1.23 |
| | 0.00003 ~ 0.0000001 | 25 | 4.31 |

It can be observed that there are linear relationships between the geometrical accuracy, build time and the value of two thresholds. For instances, based on Figure 6.4, if a user would like to fabricate the model with about 93% geometrical accuracy, the values of two thresholds can be set as 0.00003mm and 78.46 degree ($D^1_{threshold} = 0.00003mm;\ D^2_{threshold} = 78.46\ degree$) to obtain each slicing thickness of the whole model. Meanwhile, if a user would like to fabricate the model with about 46 minutes, the values of two thresholds can be set as 0.00001mm and 78.46 degree ($\mathrm{D}^1_{\mathrm{threshold}} = 0.00001\mathrm{mm};\ \mathrm{D}^2_{\mathrm{threshold}} = 78.46\ \mathrm{degree}$) to obtain each slicing thickness. In addition, based on Table 6.3, a user can improve the geometrical accuracy about 1.23% (the build time added about 12 minutes) by changing the value of threshold one from 0.001mm to 0.00003mm. Furthermore, by changing the value of threshold one from 0.00003mm to 0.0000001mm, the geometrical accuracy can improve about 4.31%, which

is about 4 times of 1.23% as above (but the build time only need added about 25 minutes, which is less than 2 times of 12 minutes in above).

Based on the above analysis, it is obvious that the developed adaptive slicing algorithms and strategies can provides an effective guideline for a user to balance the geometrical accuracy and build efficiency for complex biomedical model fabrication of RP/M, and can achieve significantly improvement of geometrical accuracy and build efficiency by choosing the right threshold values.

### 6.2.2 Part 2 (systematic application) - The adaptive tool-path generation algorithms and strategies

Based on the obtained slicing layer from the above adaptive slicing algorithms, the adaptive tool-path generation algorithms and strategies are applied for the model. The number 13 slicing layer of the model is used in here. The process for the NURBS-based contour curve generation, and the generation of contour-based tool-paths and zigzag tool-paths are shown in Figure 6.5. The result of the build time in the contour-based tool-paths is shown in Table 6.4. Table 6.5 shows the results of each build time with an incremental 10 degree for the slope from 0 degree until 170 degree.

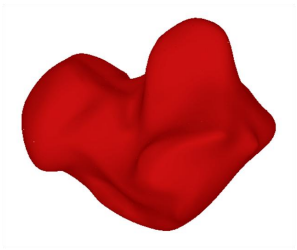

(a) The talus model

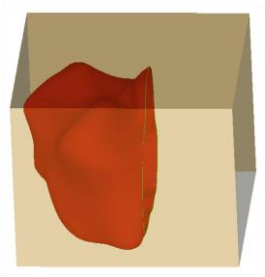

(b) The slicing layer

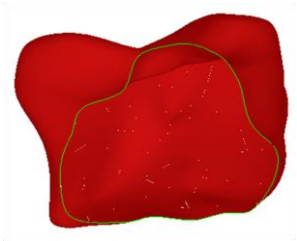

(c) The sliced model

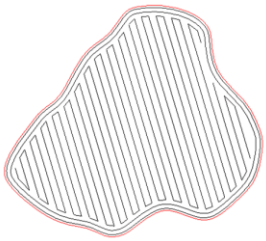

(d) The generated tool-paths for one layer

**Figure 6.5** The developed adaptive tool-path generation process for the talus model.

**Table 6.4** The RP/M nozzle/print head speed of the contour tool-paths for the talus model.

| Segment no. | 1 | 2 | 3 | 4 | 5 | 6 | 7 | 8 |
|---|---|---|---|---|---|---|---|---|
| Distance (mm) | 17.692 | 17.003 | 7.748 | 6.872 | 14.230 | 15.841 | 12.156 | 11.079 |
| Length (mm) | 18.289 | 17.552 | 7.874 | 6.986 | 15.488 | 16.288 | 13.327 | 11.176 |
| Average speed (mm/s) | 19.346 | 19.374 | 19.680 | 19.674 | 18.374 | 19.452 | 18.242 | 19.826 |
| Build time (s) | 0.946 | 0.906 | 0.400 | 0.355 | 0.844 | 0.837 | 0.731 | 0.563 |
| ***Total build time for contour tool-path = 5.581 (s)*** | | | | | | | | |

**Table 6.5** Comparisons of the different slope degrees of zigzag tool-paths for the talus model.

| Degree | 0 | 10 | 20 | 30 | 40 | 50 | 60 | 70 | 80 |
|---|---|---|---|---|---|---|---|---|---|
| Length (mm) | 642.860 | 661.545 | 650.509 | 648.605 | 659.806 | 652.450 | 650.109 | 646.745 | 642.687 |
| Time (s) | 45.652 | 47.340 | 46.606 | 47.544 | 49.362 | 48.182 | 47.816 | 47.110 | 46.442 |
| | | | | | | | | | |
| Degree | 90 | 100 | 110 | 120 | 130 | 140 | **150** | 160 | 170 |
| Length (mm) | 636.308 | 657.369 | 655.107 | 663.357 | 654.266 | 627.047 | **632.799** | 656.323 | 650.140 |
| Time (s) | 45.760 | 45.795 | 46.186 | 45.748 | 45.126 | 43.850 | **43.432** | 44.910 | 45.698 |

It can be observed that in 150 degree the build time is the shortest. The total build time for the shown layer of the tibia model = 5.581+43.432 = 49.013 seconds (contour tool-paths + zigzag tool-paths).

Figure 6.6-6.7 show the comparison results of build time and geometrical accuracy between this developed approach and typical zigzag tool-path generation approaches The series of comparisons are based on an incremental 10 degree of zigzag tool-path slope from 0 degree until 180 degree and an incremental 0.1mm of the diameter of RP/M nozzle/print head each time from 0mm until 1.9mm.

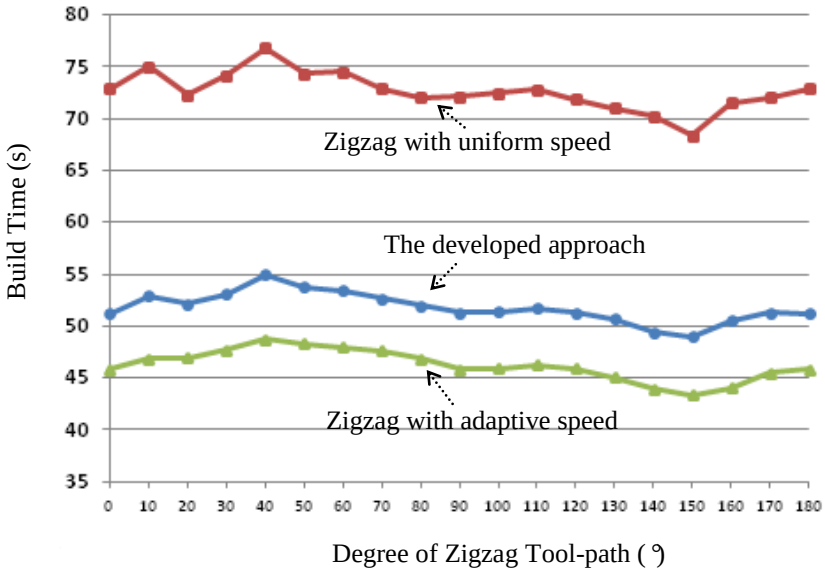


**Figure 6.6** Build time comparisons.

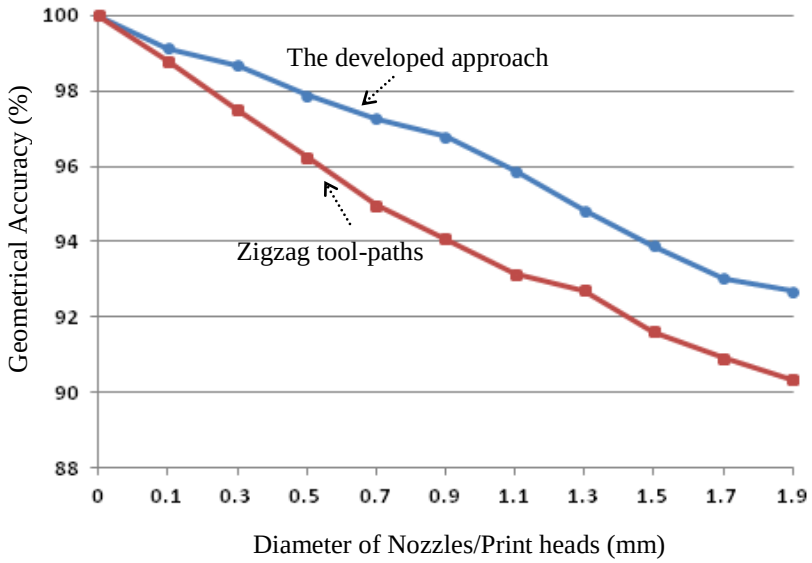


**Figure 6.7** Geometrical accuracy comparisons.

From the above data, it can be observed that the build time of this developed approach can be reduced about 25% compared to that of the zigzag tool-path generation approach in the uniform speed. Meanwhile, the developed zigzag tool-path optimisation strategy to obtain the best slope degree of the RP/M nozzle/print head can further reduce approximated 10% of the RP/M build time. The build time of this developed approach is about 7% more than that of the zigzag tool-path generation approach in adaptive speed. However, the geometrical accuracy of this developed mixed tool-paths algorithm is much better than that of the zigzag tool-path generation approaches.

It can be observed that this developed adaptive tool-path algorithms and strategies achieved much better in terms of geometrical accuracy and build time compared to that of the typical zigzag tool-path generation approaches of RP/M. Therefore, this approach can achieve an overall improvement and a better balance of build efficiency and geometrical accuracy.

### 6.2.3 Part 3 (Systematic application) - The adaptive approach for FGM-biomedical models

The process for the NURBS-based contour/offset curve generation, FGM-based representation and the generation of contour/offset and zigzag tool-paths are shown in Figure 6.8. The result of the build time for the contour/offset tool-paths is shown in Table 6.6. Figure 6.9 shows the curve built based on different slope degrees. From the curve, it can be obtained that at 50.0 degree the build time of the zigzag tool-paths is the minimum (24.320 seconds). The total build time for the shown layer of the bone model is 54.157 seconds (build times of the contour/offset tool-paths + zigzag tool-paths = 29.837 seconds +24.320 seconds).

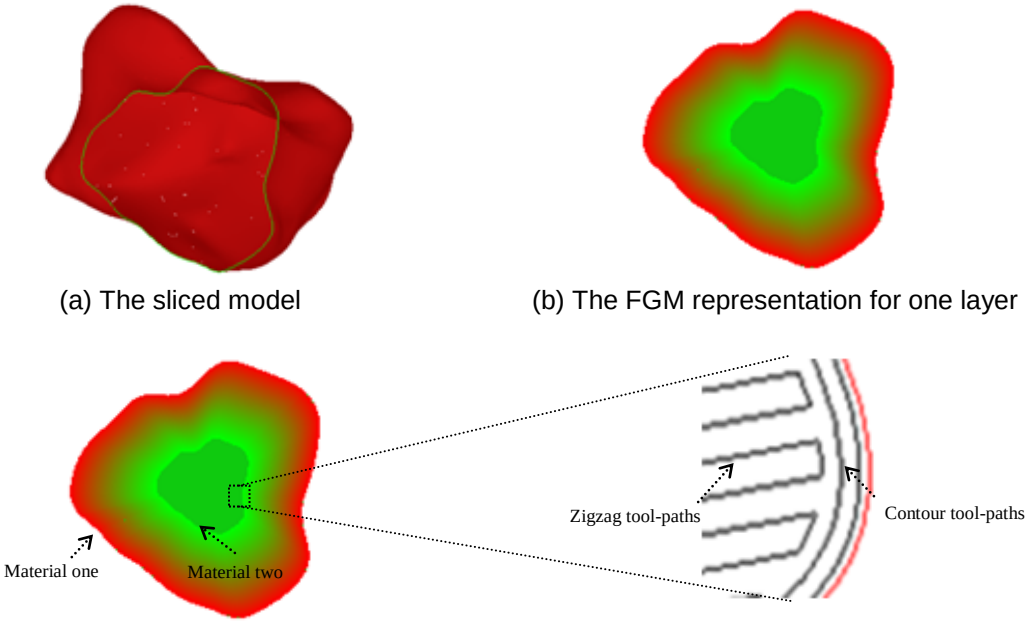


(a) The sliced model (b) The FGM representation for one layer

(c) The material distribution (d) The generated tool-paths for one layer

**Figure 6.8** The developed adaptive process for FGM-based model.

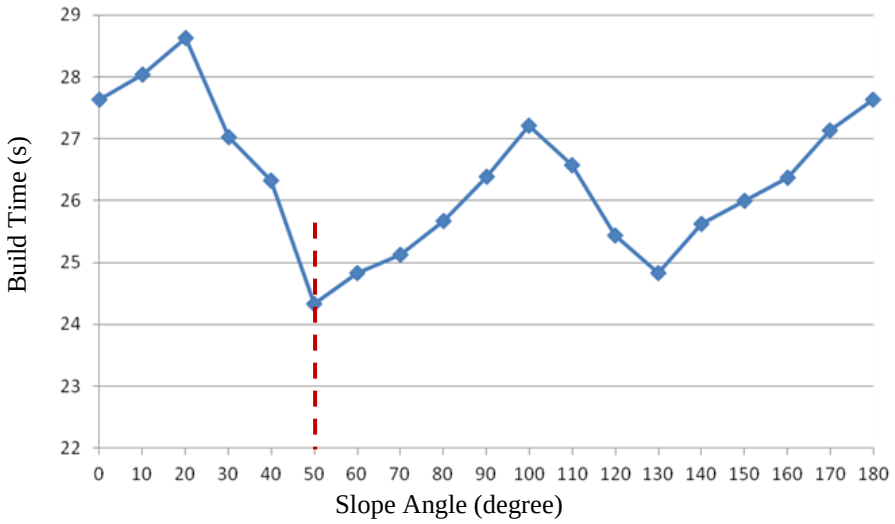


**Figure 6.9** The curve for the relation between the build times and slope degrees of zigzag tool-paths.

**Table 6.6** Build time of the contour/offset tool-paths for the bone model.

| Contour/offset tool-paths no. | 1 | 2 | 3 | 4 | 5 | 6 |
|---|---|---|---|---|---|---|
| Length (mm) | 114.290 | 96.471 | 85.044 | 77.593 | 74.399 | 68.083 |
| Build time (seconds) | 6.803 | 5.944 | 5.302 | 4.877 | 4.691 | 4.320 |

***Total build time for contour tool-paths = 29.837 (seconds)***

Figure 6.10 shows the results in five different layers of the model. The build time with a slope degree of $0^{\circ}$ has been calculated and the results are shown in Table 6.7. The results of the build time and surface accuracy for the comparison (the diameter of the RP/M nozzles/print head has been set as 1.0 mm) between our developed adaptive speed algorithms and a typical zigzag tool-path for the model in the same layer (layer 13) are shown in Table 6.8.

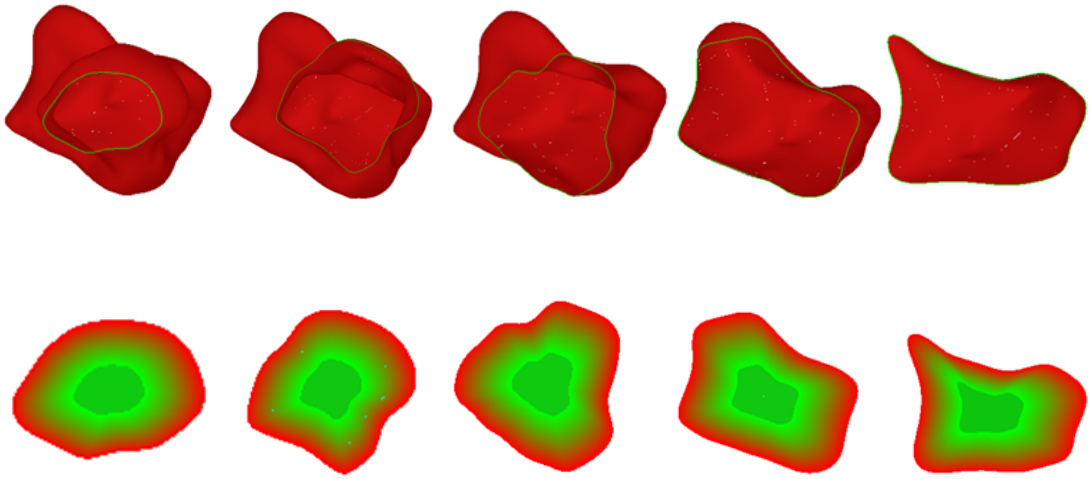

(g)The materials distribution of the corresponding sliced layers

**Figure 6.10** Five different layers of the FGM-based model.

**Table 6.7** Results of the build time with different sliced layers of developed approach.

| **Layer no.** | Layer 3 | Layer 8 | Layer 13 | Layer 17 | Layer 23 |
|---|---|---|---|---|---|
| **Build time (s).** | 38.304 | 50.662 | 57.472 | 69.763 | 61.831 |

**Table 6.8** Results of the build time comparison in the same layer (layer 13).

| | | | |
|---|---|---|---|
| The build time of uniform speed approach (s) | 86.320 | The geometrical accuracy of the typical zigzag tool-paths (%) | 94.351 |
| The build time of the developed approach (s). | 57.472 | The geometrical accuracy of this developed approach (%) | 97.640 |
| Reduced build time (%) | 28.958 | Improve geometrical accuracy (%) | 2.289 |

It can be observed that the developed adaptive approach for FGM-based talus model can reduce about 28.958% build time while 2.289% is improved compared to that of the zigzag tool-path generation approach of RP/M. Therefore, this approach can achieve an overall improvement.

## 6.3 Concept design of a multi-material RP/M system

Figure 6.11 shows the concept design of the proposed multi-material RP/M 3D nozzle deposition system, consists of four major system assemblies: (1) nozzle deposition apparatus, (2) z-axis, (3) feeding apparatus, (4) material pipe and pipe hanger. In this concept design, the nozzle deposition system is unique which consists of seven nozzles, one nozzle is used to deposit support material and other six nozzles are used to deposit different build materials, to support different materials fabrication for FGM-based biomedical model.

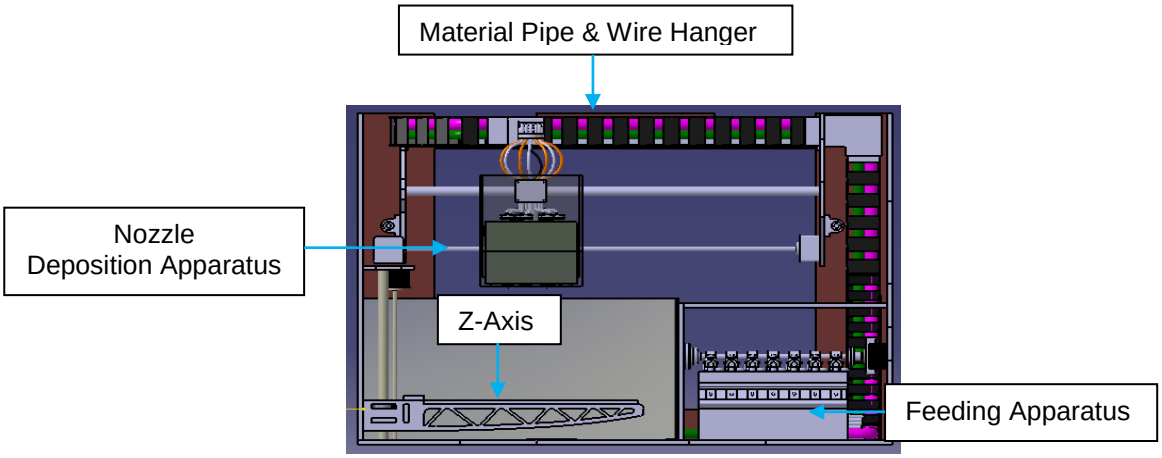


(a) Forward side

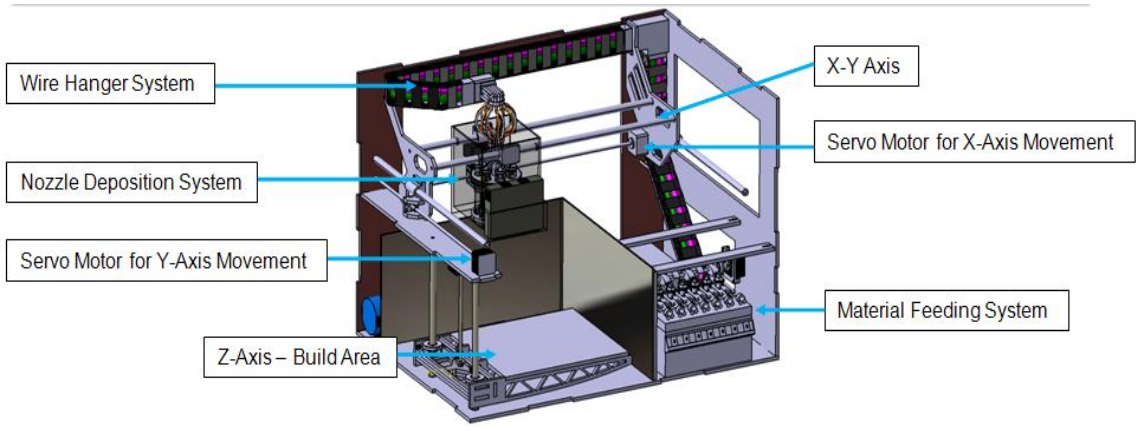


(b) Sideface

**Figure 6.11** Concept design of multi-material RP/M 3D nozzle deposition system.

The fabrication process of the concept design system for multi-material model consists of six steps and the details are depicted as follows:

**Step 1 - Feeding material process (shown in Figure 6.12)**

1. Feeding apparatus is switched on to start pumping the material from the feeding tanks to material deposition nozzle chambers. Each feeding pipe is dedicated to a specific material (one material is used as support material, another six materials are used as build material of object), its one end is connected to the material source tank and another is connected to the deposition nozzle pressure plate.
2. Feeding apparatus pumps the material with the help of a crank shaft attached to the dedicated pumps. Feeding apparatus is switched off when deposition material nozzle chamber is full.

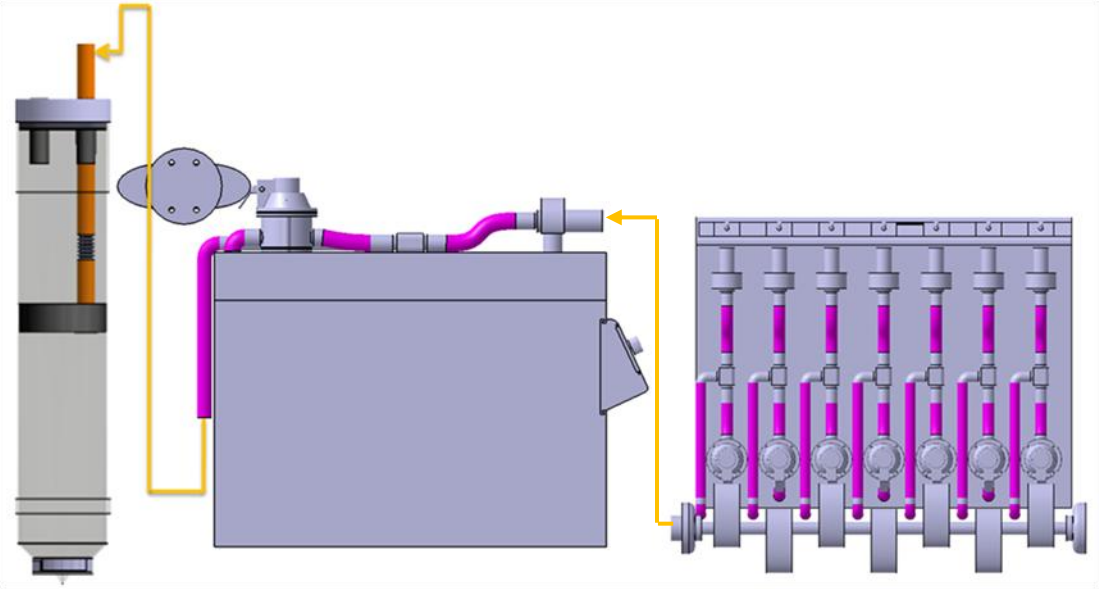

**Figure 6.12** Concept design of the feeding process.

**Step 2 - Deposition material process (shown in Figure 6.13)**

1. Deposition apparatus is initiated to start the deposition process after the material chambers of each nozzle is filled with the desired multiple materials and support material.
2. Air compressor is switched on and a constant pressure on the nozzle pressure plate is maintained.
3. The deposition flow rate is controlled by the pressure exerted on the pressure plate. The pressure of each nozzle depends on the material properties and the geometry of nozzle tip. So each nozzle‘s pressure is adjusted according to the required flow rate.

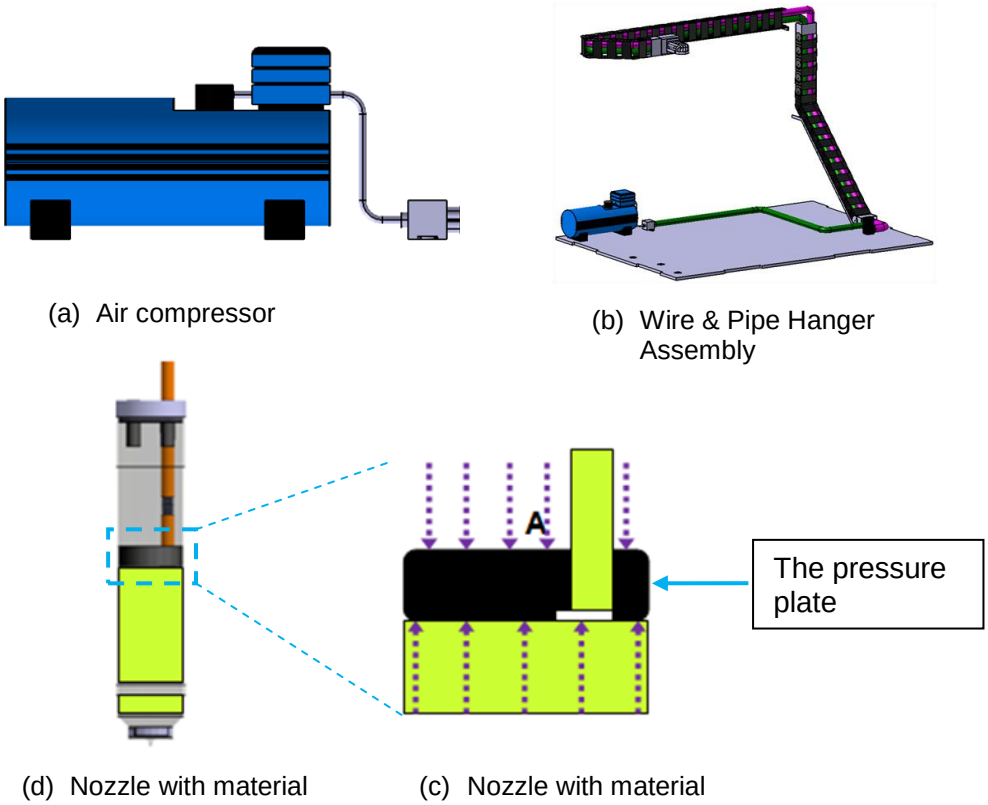


(a) Air compressor

(b) Wire & Pipe Hanger Assembly

(d) Nozzle with material

(c) Nozzle with material

**Figure 6.13** Concept design of the deposition process.

**Step 3 – Z-axis movement (shown in Figure 6.14)**

1. Z-axis is adjusted for the first deposition by moving closer to the deposition nozzle apparatus. The movement of Z-axis is controlled by a servo motor which moves the Z-axis upward or downward.

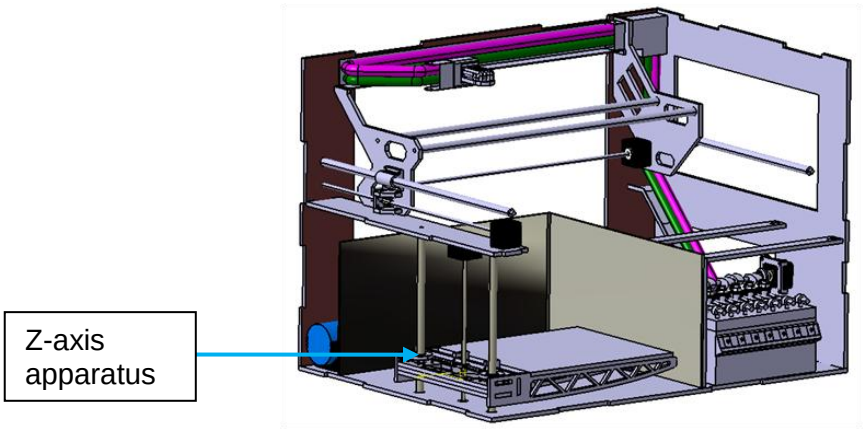


(a) Concept design system

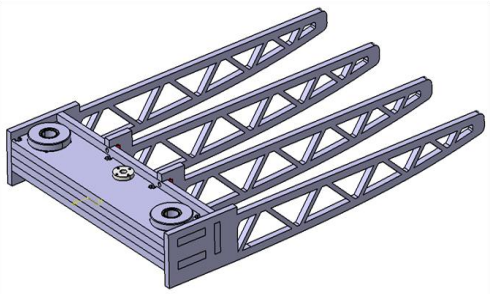

(b) Z-axis assembly

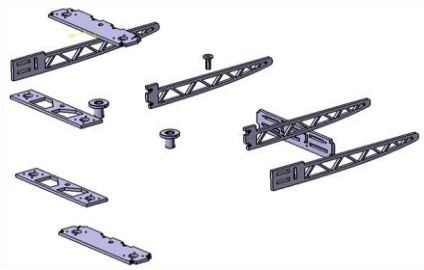

(c) Exploded view of Z-axis

**Figure 6.14** Concept design of the Z-axis.

**Step 4 – Nozzles selection process (shown in Figure 6.15)**

1. Nozzle apparatus is adjusted for the first deposition to begin by selecting the desired material nozzle. Seven nozzles are mounted on a rotation tray which is connected to a servo motor. The servo motor can rotate the nozzles 180 degree clockwise and anti clockwise to select the needed nozzles to deposited different materials for fabrication.

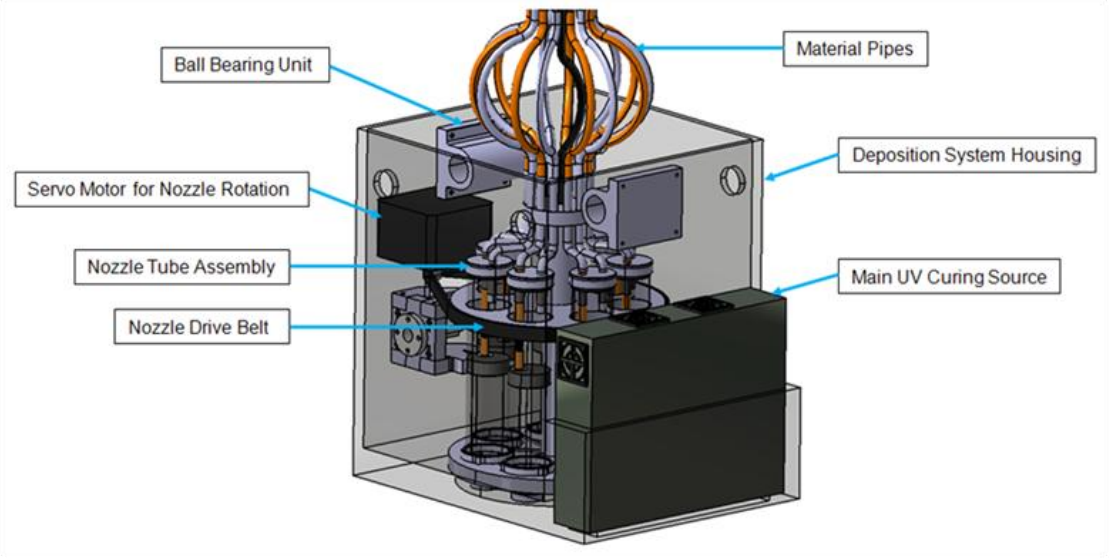


(a) Nozzle deposition system

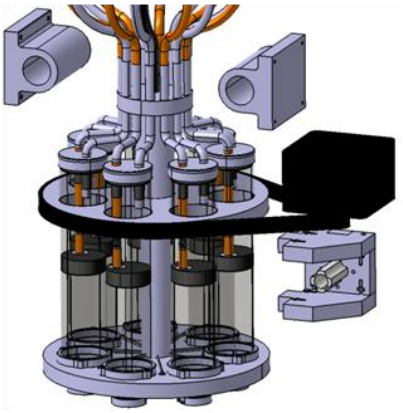

(b) Nozzle apparatus assembly

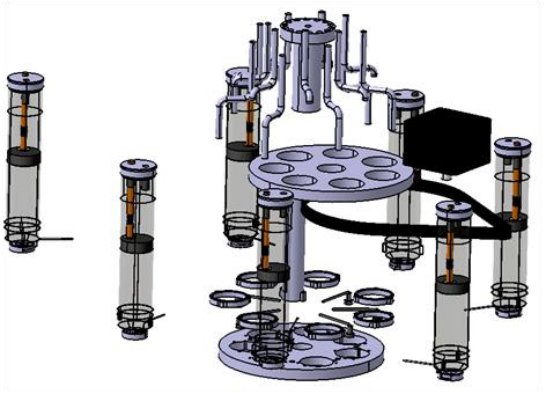

(c) Exploded view of assemblies

**Figure 6.15** Concept design of the nozzle apparatus.

**Step 5 – Material deposition control process (shown in Figure 6.16)**

1. Deposition control is actuated after the Z-axis is adjusted and nozzle is selected for the materials deposition for continues deposition.

2. Deposition control actuation is predefined when the material tool-path is defined during pre processing. It makes possible to control the material deposition quantity precisely by the deposition control valve. For quality and precision, both pressure mechanism and the deposition control need to work in perfect coordination.
3. Different materials are deposited continuously along the tool-path by activating the deposition control.

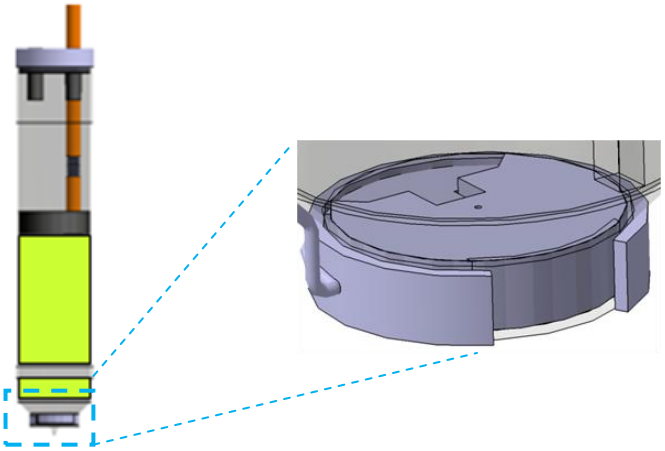

(a) Nozzle with material

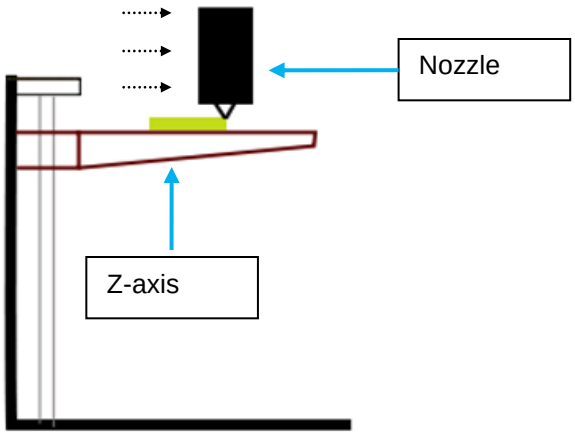


(c) Deposition material along one direction

**Figure 6.16** Concept design of material deposition control process.

**Step 6 – Curing process (shown in Figure 6.17)**

1. Material depositing process is followed by the curing process which is done layer by layer.
2. When multi-materials are deposited, the UV spot light intensity on the rotation tray can be adjusted depending on the material quantity, geometry and area which need to be cured for curing the different materials on the layer.
3. Different materials are cured continuously along the tool-path by adjusting the UV spot light control.

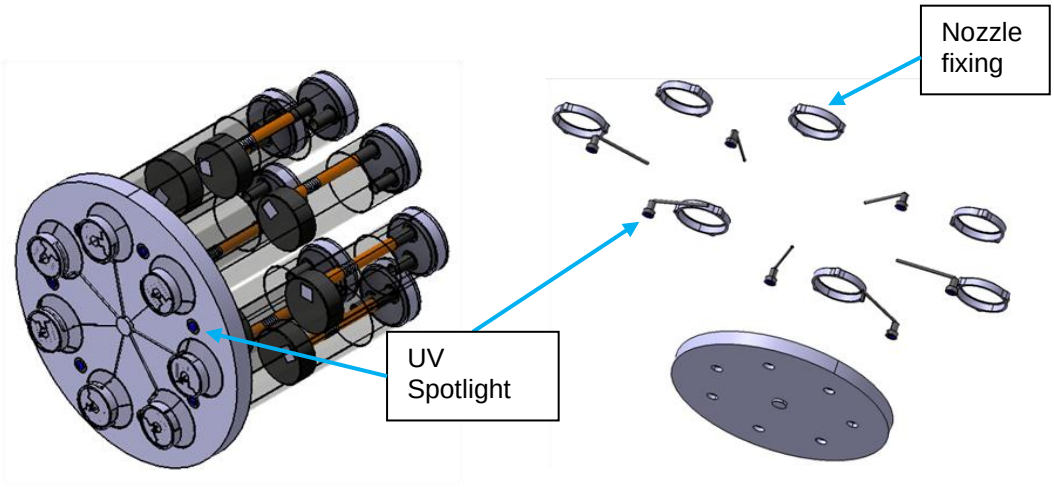


(a) Nozzle system

(b) Nozzle Fixing Plate – Exploded View

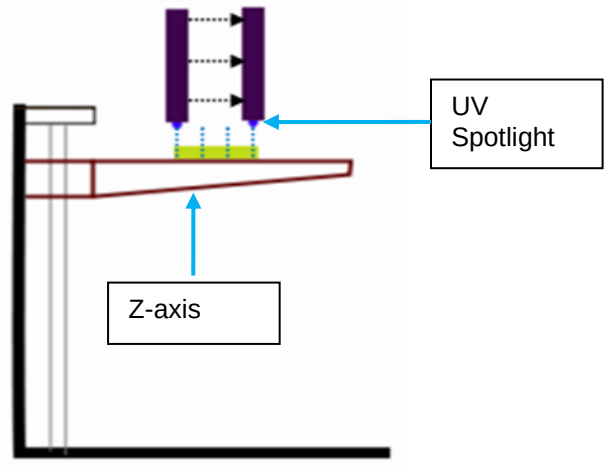


(c) Curing material along one direction

**Figure 6.17** Concept design of curing process.

Based on the above build process, the multi-material object include FGM-based biomedical model can be fabricated layer by layer from bottom to top.

## 6.4 Summary

This chapter has presented a systematic application of the developed adaptive process planning approach for a biomedical talus bone model. A series of optimisation algorithms and strategies have been applied, which include the adaptive slicing algorithms and strategies, adaptive tool-path generation algorithms and strategies and adaptive approach for FGM-based model fabrication. Meanwhile, a concept design of a multi-material RP/M system and its fabrication process also has been introduced in here. The contributions of this research are summarised as follows:

(5) The developed adaptive process planning approach can achieve significantly improvement of geometrical accuracy and build efficiency for complex biomedical model fabrication in RP/M.
(6) The introduced concept design of a multi-material RP/M 3D nozzle deposition system can be used to fabricate multi-material objects which include FGM-based biomedical models.

# CHAPTER 7
# CONCLUSIONS AND FUTURE WORK

## 7.1 Conclusions

One of the main impediments in RP/M for biomedical models is extensive build time and poor geometrical accuracy. Adaptive algorithms can effectively address the issue so as to better meet the efficiency and accuracy requirements of biomedical model fabrication. This research provides a novel and systematic adaptive process planning approach on improving geometrical accuracy and reducing build time for complex biomedical models in RP/M. A series of optimisation algorithms and strategies have been developed to optimise the tool-path generation and slicing strategy in RP/M process planning. The major features of this research are summarised as follows:

1. **Directly slicing algorithm and NURBS-based curves representations have been designed to represent each sliced layer to maintain the geometrical accuracy of original biomedical model.**

STL, which has been a widely adopted data standard in the RP/M industry, is an approximation representation scheme of product models based on triangles or quadrilaterals. However, there are some intrinsic problems in STL files such as gaps, holes, missing/degenerated/overlapping facets, etc. during the conversion process from native CAD files. On the other hand, STL is less inaccurate in geometrical representation and needs much more storage spaces for a complex model such as biomedical model than parametric mathematical representation themes such as NURBS, Bezier, B-Spline, etc.

In this research, a directly slicing algorithm and NURBS-based curves representation have been designed. It reduces the time for transferring data as the biomedical CAD model can be directly sliced and NURBS-based curves could be used to represent the sliced layer to maintain the geometrical accuracy of original biomedical models. Meanwhile, it also

establishes a good original data source for further tool-path generation, adaptive slicing and FGM-based biomedical model representation.

2. **Mixed tool-path generation algorithms have been developed to generate contour and zigzag tool-path to balance the build time and geometrical accuracy.**

In the traditional RP/M process, it only uses one tool-path type to build the whole model. The most typical tool-path method is zigzag tool-path. This method is easy to compute and implement, but it has some drawbacks which will leading to a poor building quality and warpage problem. The contour tool-path generation is another typical method, which can address the above geometrical quality issue effectively. However, the computation of the contour tool-path algorithms is complicated and for some complex model such as biomedical model, the algorithms are sometime unable to generate proper contour tool-paths.

In this research, mixed tool-path generation algorithms have been developed to combine the advantages of contour and zigzag tool-paths to balance the requirements on geometrical accuracy and fabrication efficiency for biomedical model fabrication in RP/M. In the proposed algorithms, the contour tool-paths are used to fabricate the area along the boundary of each sliced layer to improve the geometrical quality of the biomedical model. The zigzag tool-paths are used to fabricate the interior area of the biomedical model to simplify computing processes and speed up fabrication.

3. **Adaptive speed algorithms and strategies have been devised to minimise build time.**

Based on the different geometrical characteristics of contour and zigzag tool-paths, two adaptive speed algorithms are proposed to reduce build time of RP/M process for biomedical model fabrication. They include an algorithm to optimise the speed of the RP/M nozzle/print head along the contour tool-paths, and an algorithm to obtain the best slope degree to further optimise build time of the RP/M nozzle/print head along the zigzag tool-paths.

4. **Adaptive slicing algorithms and strategies have been proposed to balance the build time and geometrical accuracy.**

Uniform slicing has been widely used for commercial RP/M systems today. However, uniform slicing is difficult to achieve an optimised balance of build efficiency and geometrical accuracy. For instance, if the layer thickness is too thick, the build time is reduced but the geometrical accuracy could be relatively poor. Otherwise, the geometrical accuracy is improved but the build time is also extended significantly. Adaptive slicing can effectively address the above problems with varied thickness of layers to address the different geometrical characteristics of models. For instance, for complex shape part of the biomedical model, slicing with smaller thickness to protect feature characteristics and to improve geometrical accuracy of fabrication; for simple shape part of the biomedical model, slicing with bigger thickness to reduce build time.

In this research, a novel adaptive slicing approach has been proposed to balance the build time and geometrical accuracy for biomedical model fabrication in RP/M. In the proposed approach, rotating slicing and two thresholds strategies have been first introduced to extract the surface feature of the biomedical model. Based on the obtained outside surface feature information of the model, an adaptive slicing thickness determination algorithm has then been developed to decide the thickness of each slicing layer to balance the geometrical accuracy and build efficiency during the fabrication process of RP/M.

**5. An adaptive approach has been developed to support the realisable and customised FGM-based biomedical models effectively.**

The current RP/M systems are mainly for homogenous material-based biomedical object fabrication. Different from homogenous materials, FGM-based model contain gradual variations in composition from two or more materials. In recent years, the RP/M technology has been increasingly used in FGM-based model applications. Considering the characteristics of FGM-based products, an important research issue is how to develop more efficient and adaptive RP/M algorithms and strategies to support the realisable, customised and free-form FGM-based biomedical models.

In this research, an adaptive approach is proposed to support the realisable and customised FGM-based biomedical models in RP/M. In the proposed approach, the developed FGM-based modelling features can represent typical FGM-based biomedical models effectively based on the closed NURBS curves obtained from the directly slicing

algorithm. The linear and non-linear control parameters for FGM composition and distributions can enable users to address their specific functional needs of FGM-based biomedical model.

The proposed mixed tool-path algorithm and strategy can generate a series of contour/offset tool-paths to represent the material gradual change along the $u$ direction of NURBS surface and to ensure the surface quality, and zigzag tool-path is generated for the internal area of a single material to simplify computing and processing of FGM-based biomedical model fabrication in RP/M.

6. **Geometrical accuracy and build time analysis and control modules and strategise have been proposed to analyse and control the geometrical accuracy and build time during RP/M processing of biomedical models.**

In RP/M technology, most of the existing geometrical accuracy and build time analysis and prediction modules are applicable to relatively simple geometric product models. They are difficult to be applied to complex biomedical models which include highly customised and complex geometry.

In this research, more suitable and sensible geometrical accuracy and build time analysis and control modules have been proposed to analyse and control the geometrical accuracy and build time during RP/M processing of biomedical model.

The proposed geometrical accuracy and build time analysis modules can be used to calculate and analyze the geometrical accuracy and build time during RP/M processing with the different values of parameters. It provides an effective guideline for parameter setting of a RP/M system for biomedical models fabrication.

The proposed geometrical accuracy and build time control strategy can be used to control the geometrical accuracy and build time. They provide an effective guideline for a user to balance the geometrical accuracy and build efficiency and can achieve significantly improvement by choosing the right threshold values.

## 7.2 Recommendations for future work

The proposed adaptive process planning approach can effectively improve geometrical accuracy and reduce build time of biomedical model fabrication in RP/M, however, the studies conducted in this research can be further extended in a few important directions as follows:

1. **Integrated orientation determination, support structure generation, slicing and tool-path generation into one software platform to optimise geometrical accuracy and build time in RP/M process planning**

The process planning of RP/M is consisted by four essential tasks (1) orientation determination, (2) support structure generation, (3) slicing, and (4) tool-path generation. They are interacted between each other to affect the geometrical accuracy and build time of fabrication in RP/M. For instance, different build orientation for a CAD model will affect the surface quality, the build time, the complexity of support structure and the total number of sliced layers. Meanwhile, different designs of the support structure will affect the build time, surface quality and mechanical properties of the fabrication model.

In this research, it only focuses on slicing and tool-path generation adaptive algorithms and strategies to improve geometrical accuracy and reduce build time. There is a further work to integrate these four tasks into one software platform seamlessly to optimise the process planning for least time and cost with the highest geometrical accuracy for complex biomedical models fabrication in RP/M.

2. **More practical experiments related to this research should to be done in the future**

This research is still based on simulation, although the parameters that used to calculate and analyse the geometrical accuracy and build time of fabrication in this research, are set based on the existed commercial RP/M systems. In the future, more practical experiments need to be done to test and verify the developed algorithms and strategies.

In addition, when a practical biomedical model is built during practical experiments, its quality may be affected by warpage and shrinkage due to uneven distribution of heat

energy, and cooling and the resulting binding force, etc. of used RP/M systems. Such effects can affect the geometrical accuracy of the physical biomedical model. Therefore, it would be desirable to study the relationship between the effects of warpage and shrinkage, and the practical biomedical model geometrical accuracy. The research results can also be used to correct the developed geometrical accuracy analysis module in this research.

**3. Further enhancement in directly slicing algorithm and NURBS-based representations of complex biomedical model**

The limitation of the developed directly slicing algorithm is that the NURBS-based curve is more complex compared with a STL file to represent the CAD model. The proposed approach is only for normal biomedical model directly slicing and NURBS curve representation, and its difficult to represent extreme complex biomedical hollow models such as tissue scaffold CAD models (shown in Figure 7.1). Therefore, it would be desirable to establish a more effective directly slicing algorithm and NURBS-based curve representation to deal with tissue scaffold in the future.

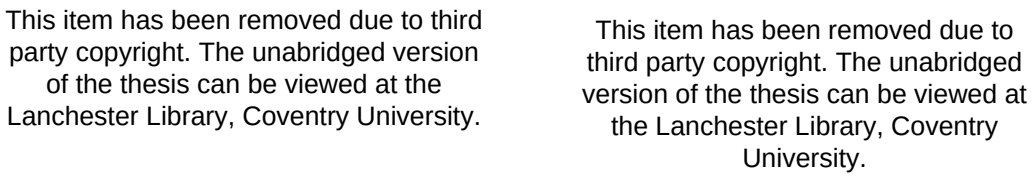


**Figure 7.1** Two examples of tissue scaffold (MedMarket Diligence, 2012).

**4. Further enhancement in mixed tool-path algorithms for FGM-based biomedical model.**

The developed adaptive approach can only be used for some special FGM-based biomedical models which have two materials and the material gradual change is along the

$u$ direction of NURBS surface. It is difficult to be applied for some complex FGM-based models that have more than two materials and the material gradual change along different direction of the model (shown in Figure 7.2). Therefore, it would be desirable to develop more effective tool-path algorithms to generate mixed tool-paths for different types FGM-based models in the future.

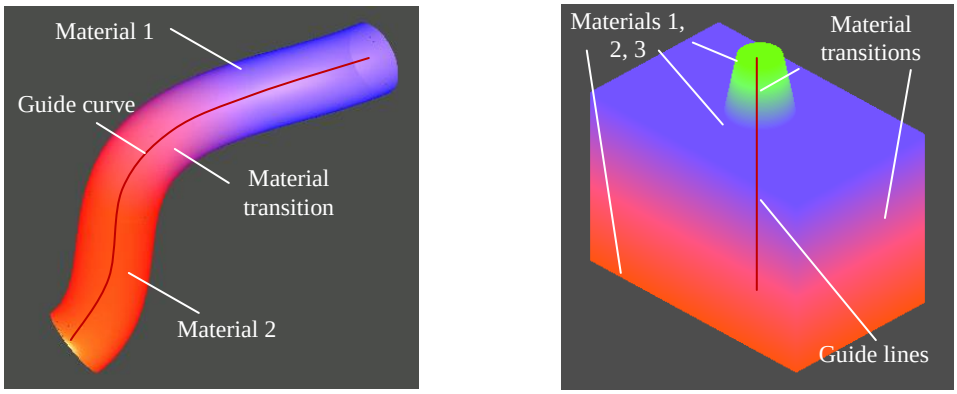


**Figure 7.2** Two examples of complex FGM-based model.

# REFERENCES


3D Systems. (2012) http://blog.3dsystems.com/

Allen, S. and Dutta, D. (1995) Determination and evaluation of support structures in layered manufacturing. Journal of Design and Manufacturing, 5: 153–162.

Armillotta, A. (2006) Assessment of surface quality on textured FDM prototypes. Rapid Prototyping Journal, 12(1): 35-41.

Bacchewar, P.B., Singhai, S.K. and Pandey, P.M. (2007) Statistical modelling and optimization of surface roughness in the selective laser sintering process. Proceedings of the Institution of Mechanical Engineers, Part B: Journal of Engineering Manufacture, 221(1): 35–52.

Bertoldi, M., Yardimci, M.A., Pistor, C.M. and Guceri, S.I. (1998) Domain decomposition and space filling curves in toolpath planning and generation. Proceedings of the 1998 Solid Freeform Fabrication Symposium. P. 267-274.

Biswas, A., Shapiro, V. and Tsukanov, I. (2004) Heterogeneous material modeling with distance fields. Computer Aided Geometric Design, 21(3): 215-242.

Bourell, D.L., Leu, M.C. and Rosen, D.W. (2009) Roadmap for additive manufacturing: Identifying the Future of Freeform Processing. The University of Texas at Austion, Austin, TX, USA.

Burstein, A.H. and Wright, T.M. (1994) Fundamentals of orthopedic biomechanics. Williams & Wilkins, Michigan, USA.

Byun, H.S. and Lee, K.H. (2005) A decision support system for the selection of a rapid prototyping process using the modified TOPSIS method. The International Journal of Advanced Manufacturing Technology, 26(11/12): 1338-1347.

Cannillo, V., Lusvarghi, L., Manfredini, T., Montorsi, M., Siligardi, C. and Sola, A. (2007) Glass–ceramic functionally graded materials produced with different methods. Journal of European Ceramic Society, 27(2/3): 1293-1298.

Cao, W. and Miyamoto, Y. (2003) Direct slicing from AutoCAD solid models for rapid prototyping. International Journal of Advanced Manufacturing Technology, 21: 739-742.

Castelino, K., D'Souza, R. and Wright, P.K. (1999) Toolpath optimization for minimizing airtime during machining. Journal of Manufacturing Systems, 22(3): 173-180.

Chang, R., Nam, J. and Sun, W. (2008) Computer-aided design, modeling, and freeform fabrication of 3D tissue constructs for drug metabolism studies. Computer Aided Design and Applications, 5(1-4): 363-370.

Chang, W.R. (1997) CAD/CAM for the selective laser sintering process. MS Thesis. University of Texas, Austin, USA.

Chen, C.C. and Sullivan, P.A. (1996) Predicting total build-time and the resultant cure depth of the 3D stereolithography process. Rapid Prototyping Journal, 2(4): 27-40.

Chen, X., Wang, C., Ye, X., Xiao, Y. and Huang, S. (2001) Direct slicing from PowerSHAPE models for rapid prototyping. International Journal of Advanced Manufacturing Technology, 17: 543-547.

Chen, K.Z., Feng, X.Y., Wang, F. and Feng, X.A. (2007) A virtual manufacturing system for components made of a multiphase perfect material. Computer-Aided Design, 39(2): 112-124.

Cheung, H.H. (2007) A versatile multi-material virtual prototyping system.
Ph.D. Thesis. The University of Hong Kong, Hong Kong.

Chiu, W.K. and Yu, K.M. (2008) Multi-criteria decision-making determination of material gradient for functionally graded material objects fabrication. Proceedings of the Institution of Mechanical Engineers, Part B: Journal of Engineering Manufacture, 222(2): 293-307.

Chiu, W.K., Yeung, Y.C. and Yu, K.M. (2006) Toolpath generation for layer manufacturing of fractal objects. Rapid Prototyping Journal, 12(4): 214-221.

Choi, S.H. and Cheung, H.H. (2006) A topological hierarchy-based approach to toolpath planning for multi-material layered manufacturing. Computer-Aided Design, 38(2): 143-156.

Chua, C.K., Leong, K.F., Tan, K.H., Wiria, F.E. and Cheah, C.M. (2004) Development of tissue scaffolds using selective laser sintering of polyvinyl alcohol/hydroxyapatite biocomposite for craniofacial and joint defects. Journal of Material Science: Mater in Medicine, 15(10): 1113-1121.

Chua, C.K., Leong, K.F. and Lim, C.S. (2005) Rapid Prototyping (2rd Edition). World Scientific Publisher.

Custompartnet. (2012) http://www.custompartnet.com/wu/fused-deposition-modeling

Das, S. and Chung, H. (2006) Processing and properties of glass bead particulate-filled functionally graded Nylon-11 composites produced by selective laser sintering. Materials Science and Engineering: A, 437(2): 226-234.

Ding, J., Colegrove, P., Mehnen, J., Ganguly, S., Sequeira Almeida, P.M., Wang, F. and Williams, S. (2011) Thermo-mechanical analysis of wire and arc additive layer manufacturing process on large multi-layer parts. Computational Materials Science, 50 (12): 3315-3322.

Dolenc, A. and Makela, I. (1994) Slicing procedures for layered manufacturing techniques. Computer-Aided Design, 26: 119-126.

EOS. (2012) http://www.eos.info/

Fang, Z. (2005) Image-guided modeling, fabrication and micromechanical analysis of bone and heterogeneous structure. Ph.D. Thesis. Drexel University, USA.

Genesan, M. and Fadel, G. (1994) Hollowing rapid prototyping parts using offsetting techniques. Proceedings of the 5th International conference on Rapid Prototyping. p. 241-251.

Giannatsis, J. and Dedoussis, V. (2009) Additive fabrication technologies applied to medicine and health care: a review. The International Journal of Advanced Manufacturing Technology, 40(1/2): 116-127.

Grimm, T. A. (2004) User's guide to rapid prototyping. Michigan: Society of Manufacturing Engineers

Gupta, A., Seifalian, A.M., Ahmad, Z., Edirisinghe, M.J. and Winslet, M.C. (2007) Novel electro hydro dynamic printing of nano composite biopolymer scaffolds. Journal of Bioactive and Compatible Polymers, 22(3): 265-280.

Han, W., Jafari, M.A., Danforth, S.C. and Safari, A. (2002) Tool path-based deposition planning in fused deposition processes. Journal of Manufacturing Science and Engineering-transactions of The Asme, 124(2): 462-473.

Han, W., Jafari, M.A. and Seyed, K. (2003) Process speeding up via deposition planning in fused deposition-based layered manufacturing processes. Rapid Prototyping Journal, 9(4): 212-218.

Hao, L., Savalani, M.M., Zhang, Y., Tanner, K.E. and Harris, R.A. (2006) Selective laser sintering of hydroxylapatite reinforced polyethylene composites for bioactive implants and tissue scaffold development. Proceedings of the Institution of Mechanical Engineers, Part H: Journal of Engineering in Medicine, 220(6): 521-531.

InstaTuts. (2012) http://instatuts.com/featured/a-rapid-prototyping-and-stl-informative-guide/

Jackson, T.R., Liu, H., Patrikalakis, N.M., Sachs, E.M. and Cima, M.J. (1999) Modeling and designing functionally graded material components for fabrication with local composition control. Materials & Design, 20(2/3): 63-75.

Jackson, T.R. (2000) Analysis of functionally graded material object representation methods. Ph.D. Thesis. Massachusetts Institute of Technology, USA.

Jafari, M., Han, W., Mohammadi, F., Safari, A., Danforth, S.C. and Langrana, N. (2000) A novel system for fused deposition of advanced multiple ceramics. Rapid prototyping Journal, 6(3): 161-175.

Kasaeian, A.B., Vatan, S.N. and Daneshmand, S. (2011) FGM materials and finding an appropriate model for the thermal conductivity. Procedia Engineering, 14: 3199-3204.

Khalil, S., Nam, F. and Sun, W. (2005) Multi-nozzle deposition for construction of 3D biopolymer tissue scaffolds. Rapid Prototyping Journal, 11(1): 9-17.

Kieback, B., Neubrand, A. and Riedel, H. (2003) Processing techniques for functionally graded materials. Materials Science and Engineering: A, 362(1/2): 81-106.

Kou, X.Y., Parks, G.T. and Tan, S.T. (2012) Optimal design of functionally graded materials using a procedural model and particle swarm optimization. Computer-Aided Design, 44(4): 300-310.

Kruth, J.P., Levy, G., Klocke, F. and Childs, T.H.C. (2007) Consolidation phenomena in laser and powder-bed based layered manufacturing. Annals of CIRP, 56: 730-759.

Kulkarni, P., Marsan, A. and Dutta, A. (2000) A review of process planning techniques in layered manufacturing. Rapid Prototyping Journal, 6(1): 18-35.

Liu, F., Zhou, H. and Li, D. (2009) Repair of STL errors. International Journal of Production Research, 47(1): 105-118.

Liu, H., Maekawa, T., Patrikalakis, N.M., Sachs, E.M. and Cho, W. (2004) Methods for feature-based design of heterogeneous solids. Computer-Aided Design, 36(12): 1141-1159.

Liu, H. (2000) Algorithms for design and interrogation of functionally graded material solid. Ph.D. Thesis. Massachusetts Institute of Technology, USA.

Liu, W., Li, L. and Kochhar, A.K. (1998) A method for assessing geometrical errors in layered manufacturing. Part 1: Error interaction and transfer mechanisms. The International Journal of Advanced Manufacturing Technology, 14(9): 637-643.

Liu, W., Li, L. and Kochhar, A.K. (1998) A method for assessing geometrical errors in layered manufacturing. Part 2: Mechanisms modeling and numerical evaluation. The International Journal of Advanced Manufacturing Technology, 14(9): 644-650.

Liu, Z., Wang, L. and Lu, B. (2006) Integrating cross-sectional imaging based reverse engineering with rapid prototyping. Computers In Industry, 57: 131-140.

Londonspine. (2012) http://www.londonspine.co.uk/

Luo, M., Zhang, D.H., Wu, B.H. and Zhang, Y. (2010) Optimisation of spiral tool path for five-axis milling of freeform surface blade. International Journal of Machining and Machinability of Materials, 8(3/4): 266-282.

Ma, W., But, W.C. and He, P. (2004) NURBS-based adaptive slicing for efficient rapid prototyping. Computer-Aided Design, 36: 1309-1325.

Ma, Y.L. and Hewitt, W.T. (2003) Point inversion and projection for NURBS curve and surface: control polygon approach. Computer Aided Geometrical Design, 20(2): 79-99.

Marsan, A. and Dutta, D. (1997) A survey of process planning techniques for layered manufacturing. Proceedings of the 1997 ASME Design Automation Conference, Sacramento, CA, USA.

Martello. (2012) http://www.martello.co.uk/rapid_prototyping.htm

Materialise. (2012) http://www.materialise.com/

McDonald, J. A., Ryall, C. J. and Wimpenny, D. I. (2001) Rapid Prototyping Casebook. London: Professional Engineering Publishing

MedMarket Diligence. (2012) http://mediligence.com/blog/

Miyamoto, Y., Kaysser, W.A., Rabin, B.H., Kawasaki, A. and Ford, R.G. (1999) Functionally graded materials: design, processing and applications. Kluwer Academic Publishers, Boston, USA.

Misra, D., Sundararajan, V. and Wright, P.K. (2005) Zig-zag tool path generation for sculptured surface finishing. Dimacs Series in Discrete Mathematics and Theoretical Computer Science, 67: 265-280.

Nagy, M.S. and Matyasi, G. (2003) Analysis of STL files. Mathematical and Computer Modeling, 38: 945-960.

Nemat-Alla, M. (2003) Reduction of thermal stresses by developing two-dimensional functionally graded materials. International Journal of Solids and Structures, 40(26): 7339-7356.

Object. (2012) http://objet.com/3d-printers

Open CASCADE. (2012) http://www.opencascade.org/

Pompe, W., Worch, H., Epple, M., Gelinsky, W., Greil, P., Hempel, U., Scharnweber, D. and Schulte, K. (2003) Functionally graded materials for biomedical applications. Materials Science and Engineering: A, 362(1/2): 40-60.

Prakash, T., Singha, M.K. and Ganapathi, M. (2011) A finite element study on the large amplitude flexural vibration characteristics of FGM plates under aerodynamic load. Internatinal Journal of Non-Linear Mechanics, 47(5): 439-447.

Qian, X.P. and Dutta, D. (2003) Physics-based modeling for heterogeneous objects. Journal of Mechanical Design, 125(3): 416-427.

Ren, L., Sparks, T., Ruan, J.Z. and Liou, F. (2008) Process planning strategies for solid freeform fabrication of metal parts. Journal of Manufacturing Systems, 27: 158-165.

Rianmora, S. and Koomsap, P. (2010) Recommended slicing positions for adaptive direct slicing by image processing technique. International Journal of Advanced Manufacturing Technology, 46: 1021-1033.

Ryan, G.E., Pandit, A.S. and Apatsidis, D.P. (2008) Porous titanium scaffolds fabricated using a rapid prototyping and powder metallurgy technique. Biomaterials, 29(27): 3625-3635.

Sabourin, E. (1996) Adaptive high-precision exterior, high-speed interior, layered manufacturing. MS thesis. Virginia Polytechnic Institute and State University, Blacksburg, Virginia.

Sabourin, E., Houser, S.A. and Bohn, J.H. (1997) Accurate exterior, fast interior layered manufacturing. Rapid Prototyping Journal, 3: 44-52.

Samanta, K. and Koc, B. (2005) Feature-based design and material blending for free-form heterogeneous object modeling. Computer-Aided Design, 37(3): 287-305.

Shi, Y., Chen, X., Cai, D. and Huang, S. (2004) Application software system based on direct slicing for rapid prototyping. International Journal of Product Research, 42: 2227-2242.

Shin, K.H. (2002) Representation and process planning for layered manufacturing of heterogeneous objects. Ph.D. Dissertation. University of Michigan, USA.

Siu, Y.K. and Tan, S.T. (2002) Source-based heterogeneous solid modeling. Computer-Aided Design, 34(1): 41-55.

Singhal, S.K., Jain, P.K. and Pandey, P.M. (2008) Adapitve slicing for SLS prototyping. Computer-Aided Design and Applications, 5(1-4): 412-423.

Suh, Y.S. and Wozny, M.J. (1994) Adaptive slicing of solid freeform fabrication processes. Proceedings of Solid Freeform Fabrication Symposium, University of Texas at Austin,Texas. p. 404-411.

Sun, W., Starly, B., Nam, J. and Darling, A. (2005) Bio-CAD modelling and its applications in computer-aided tissue engineering. Computer-Aided Design, 37(11): 1097-1114.

Starly, B., Lau, A., Sun, W., Lau, W. and Bradbury, T. (2005) Direct slicing of STEP based NURBS models for layered manufacturing. Computer-Aided Design, 37: 387-397.

Syed, I. (2011) Feasibility study of key components and algorithm design for multi-material RP/M machine. Master Dissertation, Coventry University, UK.

TECHSOFT3D. (2012) http://docs.techsoft3d.com/visualize/

Thompson, D.C. (1995) The optimization of part orientation for solid freeform manufacture. MS Thesis. The University of Texas at Austin, USA.

Torshizian, M.R., Kargarnovin, M.H and Nasirai, C. (2011) Mode III fracture of an arbitrary oriented crack in two dimensional functionally graded material. Mechanics Research Communications, 38(3): 164-169.

Ultrasound-scanners. (2012) http://www.ultrasound-scanners.co.uk/

Wah, P.K., Murty, K.G., Joneja, A. and Chiu, L.C. (2002) Toolpath optimization in layered manufacturing. IIE Transactions, 34(4): 335-347.

Wang, C.S. and Chang, T.R. (2008) Re-triangulation in STL meshes for rapid prototyping and manufacture. International Journal of Advanced Manufacturing Technology, 37: 770-781.

Warkhedkar, R.M. and Bhatt, A.D. (2009) Material-solid modeling of human body: A heterogeneous B-spline based approach. Computer-Aided Design, 41(8): 586-597.

Watanabe, Y., Iwasa, Y., Sato, H., Teramoto, A., Abe, K. and Fujiwara, E.M. (2011) Microstructures and mechanical properties of titanium/biodegradable-polymer FGM for bone tissue fabricated by spark plasma sintering method. Journal of Materials Processing Technology, 211(12): 1919-1926.

Watari, F., Yokoyama, A., Omori, M., Hirai, T., Kondo, H., Uo, M. and Kawasaki, T. (2004) Biocompatibility of materials and development to functionally graded implant for bio-medical application. Composites Science and Technology, 64(6): 893-908.

Weiss, L.E., Amon,C.H., Finger, S., Miller, E.D., Romero, D., Verdinelli, I., Walker, L.M. and Campbell, P.G. (2005) Bayesian computer–aided experimental design of heterogeneous scaffolds for tissue engineering. Computer-Aided design, 37: 1127-1139.

Wohlers, T. (2008) Wohlers Raport 2008: Rapid Prototyping & Tooling State of the Industry, Wohlers Association Inc., USA.

Worldmedassist. (2012) http://www.worldmedassist.com/procedures/hip-replacement-abroad/

WRAMC. (2012) http://wramc.amedd.army.mil/

Xia, Q. and Wang, M.Y. (2008) Simultaneous optimization of the material properties and the topology of functionally graded structures. Computer-Aided Design, 40(6): 660-675.

Xpress3d. (2012) http://www.xpress3d.com/SLA.aspx

Xu, F., Loh, H.T. and Wong, Y.S. (1999) Considerations and selection of optimal orientation for different rapid prototyping systems. Rapid Prototyping Journal, 5(2): 54-60.

Yakovlev, A., Trunova, E., Grevey, D., Pilloz, M. and Smurov, I. (2005) Laser-assisted direct manufacturing of functionally graded 3D objects. Surface and Coatings Technology, 190(1): 15-24.

Yang, Y., Loh, H.T., Fuh, F.Y.H. and Wang, Y.G. (2002) Equidistant path generation for improving scanning efficiency in layered manufacturing. Rapid Prototyping Journal, 8(1): 30-37.

Yang, P. and Qian, X.P. (2007) A B-spline-based approach to heterogeneous objects design and analysis. Computer-Aided Design, 39(2): 95-111.

Yin, Z.W. (2004) Direct integration of reverse engineering and rapid prototyping based on the properties of NURBS or B-spline. Precision Engineering, 28(3): 293-301.

Z corp. (2012) http://www.zcorp.com/

Zhao, Z. and Laperriere, L. (2000) Adaptive direct slicing of the solid model for rapid prototyping. International Journal of Production Research, 38(1): 69-83.

Zhou, M.Y. (2004) Path planning of functionally graded material objects for layered manufacturing. International Journal of Production Research, 42(2): 405-415.

Zhu, J., Ye, G.R., Xiang, Y.Q. and Chen, W.Q. (2011) Recursive formulae for wave propagation analysis of FGM elastic plates via reverberation-ray matrix method. Composite Structures 93: 259-270.